The contribution of bone marrow-derived cells to angiogenesis and lymphangiogenesis in murine models of carcinogenesis

Inauguraldissertation

zur Erlangung der Würde eines Doktors der Philosophie
vorgelegt der
Philosophisch-Naturwissenschaftlichen Fakultät
der Universität Basel

von

Adrian Zumsteg
aus Solothurn/ Schweiz

Basel, Februar 2009

Genehmigt von der Philosophisch-Naturwissenschaftlichen Fakultät
auf Antrag von

Prof. Dr. Gerhard Christofori
Prof. Dr. Christoph Dehio
Prof. Dr. Kurt Ballmer-Hofer

Basel, den 17. Februar 2009

Prof. Dr. Eberhard Parlow
Dekan

Summary

Cancer is a class of diseases in which a group of cells display uncontrolled growth (division beyond the normal limits), invasion (intrusion on and destruction of adjacent tissues), and sometimes metastasis (spread to other locations in the body via the circulatory system). In addition to tumor cell-intrinsic genetic and epigenetic alterations, the tumor stroma, i.e. endothelial cells, pericytes, fibroblasts and a diverse immune cell infiltrate, might substantially contribute to tumor progression, metastatic potential and resistance to therapy.

I therefore investigated the influence of immune cells on the growth of tumors in the Rip1Tag2 mouse insulinoma model of multistage carcinogenesis. I detected a strong infiltration of myeloid cells, i.e. macrophages and granulocytes, into insulinomas. Functional experiments *in vivo* revealed that depletion of macrophages in tumors led to reduced angiogenesis but did not affect tumor growth.

During the characterization of the immune cell contribution to tumor growth in the Rip1Tag2 tumor model, I detected bone marrow-derived cells at unexpected sites. In particular, when I analyzed the spatial contribution of GFP-tagged bone marrow cells in tumors of lymphangiogenic Rip1Tag2;RipVEGF-C mice, I detected bone marrow-derived cells in lymphatic endothelium surrounding the tumors.

Detailed analysis of the integrated GFP^+-cells revealed the expression of a complete set of markers that are characteristic for lymphatic endothelial cells, the cell surface proteins LYVE-1 and Podoplanin, as well as the homeo-box transcription factor Prox-1. Depending on the analysis technique applied, either confocal microscopy followed by 3D reconstitution or flow cytometry, between 3 and 9% of lymphatic endothelial cells in tumors are derived from the bone marrow. These studies were expanded to a second tumor model, the subcutaneous growth of TRAMP-C1 prostate cancer cells in syngenic mice, which confirmed the findings made in Rip1Tag2; RipVEGF-C mice, and allowed to further substantiate the suggested ontogeny of the integrated, bone marrow-derived cells.

Cell sorting and genetic lineage tracing experiments indicated that the bone marrow-derived tumor lymphatic endothelial cells were at least partially derived from the myeloid lineage. Tumor mice were adoptively transferred with labeled myeloid (progenitor) cells, and subsequent integration of these cells into tumor lymphatic endothelium was detected. Cre/Lox technology resulting in myeloid-specific marker gene expression was employed to come to similar conclusions in a pure genetic experimental system without bone marrow cell-transfer or irradiation.

In a loss-of-function approach, macrophages were pharmacologically depleted in Rip1Tag2;RipVEGF-C mice. Peritumoral lymphatic vessel coverage was found to be reduced in

macrophage-depleted mice as compared to control mice. Expression level analysis of the lymphangiogenic factors VEGF-C and VEGF-D by tumor-infiltrating macrophages indicated that their contribution to lymphangiogenesis by supplying growth factors is negligible and that the reduced lymphangiogenesis might indeed come from the reduced availability of macrophages as building blocks of lymphatic endothelia.

The same plasticity of myeloid cells I detected *in vivo* was also observed *in vitro*, where bone marrow-derived macrophages start forming tube like structures and also start expressing lymphatic endothelial markers, when cultured under pro-inflammatory and endothelial specific conditions.

In conclusion, this data indicates a myeloid origin of cells that trans-differentiate into lymphatic endothelial cells in an inflammatory tumor environment.

The increasing use of *non-invasive* imaging technologies prompted us to evaluate an approach resulting in bioluminescent pancreatic insulinoma, principally an improved Rip1Tag2 tumor model of multistage pancreatic β-cell carcinogenesis**.** I therefore constructed a bicistronic expression cassette in which SV40 early region is followed by an internal ribosomal entry site and a firefly luciferase coding sequence, under the transcriptional control of the Rat insulin promoter 1. Transgenic expression in mice resulted in β-cell carcinogenesis that could be monitored non-invasively by *in vivo* bioluminescence. Numerous tumors of different malignancy stages can be detected in individual mice, indicating that this model recapitulates multistage carcinogenesis. In addition, in this mouse strain called *RL-1* (*R*ipTag-IRES-*L*uciferase line *1*), due to the very stringent expression exclusively in the β-cells of Langerhans islets, we could determine micro-metastasis in liver via luciferase expression of metastatic cells. This mouse line will be of value to study anti-tumoral therapeutic approaches in real-time, as well as to define roles for tumor-promoting as well as metastasis-related genes when crossed to other transgenic or gene-targeted mice.

Zusammenfassung

Krebs umfasst eine Gruppe von Krankheiten, in deren Verlauf Zellen unkontrolliert wachsen, in angrenzende Gewebe eindringen, diese eventuell zerstören und die auch Metastasen bilden können (Ausbreitung der Krebszellen im Körper mittels des Kreislaufsystems). Nicht nur genetische und epigenetische Mutation innerhalb der Tumorzellpopulation, sondern auch das Tumorstroma, welches Endothelzellen, Perizyten, Fibroblasten und veschiedene Immunzellen umfasst, kann einen grossen Einfluss auf die Tumorentwicklung und das Metastasierungspotential bzw. die Therapieresistenz von Tumoren haben.

Daher habe ich den Einfluss von Immunzellen auf das Wachstum von Tumoren im Rip1Tag2 Insulinom Mausmodell für stufenweise Krebsentwicklung untersucht. Eine substantieller Anteil aller in der Tumormasse gefundenen Zellen sind myeloide Zellen, eine Immunzellgruppe, die u.a. Makrophagen und Granulozyten umfasst. Experimentelle Depletion von Makrophagen in Tumoren führte zu verminderter Blutgefäss-Bildung ohne jedoch einen Einfluss auf das Tumorwachstum zu entfalten.

Im Verlaufe meiner Studien über den Beitrag von Immunzellen zur Tumorentwicklung im Rip1Tag2 Tumor-Modell, habe ich dem Knochenmark entstammende Immunzellen an unerwarteter Stelle gefunden. Als ich die räumliche Verteilung von GFP-markierten Knochenmark-Zellen in lymphangiogenen Rip1Tag2;RipVEGF-C Mäusen analysierte, habe ich markierte Zellen im lymphatischen Endothel gefunden, welches die Tumoren umgibt.

Analyse der integrierten GFP^+-Zellen hat ergeben, dass die wichtigsten Marker, welche zur Definition von lymphatischem Endothel gebräuchlich sind, nämlich die Oberflächenmoleküle LYVE-1 und Podoplanin sowie der Transkriptionsfaktor Prox-1, auf den GFP^+-Zellen ko-exprimiert sind. Je nach Analyse-Methode, entweder konfokale Mikroskopie oder Durchflusszytometrie, waren 3 – 9% aller Tumor-Lymphendothelzellen dem Knochenmark entstammende Zellen. Diese Studien habe ich daraufhin um ein andersartiges Tumormodell erweitert, das subkutane Wachstum von der Prostata-Karzinom-Zelllinie TRAMP-C1 in syngenen Mäusen. In diesem Modell bin ich zu gleichen Resultaten gekommen, insbesondere hat sich die vermutete Ontogenese der im Lymphendothel integrierten Knochenmark-Zellen bestätigt.

Zell-Sortierungs- und genetische Markierungs-Experimente deuten darauf hin, dass dem Knochenmark entstammende Tumor-Lymphendothelzellen zumindest teilweise von myeloiden Zellen abstammen. In Tumormäusen, welche adaptiv mit markierten myeloiden (Vorläufer)-Zellen transferiert worden waren, wurde die gleiche Art von Integration in lymphatische Gefässe entdeckt. Mit Hilfe der Cre/Lox Technologie konnte ein Marker-Gen spezifisch in myeloiden Zellen und deren Abkömmlingen exprimiert werden und so die adoptiven Transfer-Experimente in einem rein

genetischen Ansatz bestätigt werden, der ohne Knochenmarks-Transfer und Bestrahlung auskommt.

In einem Funktionsverlust-Experiment habe ich Makrophagen pharmakologisch in Rip1Tag2;RipVEGF-C Mäusen depletiert. Daraufhin bildeten sich weniger Tumor-umgebende Lymphgefässe. Expressionsanalysen der lymphangiogenen Faktoren VEGF-C and VEGF-D in Tumor-infiltrierenden Makrophagen deuten darauf hin, dass Makrophagen in diesem Modell nicht primär Quelle von lymphangiogenen Wachstumsfaktoren sind, sondern eher eine Funktion als Bausteine von lymphatischem Endothel einnehmen.

Die gleiche Plastizität, die *in vivo* festgestellt wurde, konnte auch *in vitro* festgestellt werden. Aus dem Knochenmark gewonnene Makrophagen beginnen röhrenförmige Gebilde zu formen und lymphatische Marker zu exprimieren, wenn man sie unter inflammatorischen und endothel-spezifischen Bedingungen kultiviert.

Wir schliessen aus diesen Daten, dass myeloide Zellen in einer inflammatorischen Tumor-Umgebung zu Lymphendothel-Zellen trans-differenzieren können.

Der zunehmende Gebrauch von *nicht-invasiven* Bildgebungsverfahren veranlasste mich, einen Ansatz in Richtung biolumineszenter pankreatischer Insulinome zu entwickeln, also eine Art erweitertes Rip1Tag2 Modell der mehrstufigen β-Zell-Krebsentwicklung zu schaffen. Zu diesem Zweck wurde eine bicistronische Expressionskassette konstruiert, welche unter Kontrolle des Rip ("Rat insulin promoter") Promoters das SV40 grosse T Antigen kodiert, gefolgt von einer internen Ribosomen-Eintrittsstelle und der Glühwürmchen-Luziferase kodierenden Sequenz. Transgene Expression in Mäusen führte zu Tumorentwicklung, die durch *in vivo* Biolumineszenz verfolgt werden kann. Da verschiedene Tumorgrade in einer Maus beobachtet werden können, ist dieses Mausmodell geeignet, um stufenweise Krebsentwicklung zu untersuchen. Zusätzlich detektierten wir in dieser Mauslinie, genannt RL-1 (*R*ipTag-IRES-*L*uciferase line *1*), aufgrund der hochspezifischen Expression der Luziferase in β-Zellen, Mikrometastasen in der Leber mittels der Luziferase-Aktivität der metastasierten Zellen. Diese Maus-Linie wird von Nutzen sein zur Echtzeit-Analyse von experimentellen Krebstherapieansätzen und zur Untersuchung von Tumor-beschleunigenden und Metastasen-relevanten Genfunktionen, wenn man die RL-1 Maus mit weiteren genetisch veränderten Mauslinien kreuzt.

1. Introduction

1.1. Hallmarks of cancer

Cancer is a disease in which a group of cells display uncontrolled growth (division beyond the normal limits), invasion (intrusion on and destruction of adjacent tissues), and sometimes metastasis (spread to other locations in the body via lymph or blood). These three malignant properties of cancers differentiate them from benign tumors, which are self-limited, do not invade or metastasize. In developed countries, cancer is presently responsible for about 25% of all deaths, and on a yearly basis, 0.5% of the population is diagnosed with cancer. As cancer rates increase with age and average life expectancy goes up, cancer is projected to be the major cause of death in the developed countries at around 2010. Many cancers are not yet curable, and a more detailed understanding of cancers and their resistance to treatment is warranted and might lead to novel therapeutic approaches.

Murine models of cancer have been used for more than two decades to model human cancer in animal experiments, the mouse being an animal amenable to genetic manipulation (see section “1.2. Mouse models of cancer”). Combining results from clinical observations and animal experiments allowed to define many clinical and genetic parameters with prognostic (overall outcome of a certain cancer type) or predictive (likeliness to respond to therapy) value. Predictive biomarkers can be targets for therapy. Examples of genes that have proven to be of relevance are well-known markers such as estrogen receptor (ER), progesterone receptor (PR) and HER2/neu in breast cancer, BCR-ABL fusion protein in chronic myeloid leukemia, c-KIT mutations in gastro-intestinal stroma tumors (GIST) and EGFR1 mutations in non-small cell lung cancer (NSCLC).

In addition to tumor cell intrinsic genetic and epigenetic alterations, the tumor stroma might substantially contribute to tumor progression, angiogenesis, metastatic potential and resistance to therapy (see “1.4. Interactions tumor – immune system”).

Douglas Hanahan and Robert Weinberg have defined six traits – acquired capabilities – shared by most types of human cancer (Hanahan and Weinberg, 2000), which are shortly summarized in the following paragraphs.

Self-sufficiency in growth signals

Normal cells require extrinsic mitogenic growth signals before they can move from a quiescent state into an active proliferative state. Such signals are conveyed to the cells by diffusible growth factors, cell-cell contacts and extracellular matrix components. Whereas normal cells have to be cultured in presence of the appropriate exogenous mitogenic factors and on a suitable substratum for correct ligation of integrins, tumor cells show a reduced dependence on

exogenous growth stimulation. In order to obtain a self-sufficient mitogenic stimulus, three molecular strategies are applied by cancer cells: synthesis of growth factors by the cancer cell, mutation/ over-expression of cell surface receptors leading to increased mitogenic stimulation, and alterations in components of the downstream cytoplasmic signaling circuitries that receive and processes the signals, elicited by the previously mentioned ligands and receptors. A central role among these cytoplasmic circuitries assigns to the SOS-Ras-Raf-MAP kinase pathway. Receptor tyrosine kinases, HER2/*neu* for example over-expressed in some breast cancers, principally elicit their mitogenic signals through this pathway. In another example, in the case of human colon cancer, about half of the tumors have a mutant *ras* oncogene.

Insensitivity to antigrowth signals

Not only the absence of mitogenic stimuli but also anti-proliferative signals, being either soluble or mediated by the extra-cellular matrix, are responsible for keeping cells in a quiescent state and tissues in a homeostasis. Much of the circuitry that enables normal cells to respond to antigrowth signals is associated with proper cell cycle regulation, specifically the components governing the transit of the cell through the G1 phase of its growth cycle. Most anti-proliferative signals funnel into the retinoblastoma protein family members pRB, p107 and p130. In a hypo-phosphorylated state, pRb blocks proliferation by sequestering E2F transcription factors that control the expression of genes essential for progression from G1 to S phase. pRb has been shown to be inactivated by a number of viral oncogenes, including the human papillomavirus E7 protein, and simian virus 40 large T antigen. In contrast, the soluble transforming growth factor-β (TGF-β) has been shown to elicit a very potent anti-proliferative signal, through blocking of c-myc expression controlling G1 cell cycle machinery and induction of p15INK^{4B} and p21 proteins responsible for blockade of pRb phosphorylation by cyclin:CDK complexes. Members of the TGF-β signaling machinery have been shown to be inactivated in cancers, e.g by down-regulation or mutation/ inactivation of the TGF-β receptors or by the inactivation of the SMAD4 gene, encoding a cytoplasmic mediator of TGF-β signaling.

Apoptosis evasion

The machinery for programmed cell death – apoptosis – is present in a latent form in virtually all cell types in the body. The p53 tumor suppressor gene product is critical for sensing DNA damage and upon activation induces either cell cycle arrest or apoptosis. Consequently, more than 50% of human cancers harbor a functional inactivation of the p53 tumor suppressor. Uncontrolled cell growth, for example by forced expression of the oncogene c-myc, often induces apoptosis. This is due to sensory machinery detecting cellular imbalances, e.g. an improper chromosomal segregation. Besides the inactivation of p53, tumor cells have other strategies to

circumvent these pro-apoptotic stimuli. Either anti-apoptotic proteins are up-regulated, including the members of the pro-apoptotic Bcl-2 family or activation of the insulin like growth factor (IGF)/ IGF-1R system resulting in activation of the AKT survival signaling pathway, or by disruption of the FAS death signaling circuit.

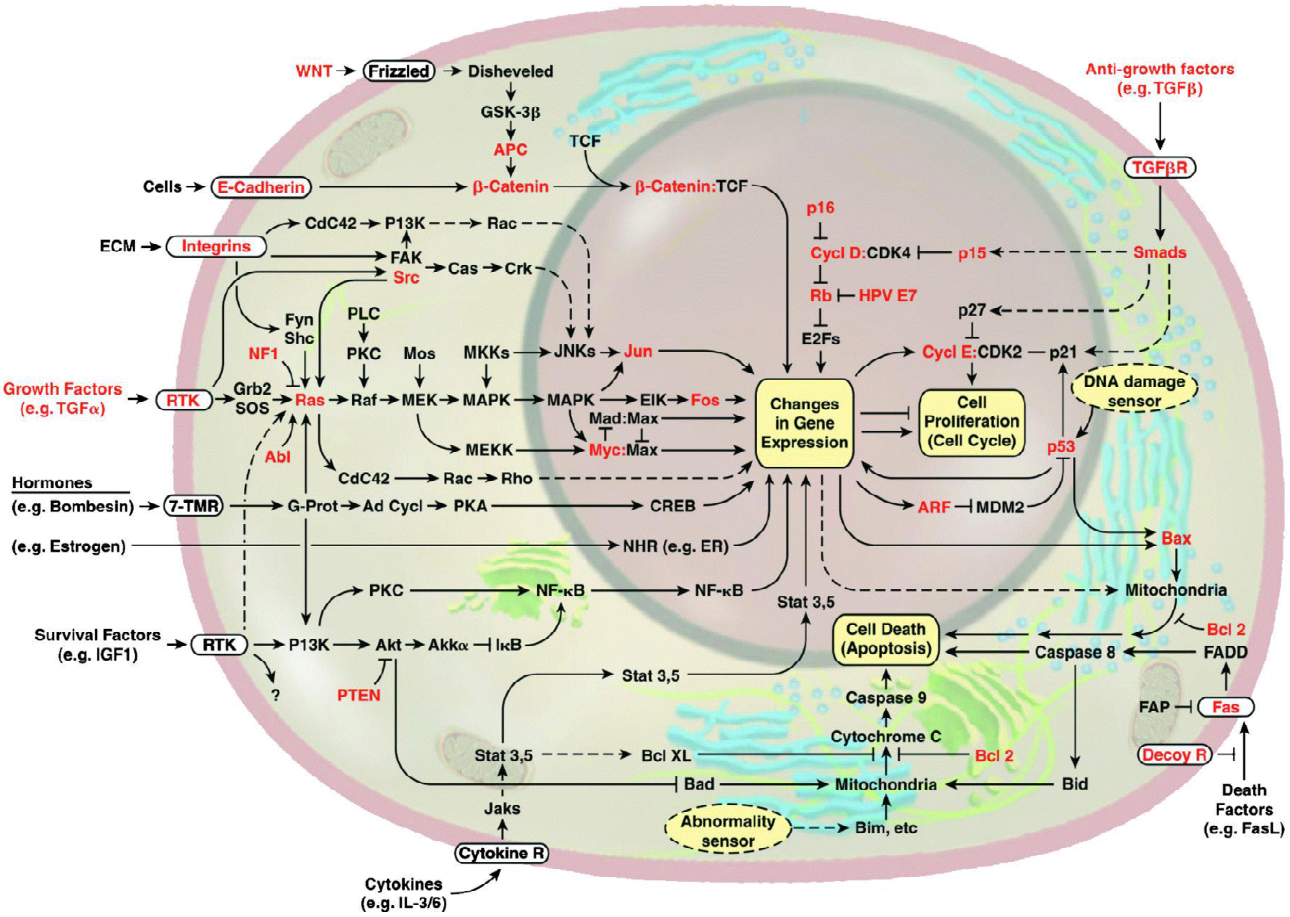

Figure 1. Main players of the integrated circuit of the cell and molecular players found to be mutated/ deregulated in cancers discussed in the previous paragraphs. (From (Hanahan and Weinberg, 2000))

Limitless replicative potential

Most mammalian cells carry an intrinsic, cell-autonomous program that limits their multiplication, working independently of the above-mentioned cell-to-cell signaling pathways. The cellular counting devices, the chromosomal ends called telomeres are shortened during each replicative division by 50-100 nucleotides. Cultured “normal” human cells have the capacity for 60 – 70 cell doublings, before the shortened chromosomal ends cause a karyotype disarray, resulting in a state called crisis, accompanied by massive apoptosis. An estimated 1 in 10^7 cells emerges during crisis and will acquire the ability to multiply without limit, called immortalization. Telomere maintenance is evident in most malignant cells and most of them so do so by up-regulating telomerase, the enzyme counteracting telomere shortening. However, from a numbers perspective, this doubling capacity would easily be sufficient to allow single tumor cell clones to grow to

macroscopic size. Clues to resolve this paradox come from animal studies and analysis of human tumors, in which it became evident that evolving pre-malignant and malignant cell populations have chronic and widespread apoptosis. Emerging tumors therefore result from a slight outbalancing of apoptosis by proliferation, and the numbers of cells constituting a tumor greatly under-represents the generations required to produce it. Hence, the generational limit of normal somatic cells arises as a barrier to cancer.

Sustained angiogenesis

Gain- and loss-of-function experiments indicate that neovascularization is a prerequisite to the formation of macroscopic tumors. Also, compelling evidence arose that lymphangiogenesis promotes tumor metastasis. For further details see “1.3.3. Tumor angiogenesis and lymphangiogenesis”.

Tissue invasion and metastasis

Sooner or later, most solid tumors leave the primary tumor site and seed to distant organs, a process called metastasis. Tissue invasion and metastasis are mechanistically closely related, and cellular changes observed in invading tumor cells are often mirrored by the metastasis. Several classes of proteins involved in the tethering of cells to their surroundings in a tissue are altered in cells possessing invasive or metastatic capabilities. These include cell-cell adhesion molecules (CAM) of the immunoglobulin superfamily and the calcium-dependant cadherins, as well as integrins, connecting cells with the extracellular matrix. Many tumors derived from epithelial tissues, called carcinomas, lose their principal cell-cell contact molecule E-Cadherin. This results in reduced cell-cell contact and liberation of β-catenin from the cell membrane, where it binds to the E-Cadherin intracellular domain. Stabilized cytoplasmatic β-catenin can, potentiated by Wnt and TGF-β signaling pathways, enter the nucleus and induce Tcf/Lef mediated transcription of pro-migratory and anti-adhesive genes. Apart from expression changes of molecules conferring adhesive properties to the cells, increased extracellular proteolytic activity is observed during cancer progression. This increased proteolytic activity might facilitate the invasion of cancer cells into nearby stroma, across blood vessel walls and through normal epithelial cell layers.

An additional level of complexity has come from the recent discovery of micro RNAs (miRNA), a class of non-protein coding RNA species. miRNAs regulate gene expression on a post-transcriptional level by modulating messenger RNA (mRNA) stability and translation efficiency through the formation of miRNA/ mRNA duplexes. As a single miRNA can target multiple mRNAs, the genetic loss of a single miRNA can have a tremendous influence on protein expression levels of many genes. For example, miR-34 miRNA family members have been show to be direct

transcriptional targets of p53. miR-34 activation can recapitulate elements of p53 activity, including induction of cell-cycle arrest and promotion of apoptosis, and loss of miR-34 can impair p53-mediated cell death (He et al., 2007).

1.2. Mouse models of cancer

Cancer is a disease that hits humans mainly in their post-reproductive period of life. To acquire all cellular traits required for carcinogenesis, many decades of life are necessary, time scales that are obviously un-suited for laboratory studies. However, also laboratory animals are prone to spontaneous carcinogenesis. Inbred rat strains show a higher incidence of cancer as compared to mice, e.g. rats can spontaneously develop prostate adenocarcinoma and endometrial tumors. Also in rodents, spontaneous cancer incidence correlates with age. With the availability of transgenic and gene-targeting strategies in mice, becoming standard laboratory techniques, it is feasible to alter the function of central cellular gatekeepers involved in protection of organism from neoplasia, the alteration resulting in hereditary and relatively homogenous tumor formation. Combinatorial crossing of genetically modified mice has generated a plethora of knowledge about genes modifying tumor development and is nowadays the most commonly used way to study cancer development in basic research.

In addition to genetically engineered mice, chemical and physical carcinogenesis protocols have also been established for mice and other animals, generally also producing relatively homogenous tumor types. Tumor transplantation has also been widely used to study tumor growth in mice. In this kind of tumor studies, primary or cell line-derived tumor cells are transferred into mice. This can either happen in a syngenic background, i.e. the tumor cell and recipient are genetically matched, or in mice with a restricted immune system allowing engraftment and growth of cells derived from a non-matched genetic origin, e.g. when human cancer cells are injected into immune-compromised mice. Topologically, tumor cells can be placed in the mouse at the location of their origin, e.g. pancreatic adenocarcinoma cells can be injected into the murine pancreas, called orthotopic transplantation. On the other hand, many studies are interested in the effects on primary growth of the tumor cells and the cells are therefore injected at sites accessible without surgery: subcutaneous, intraperitoneal or intravenous. Transplantation studies are convenient to study the role of cancer cell intrinsic factors because genetic manipulation of cell lines is much faster than of mice. However, the use of already transformed cells hampers their use in the investigation of initiating events in cancer and transplantation models also fail to faithfully mirror tumor-stroma interactions developing in transgenic mouse models of cancer.

1.2.1. Transgenic mouse models of cancer

Genetic mouse tumor models short-circuit the multi-hit concept described above, as they directly target central genes and proteins involved in preventing cancer. Conceptually, malignant transformation can be mediated and catalyzed by the over-expression of a proto-oncogene or by the knockout of a tumor suppressor gene. The first transgenic cancer models in mice have been established in the 1980ies, using simian virus 40 (SV40) derived T antigen oncoproteins, myc, ras and fos, whose expression was driven by tissue specific or viral promoters. This over-expression resulted in brain, mammary, bone, pancreatic acinar cell or endocrine tumors and, in the case of myc over-expressed in B lymphocytes, in lymphoma (Hanahan et al., 2007).

Mouse models for tumorigenesis have been established for the gastrointestinal tract, hematopoietic system, lung, liver, mammary gland, nervous system, ovary, prostate, skin and pancreas (http://emice.nci.nih.gov/emice/mouse_models). A common strategy is the tissue-specific expression of viral oncogenes, which are very potent by their inactivation of central tumor suppressors. For example, using transgenic and gene-targeting approaches, several prostate cancer mouse models have been established. Prostate specific expression of SV40 large and small antigen under either probasin or C3 promoter results in prostate intraepithelial neoplasia (PIN) as well as in invasive adenocarcinoma (Greenberg et al., 1995; Maroulakou et al., 1994). Over-expression of c-myc, IGF-I, androgen receptor or fibroblast growth factor 7, all of them implicated in human prostate carcinogenesis, under the control of prostate specific promoters also gave rise to low grade PIN but generally resulted in less aggressive tumor phenotypes. A central role of the PI3K/ Akt pathways was confirmed by the prostate-specific knockout of PTEN, which resulted in metastatic, invasive adenocarcinoma (Wang et al., 2003).

1.2.2. The Rip1Tag2 model of insulinoma

Using the strategies described above, the Rip1Tag2 transgenic mouse model of β-cell carcinogenesis was established more than 20 years ago. In these mice, the early region of SV40 encoding large T antigen (Tag) is expressed under the control of the rat insulin gene promoter (Rip), and thereby targeted to the insulin-producing β-cells of the endocrine pancreas (Hanahan, 1985). Tag displays direct transforming functions and disrupts cell cycle control by sequestering and inactivating the tumor suppressors p53 and pRb (Sachsenmeier and Pipas, 2001). Inactivation of these tumor suppressors results in malignant transformation and uncontrolled proliferation of β-cells triggering the sequential formation of insulinoma over a period of 12-14 weeks.

The murine pancreas contains approximately 400 islets of Langerhans, which together constitute the endocrine part of the organ. Islets consist of several types of hormone-producing cells, including α-, β-, δ- and PP-cells, with β-cells being the most abundant (80%). In Rip1Tag2

mice, β-cells start to express the transgene at embryonic day 8.5. Hyperplastic islets begin to appear at around 4 weeks of age, and although all islets express Tag, only about 50% of the islets become hyperplastic at 10 weeks. The onset of an angiogenic switch in a subset of hyperplastic islets triggers the formation of new blood vessels, resulting in the sequential emergence of angiogenic islets at 6 weeks and solid tumors at 9 to 10 weeks of age. At 12 to 14 weeks, 2-4% of all initial islets have progressed into well-encapsulated, non-invasive benign tumors (adenomas) and about 0.5% of islets into malignant, invasive carcinoma, the latter having the potential to metastasize. Importantly however, metastases are rarely found in Rip1Tag2 mice because the animals succumb already at 12-14 weeks of age due to hyperglycemia caused by the massive production of insulin by the tumors. The predictability and reproducibility of Rip1Tag2 tumorigenesis allows the study of distinct molecular events that may influence tumor growth and progression as well as tumor angiogenesis, lymphangiongenesis, metastasis and tumor-stroma interactions.

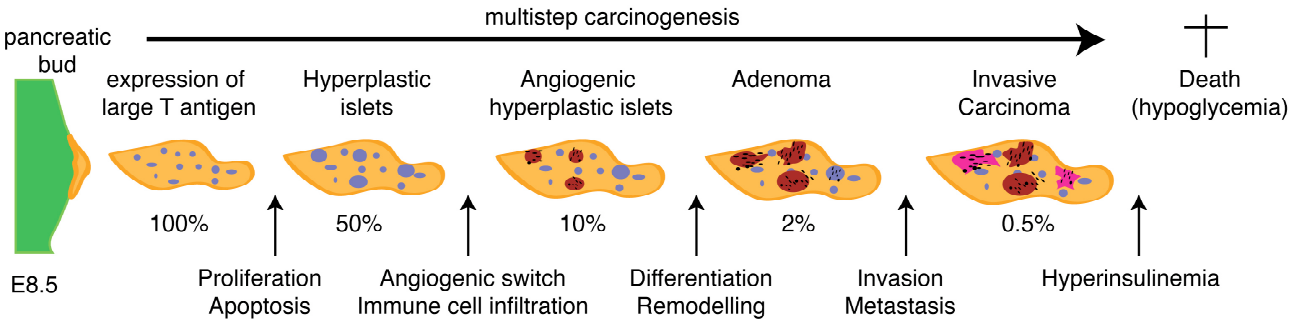

Figure 2. Multistep β-cell carcinogenesis in Rip1Tag2 transgenic mice. As indicated, islets (blue) sequentially progress into hyperplastic islets (enlarged, blue), angiogenic islets (red), benign adenoma (enlarged, red), and malignant carcinoma (magenta). From the time of the angiogenic switch, immune cell infiltration is prominent (black dots). Percentages indicate the subset of initial islets that have developed into a specific tumor grade at 12-14 weeks of age. The exocrine pancreatic tissue is drawn in brown, the foregut in green. E8.5, embryonic day 8.5. (Modified from (Christofori et al., 1995b))

1.3. Vasculogenesis, angiogenesis and lymphangiogenesis

1.3.1. Hematopoietic vs. endothelial fate specification

Developmentally, the endothelial lineage comprising blood and lymphatic vessels, and the hematopoietic system are likely to be closest relatives by their ontogeny, and, in the case of the extra-embryonic yolk sac (YS), are derived from a common precursor called the hemangioblast (reviewed in (Cumano and Godin, 2007; Lugus et al., 2005)). At embryonic day (E) 7.5, primitive blood cells are detected in the YS surrounded by cells that evolve to resemble endothelial cells morphologically. Cells isolated from this anatomical region were able to give rise to erythroid and myeloid compartment when transplanted into Rag-2$^{-/-}$;γc$^{-/-}$ mice (Cumano et al., 2001). However, only after a vascular connection between the YS and the inner embryo (embryo proper) was

established, cells isolated from the YS are also able to give rise to lymphoid cells upon transplantation. More recent data indicate that the main site of generation of definitive hematopoietic stem cells (HSC) is the para-aortic splanchnopleura (P-Sp)/aorta-gonad-mesonephros (AGM) region. Indeed, cells isolated from this region are able to provide long-term multi-lineage reconstitution even before the establishment of embryonic circulation when transplanted into Rag-$2^{-/-}$;$\gamma c^{-/-}$ mice (Cumano et al., 2001). HSC appear in two defined locations around the dorsal aorta between E9 and E12, in hematopoietic intra-aortic clusters (HIAC) inserted inside the ventral wall of the dorsal aorta or in subaortic patches (SAP). Independent of their origin, either YS or P-Sp/AGM region, HSC generated *in situ* will then populate the fetal liver, the main site of embryonic hematopoiesis.

The notion that multi-lineage repopulating competent cells isolated from the P-Sp/AGM region expressed the endothelial marker CD31, VE-Cadherin, Tie2 and CD34 prompted investigators to propose an close ontogenic relationship between hematopoietic and endothelial lineage, in the YS as well as in the AGM region. However, experiments in which genetically labeled epiblast fragments were orthotopically grafted into normal embryos and then allowed to develop *in vitro* for a few days showed that simultaneous contribution to endothelial and hematopoietic cells constitutes a rare event in the YS (Kinder et al., 1999), suggesting a polyclonal origin of the lineages. In the embryo proper, the occurrence of vasculature precedes hematopoietic cell production. Whereas this renders the existence of a common, bipotent hemangioblastic precursor unlikely, the close association of HSC with the dorsal aorta occurring in the embryo proper established the concept of hemogenic endothelium (de Bruijn et al., 2002). According to this concept, endothelial cells are able to give rise to intra-embryonic HSC through a transient trans-differentiation process.

Knockout and *in vivo* tracing studies using Cre/Lox technology and *in vitro* differentiation assays, using embryonic bodies, assigned an outstanding role for fetal liver kinase-1 (Flk-1/ VEGFR2) and the transcription factor Scl in the generation of cells with endothelial and hematopoietic potential from mesoderm (Figure 3). Lineage tracing experiments using Flk-$1^{+/Cre}$;Rosa26R-LacZ mice demonstrated that not only endothelial and hematopoietic but also cardiac and skeletal muscle as well as smooth muscle cells originate from a Flk-1 expressing precursor cell (Motoike et al., 2003). Knockout of Scl blocked the ability of ES cells to differentiate into endothelial and hematopoietic cells; rather these cells became smooth muscle cells (Yamashita et al., 2000). A recent report, utilizing either Flk-$1^{+/Cre}$;Rosa26R-EYFP or Flk-$1^{+/Cre}$;Rosa26R-LacZ mice, demonstrated that all blood cells within the yolk sac and aorta were of Flk-1^{+} origin. Additionally, nearly all $CD45^{+}$ cells in bone marrow and circulating blood in adults were of Flk-1^{+} origin, further substantiating that all blood cells, primitive and definitive, in mice are derived from Flk-1^{+} mesodermal cells (Lugus et al., 2008).

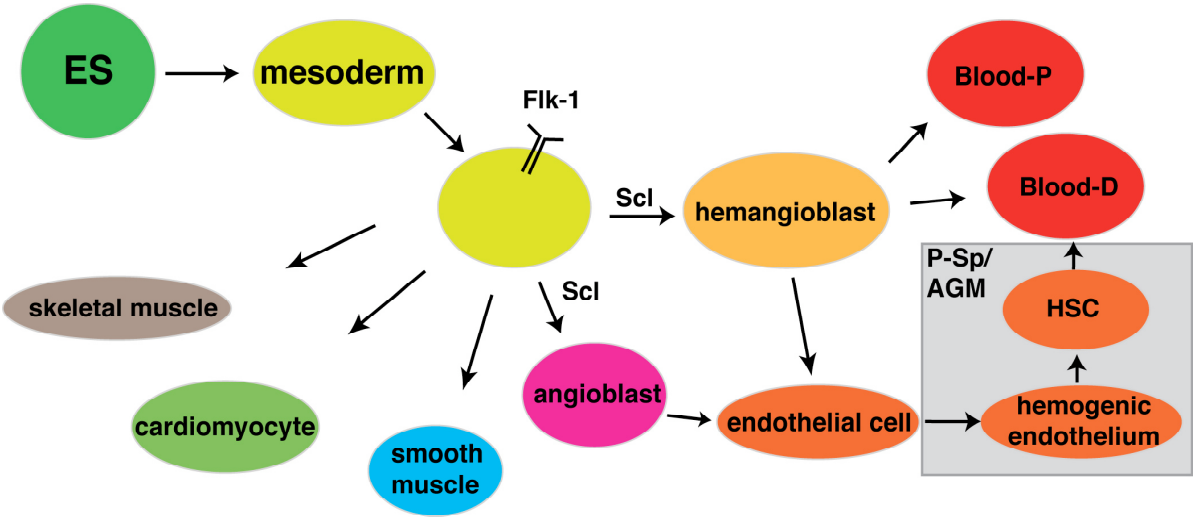

Figure 3. Embryonic ontogeny of endothelial and hematopoietic lineages. Flk-1 expressing mesoderm establishes the circulatory system. Flk-1 is expressed in mesoderm very early during development and Flk-1$^{-/-}$ embryos are unable to form blood islands and to generate hemopoietic precursors. Lineage tracing studies showed that Flk-1 is also expressed on progenitor cells of smooth muscle cells, skeletal muscle cells and cardiomyocytes. Whether there is a multi-potent common precursor (as suggested here) is unknown at present. Expression of the transcription factor Scl (also known as Tal1) is indispensable for the generation of endothelial and hematopoietic lineages. In the P-Sp/AGM region of the embryo proper, HSC are derived from hemogenic endothelium. ES: embryonic stem cell, HSC: hematopoietic stem cell, Blood-P: primitive blood (comprising erythroid and myeloid lineages), Blood-D: definitive blood (comprising all lineages). P-Sp/AGM: para-aortic splanchnopleura/aorta-gonad-mesonephros. (Modified from (Lugus et al., 2005))

1.3.2. Lymphatic vessel development

The cardiovascular system is the first organ that develops during embryogenesis. During the process called vasculogenesis, the *de novo* forming angioblasts aggregate in the embryo and YS into a primitive network of endothelial tubes, called the primary vascular plexus (Risau and Flamme, 1995). Induction by fibroblast growth factors (FGF) of mesoderm during gastrulation leads to the generation of angioblasts and hematopoietic cells. Vascular endothelial growth factor (VEGF) and its high-affinity receptor tyrosine kinase Flk-1 represent a paracrine signaling system crucial for the differentiation of endothelial cells and the development of the vascular system. Specific cell adhesion molecules such as VE-Cadherin and CD31, and transcription factors such as Ets-1, as well as mechanical forces and vascular regression and remodeling are involved in the subsequent events of endothelial cell differentiation, apoptosis, and angiogenesis.

The lymphatic system however, develops only after appearance of blood vasculature, which was the first indication that lymphatics might have a blood vasculature origin (reviewed in (Oliver, 2004)). The lymphatic system is composed of a vascular network of blind-ended, thin-walled capillaries and larger vessels that drain protein-rich interstitial fluid (lymph) from the extracellular spaces within organs into larger collecting ducts. In contrast to blood capillaries, lymphatic capillaries lack fenestrations, a continuous basal membrane and pericytes; instead, these vessels are lined with a continuous, single layer of overlapping endothelial cells that form loose intercellular

junctions. These characteristics make the lymphatic capillaries highly permeable to large macromolecules, pathogens and migrating cells.

Nowadays, most experimental data support the hypothesis proposed by Florence Sabin in 1902 that lymphatic endothelial cells arise by sprouting from embryonic veins (Oliver, 2004; Sabin, 1902). According to this model (Figure 4), cells within the venous compartment of the blood vasculature become competent to respond to induction signals towards the lymphatic lineage at embryonic day 9.5, morphologically indicated by the expression of LYVE-1 by a few endothelial cells lining the anterior cardinal vein of mice. Neither are the signals known that induce this competence nor is LYVE-1, a hyaluronan receptor and lymphatic specific marker, required for the lymphatic competence (Gale et al., 2007).

Following this initial step, polarized expression of the homeobox protein Prox-1 is detected in the anterior cardinal vein in a subpopulation of “competent” LYVE-1-expressing venous endothelial cells. As development progresses, the number of Prox-1 expressing cells increases and is also detected in more caudally located veins. After the initial phase of Prox-1 expression in the veins, Prox-1-expressing lymphatic endothelial cells (LEC) progenitors migrate from the veins and form the primitive lymph sacs, scattered along the anteroposterior axis (Wigle and Oliver, 1999). In parallel, VEGFR3 becomes expressed and activated by its cognate ligand VEGF-C, uniformly produced by the mesenchyme surrounding the cardinal veins. Even though uniformly expressed, VEGF-C and its receptor constitute at least one of the mechanisms required for the polarized budding of Prox-1 expressing LEC, as evidenced by the inability of Prox-1^{+} LEC progenitor to leave the embryonic veins in VEGF-C deficient mice (Karkkainen et al., 2004). At around E14.5, the lymphatic vasculature has spread throughout the developing embryo by budding and sprouting from the primary lymph sacs, and the immature LEC are in the process of terminal differentiation.

Late embryonic and postnatal remodeling of the lymphatic vasculature includes sprouting of lymphatic capillaries from the primary lymphatic plexus, whereas bigger lymphatic vessels recruit smooth muscle cells and develop lymphatic valves, thereby acquiring a collecting vessel phenotype. These processes critically depend on Neuropilin-2, Angiopoeitin-1 & -2/ Tie2 as well as ephrinB2 signaling pathways (Gale et al., 2002; Yuan et al., 2002) and lead to the expression of the full panel of lymphatic specific markers, as indicated in Figure 4.

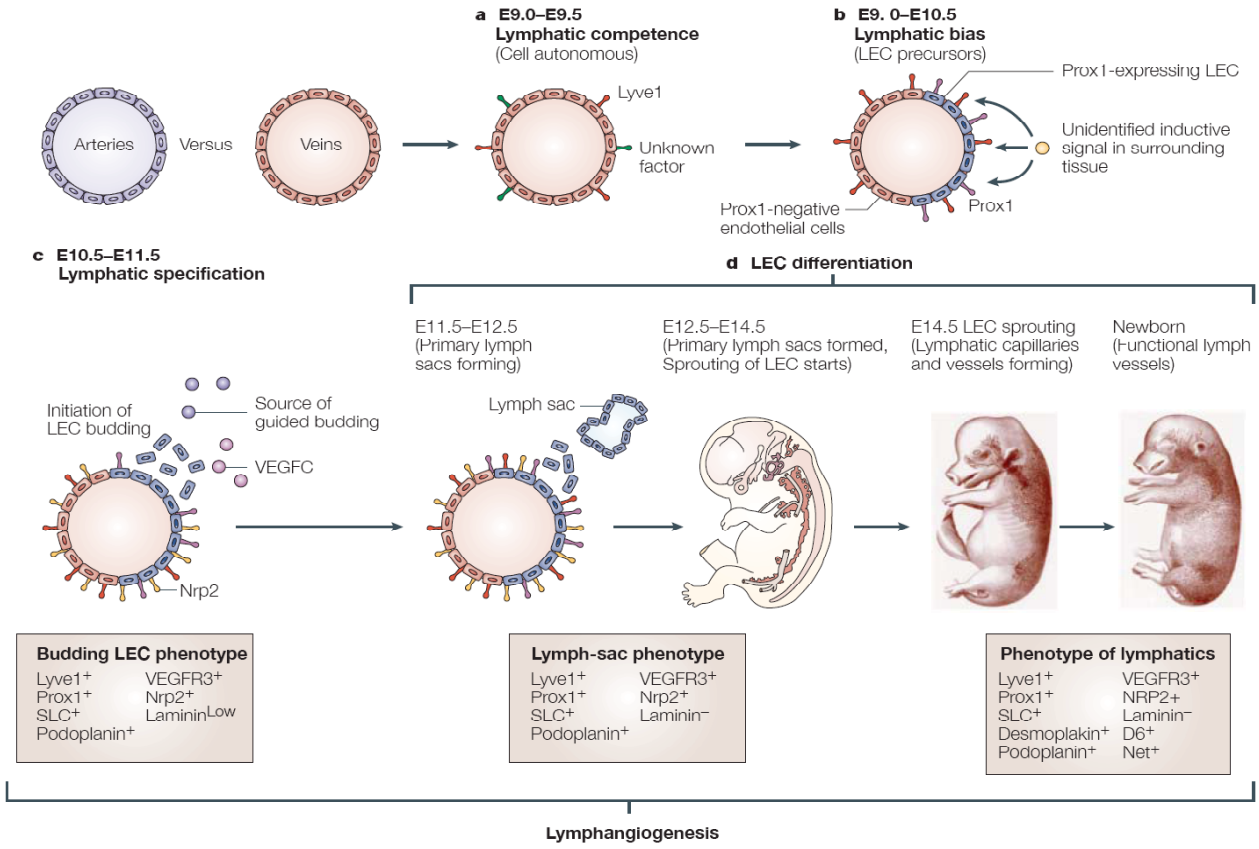

Figure 4. Model for generation of the lymphatic vasculature from venous endothelium. See text for details. (Taken from (Oliver, 2004))

In addition to a strict origin of LEC from venous vasculature, the existence of mesenchymal lymphangioblasts was proposed by studies on avian embryos and Xenopus tadpoles (Ny et al., 2005; Schneider et al., 1999). Similar observations were made very recently in mouse, where proliferating cells co-expressing lymphatic and monocytic markers (Prox-1^{+}/ LYVE-1^{+}/ F4/80^{+}) located in the mesoderm, immediately adjacent to, and within lymph vessels were detected (Buttler et al., 2008). If these cells are derived from lymphangioblasts, by chance phenocopy a mixed lymphatic/ hematopoietic marker profile or rather represent a lymphatic differentiation of monocytic cells (or *vice versa*) cannot be decided at this point. However, our experimental data (see “4.2. Myeloid cells contribute to tumor lymphangiogenesis”) indicate that at least in the adult, there is a trans-differentiation potential of monocytic cells to the lymphatic lineage under inflammatory conditions.

1.3.3. Tumor angiogenesis and lymphangiogenesis

Tumor angiogenesis and its molecular regulation

In normal tissues, oxygen and nutrients are only efficiently delivered to cells residing within a 200μm diameter around a blood capillary. To ensure this proximity, growth of parenchyma and expansion of the vasculature are carefully coordinated. Once a tissue is formed, the growth of new blood vessels, angiogenesis, only occurs transitory and under tight molecular control. For example, during wound healing in the skin, dermal endothelial cells first have to be activated in order to expand and then reestablish blood vasculature function in the wound area. This happens via a coordinated local action of immune cells, coagulation factors, and activation of matrix components - all initially triggered by physical stress like oxygen and nutrient deprivation as well as loss of matrix integrity. After the tissue components were successfully repaired, the vasculature will re-enter quiescence and a pre-wound immune cell status will be reestablished.

The quiescence phenotype of the vasculature in adults is mediated by the balance of pro- and anti-angiogenic factors within a given tissue (Figure 5). Over time it had become clear, that organs as well as tumors produce pro- and antiangiogenic factors, and only upon dominance of the pro-angiogenic factors, angiogenesis will take place. The existence of a “tumor angiogenesis factor (TAF)” was proposed by Judah Folkman in 1971 (Folkman et al., 1971), but it took more than ten years to isolate basic fibroblast growth factor (bFGF) and vascular endothelial growth factor A (VEGF-A) and to assign a clear pro-angiogenic role to them (Klagsbrun et al., 1986; Leung et al., 1989; Senger et al., 1983).

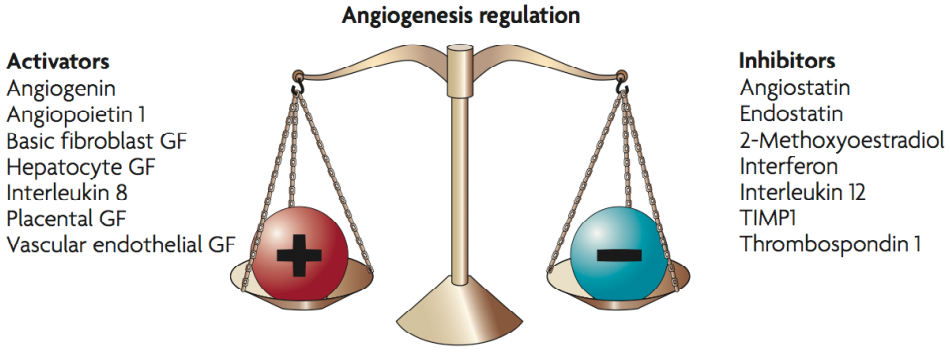

Figure 5. Abundance of pro- and antiangiogenic factors defines vascular quiescence, regression or angiogenic expansion. (From (Zetter, 2008))

Multiple studies have established VEGF-A as a key angiogenic player in cancer (reviewed in (Dvorak, 2002)). It is expressed by most tumors and its expression correlates with tumor microvessel density and tumor proliferative status, and exerts its function via activation of VEGF receptor 2 (VEGFR2) and, eventually, VEGFR1 on endothelial cells. Also tumor and immune cells

have been shown to express VEGF receptors to varying degrees, however the significance of these potentially stimulatory signaling circuits is poorly understood. VEGF-A action on endothelial cells has mitogenic as well as chemotactic effects. One of the earliest factors implicated in angiogenesis that is detected in tumor initiating nodules is Angiopoietin-2 (Ang-2) (Holash et al., 1999). Ang-2 is a ligand for the receptor tyrosine kinase Tie2, and at least in some settings, Ang-2 acts antagonistically on Tie2, a function implicated in destabilizing the endothelium and rendering it susceptible to VEGF-A stimulus (Figure 6) (Yancopoulos et al., 2000). Ang-2 stimulation without concomitant VEGFR2 stimulation rather leads to blood vessel regression. Ang-1, another Tie-2 ligand, is involved in stabilizing blood vessels, as evidenced by larger vessel size and reduced vascular permeability in mice over-expressing Ang-1 in the skin (Thurston et al., 1999).

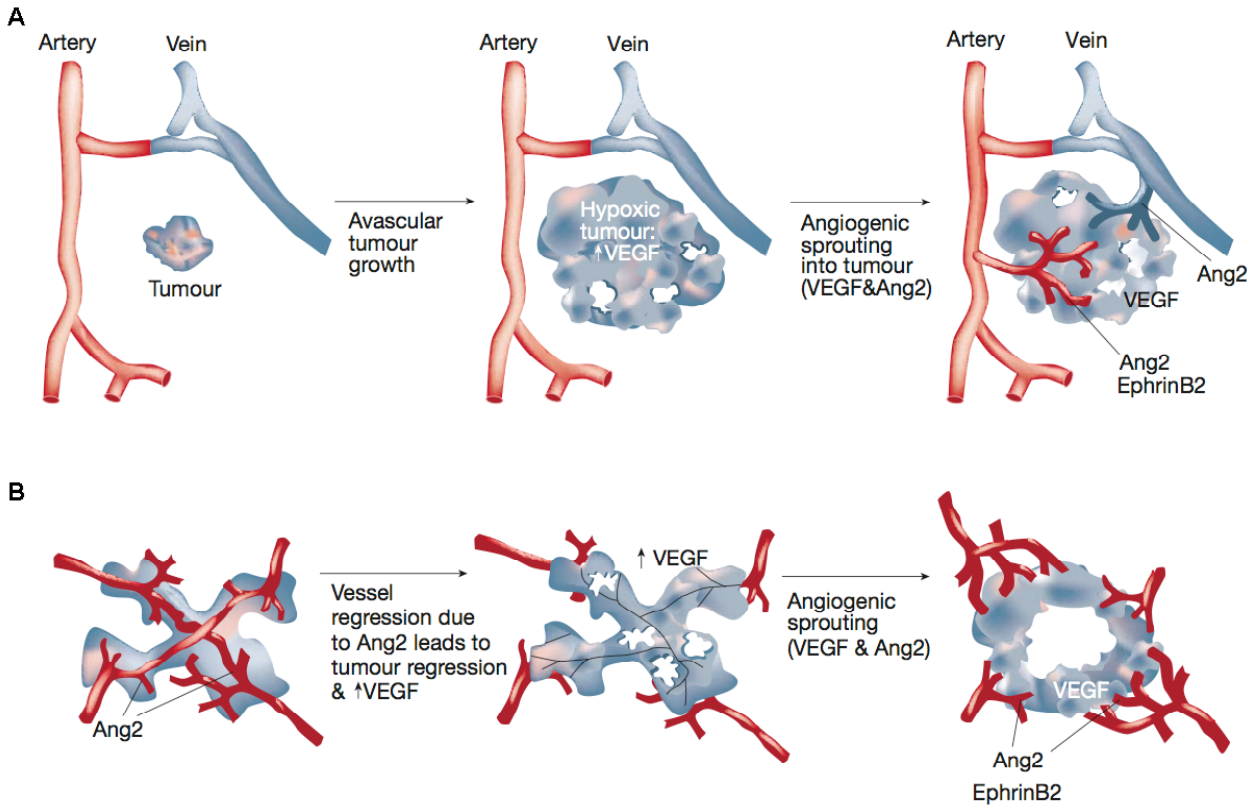

Figure 6. Interplay of VEGF and Angiopoietin system in tumor angiogenesis. (**A**) Tumor initially grows avascular and upon hypoxia VEGF-A is induced and host vessels destabilized/ activated by Ang-2 expression. (**B**) Tumor initiation with concomitant co-option of host vessels, expressing Ang-2, results in temporary vessel and tumor regression, only secondary to which tumoral VEGF expression and angiogenic sprouting are induced. (Taken from (Yancopoulos et al., 2000))

The molecular proof of the necessity for tumor angiogenesis came with mouse models in which angiogenesis and subsequent tumor growth was impaired upon blockade of the VEGF axis by anti-VEGF antibody or dominant negative VEGFR2 in xeno-transplantation studies (Kim et al., 1993; Millauer et al., 1994). Similarly, treating transgenic tumor mice with anti-angiogenic

compounds also proved to be effective in limiting angiogenesis and reducing tumor growth (Bergers et al., 1999; Sacco et al., 2001)

Expression of VEGF can be induced by multiple cellular pathways: Hypoxia leads to stabilization of hypoxia inducible factor 1α (HIF1α) that in turn induces VEGF-A expression via HIF-responsible elements in the VEGF-A promoter; a different pathway of VEGF induction is mediated by pro-inflammatory cytokines such as TNF-α and TGF-β2. Recently, the transcriptional co-activator PGC-1α was shown to induce VEGF-A independent of the HIF pathway; PGC-1α is a potent metabolic sensor and regulator of mitochondrial function, but its significance for tumor angiogenesis is currently not clear (Arany et al., 2008).

A series of publications have recently revealed a mechanism that prevents overshooting of sprout formation during angiogenesis via the delta-like ligand 4 (Dll4) – Notch1 pathway (reviewed in (Thurston et al., 2007)). Even though tumors elicit a kind of aberrant angiogenesis, resulting in leaky vessels and intra-tumoral hemorrhage, the Dll4-Notch1 pathway, already essential during vasculature development in the embryo, is tightly controlled in tumor blood vessels to allow productive angiogenesis. Blockade of Dll4 inhibited tumor growth by promoting non-productive angiogenesis. Mechanistically it was found that Dll4 is induced by VEGF-A as a negative regulator of angiogenic sprouting.

Judah Folkman stated in 1971 "...antiangiogenesis therapy, perhaps by immunization against TAF, should provide a powerful adjunct to the control of solid neoplasms". The prediction was that control of vascularity within a tumor would facilitate control of the tumor. If, in fact, one substitutes VEGF for TAF, then it is clear that Folkman anticipated the clinical use of anti-angiogenic antibodies such as bevacizumab (Avastin) decades before they were available in the clinic. Aspects of clinical interference with tumor angiogenesis are further discussed in section “1.4.4. Perspectives for therapy”.

Tumor lymphangiogenesis and its molecular regulation

The metastatic spread of tumor cells is the most lethal aspect of cancer and often occurs via the lymphatic vasculature (reviewed in (Achen and Stacker, 2008; Das and Skobe, 2008)). Cancer cells may also spread via blood vessels or seed directly to body cavities. Experimental tumor models as well as human clinicopathologic data indicate that growth of lymphatic vessels – lymphangiogenesis – in or around solid tumors is often associated with lymph node metastasis. Correlation studies in humans indicate a clear positive correlation between tumor-associated lymphangiogenesis and lymph node metastasis in cutaneous melanoma, inflammatory breast cancer, non-small cell lung cancer and bladder carcinoma as well as in head & neck cancer. The location of the lymphatic vessel might be crucial as animal experiments revealed most *intra-*

tumoral lymphatics to be non-functional and therefore rather suggest peri-tumoral lymphatics to be the entry points for tumor cells into the vascular bed (Padera et al., 2002).

The most specific lymphangiogenic growth factors promoting formation of (tumor) lymphatics that have been identified are the secreted glycoproteins vascular endothelial growth factors C (VEGF-C) and VEGF-D (Jeltsch et al., 1997; Stacker et al., 2001). Both ligands bind their cognate receptor VEGFR3, which is mainly expressed in lymphatic vasculature in adults, but might be re-expressed on blood endothelial cells during tumor angiogenesis (Tammela et al., 2008). VEGF-C and -D are proteolytically processed and in fully processed form, they also bind and activate VEGFR2, which is expressed on blood and lymphatic endothelial cells. These findings implicate that over-lapping ligand/ receptor signaling between VEGFR2/ VEGF-A and VEGFR3/ VEGF-C & -D is reactivated in tumors similar to the situation during development, stimulating both blood and lymphatic endothelial cells.

Tumoral expression of VEGF-C emerges as a reliable marker for ongoing tumor lymphangiogenesis and increased risk of regional lymph node metastasis in many carcinomas. Data for VEGF-D are less consistent, suggesting that its ability to promote metastatic spread via lymphatics depends on the investigated tumor type and/ or grade. Expression of VEGF-C is stimulated by the inflammatory mediators interleukin-1β, tumor necrosis factor-α, COX-2 and its induced prostaglandins (Ristimaki et al., 1998; Su et al., 2004). Induction of VEGF-C mediated lymphangiogenesis could counteract inflammation-induced edema, a situation often occurring in cancer due to high immune cell infiltration.

Experimental mouse models have clearly shown a firm link between expression of VEGF-C/ or –D in cancerous tissue and tumor associated lymphangiogenesis and metastasis in experimental insulinoma and in xeno-transplantation studies (Mandriota et al., 2001; Skobe et al., 2001; Stacker et al., 2001).

Increasing evidence suggests that lymph node lymphangiogenesis can precede and facilitate lymph node metastasis. This was observed in a chemically induced skin cancer model, where either transgenically expressed VEGF-A or VEGF-C could induce tumor and draining lymph node lymphangiogenesis (Hirakawa et al., 2006; Hirakawa et al., 2005). Amazingly, the expansion of lymph node lymphatic vasculature seemed to significantly promote distant metastases. In human melanoma, multivariate analysis revealed that tumor lymphangiogenesis was the most significant independent prognostic indicator for the presence of sentinel lymph node metastasis (Dadras et al., 2005). In retrospective studies, increased melanoma-associated lymphangiogenesis was found to be inversely correlated with disease-free and overall survival of melanoma patients (Dadras et al., 2003).

The identification of a link between tumoral expression of lymphangiogenic factors, associated lymphangiogenesis and the correlation of these events with metastatic events

suggested that interference with this system might prevent metastasis. Indeed, studies aiming at interfering with VEGFR3 signaling by sequestering the ligands VEGF-C and –D using soluble VEGFR3 traps or by neutralizing the receptor with anti-VEGFR3 antibodies successfully reduced lymph-angiogenesis and lymph node metastases in murine models of breast, prostate, mammary cancer and in malignant melanoma (Lin et al., 2005; Roberts et al., 2006). Interestingly, the re-expression of VEGFR3 on angiogenic tumor blood endothelial cells also allowed blockade of tumor angiogenesis via interference with the VEGFR3 axis (Tammela et al., 2008).

Over the last few years, many more signaling pathways stimulating lymphangiogenesis in certain systems have been identified, including hepatocyte growth factor/ c-Met (Kajiya et al., 2005), FGF-2 (Chang et al., 2004), platelet-derived growth factors (Cao et al., 2004) and insulin like growth factors (IGF) (Bjorndahl et al., 2005). These receptor/ ligand pairs do not exclusively act on lymphatic endothelial cells but also on other cells; additionally, some of the actions observed might be due to indirect effects on the VEGF-C/-D VEGFR3 axis. For example, it was shown that IGF-1R stimulates the expression of VEGF-C in Lewis lung carcinoma cells (Tang et al., 2003).

Very recently, the adrenomedullin/RAMP2/Calcrl signaling pathway has been demonstrated to be important for the development of balanced blood and lymphatic endothelial systems. Two groups have shown by knockout studies that loss of this signaling pathway results in tissue edema and embryonic death due to increased blood vasculature permeability and reduced lymphatic uptake of interstitial fluid (Fritz-Six et al., 2008; Ichikawa-Shindo et al., 2008).

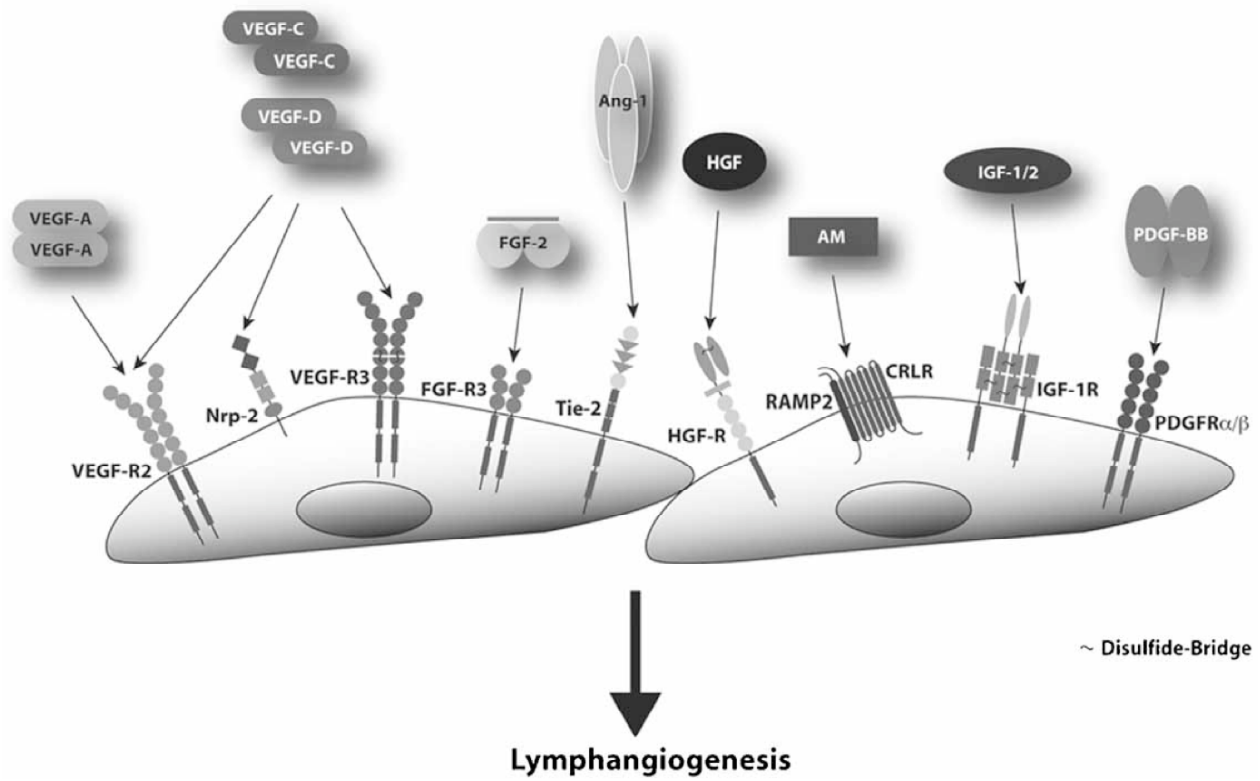

Figure 7. Signaling pathways involved in lymphangiogenesis. Whereas the VEGF-C/ -D and VEGFR3 system specifically promotes lymphangiogenesis, the other signaling pathways depicted here are also employed by blood endothelial cells and/ or other cell types. (From (Rinderknecht and Detmar, 2008))

1.4. Interactions tumor – immune system

Zumsteg and Christofori: "**Corrupt policemen: inflammatory cells promote tumor angiogenesis**" *Current Opinion in Oncology 2009, 21:60–70*

Purpose of the review

The last decade has seen a paradigm change in that tumor stroma contributes to malignant tumor progression in a manner comparable to genetic and epigenetic changes within cancer cells. This review summarizes recent novel insights into how inflammatory conditions stimulate the formation and expansion of blood and lymphatic vessels within tumors and, thus, allow tumors to grow, to gain invasive capabilities, and to finally seed metastasis in distant organs.

Recent findings

Different cancer types have a highly defined microenvironment, which is composed of cancer-associated fibroblasts, blood vessel and lymphatic endothelial cells, pericytes, and a heterogeneous infiltrate of cells of the immune system. In addition to the local stimulation of tumor angiogenesis and tumor lymphangiogenesis, cytokines released by the primary tumor and by the immune cell infiltrate also instruct bone marrow-derived cells to colonize distant organs and to prepare these sites for future metastasis.

Summary

Inflammatory reactions coinciding with carcinogenesis can be visualized by the presence of specific bone marrow-derived, inflammatory cells in patients' peripheral blood. Recent findings suggest that such inflammatory fingerprints may better define the inflammatory nature of the primary malignancy and, thus, allow the design of therapeutic strategies targeting the pro-tumorigenic immune cell stroma compartment.

1.4.1. Introduction

The notion that angiogenesis is critical for supplying tumors with sufficient oxygen and nutrients to grow beyond a certain size is well established. However, only recently it has been appreciated that activation, expansion and maintenance of the tumor vascular system extends beyond the function of angiogenic factors released by hypoxic tumor cells. A tumor is usually composed of many different cell types, and this composition is spatially and temporally highly dynamic and, thus, the causal link between a specific modulating factor and tumor progression has been rather speculative than direct. In the past few years, transgenic mouse models of cancer have served a critical role in unraveling the complex interplay between tumor cells, infiltrating

leukocytes, cancer-associated fibroblasts (CAF), and the tumor blood and lymphatic vasculature. Major attention has been paid to the contribution of cells of the immune system to tumor progression, mainly by employing bone marrow transplantations and the use of genetically modified mice. These experiments have revealed that most immune cell lineages exert anti- as well as pro-tumorigenic functions and that established tumors often skew immune cells into a pro-angiogenic and immunosuppressive state (Figure 8). The use of inducible genetic or pharmacological ablation strategies may set the stage for future, even more relevant animal studies.

1.4.2. Immune cells as critical drivers of tumor angiogenesis

The critical functions of CAF and pericytes in angiogenesis, extracellular matrix remodeling and metastasis have been recently reviewed (Gerhardt and Semb, 2008; Kalluri and Zeisberg, 2006). Here, we focus on the role of the immune system in tumor progression, with the innate immune system playing a more prominent role than the adaptive immune system in most experimental settings. The majority of recent studies discussed in this review are summarized in Table 1.

1.4.2.1. Myelomonocytic cells and tumor associated macrophages (TAM)

Tissue macrophages, derived from the peripheral blood monocytic branch of myeloid cells, have been found to be present in virtually all solid tumors. High TAM content in human epithelial tumors usually links to poor prognosis with few exceptions (Bingle et al., 2002). TAMs are, alongside with myeloid-derived suppressor cells (MDSC, see below), mobilized from the bone marrow and recruited to the tumor site upon specific tumor-derived stimuli, such as vascular endothelial growth factor (VEGF), placental growth factor (PlGF), CC-chemokine ligand 2 (CCL2), granulocyte macrophage colony-stimulating factor (GM-CSF), interleukin-3 (IL3), macrophage CSF (M-CSF), IL6 or soluble Kit ligand (sKitL). In a tumor microenvironment, macrophages can be polarized to a M1 (classically activated) state, eliciting Th1 adaptive immune cell reactions, host defense and tissue destruction, mainly by secretion of high levels of IL1β, tumor necrosis factor-α (TNFα), and IL6 and the production of reactive nitrogen and oxygen intermediates. Alternatively, macrophages can be polarized to a M2 state, suppressing Th1 adaptive immunity and promoting wound healing, angiogenesis and tissue remodeling (Allavena et al., 2008). TAM are rather M2 polarized and confer immunotolerance to a tumor environment. Macrophages themselves have been shown to produce various pro-angiogenic factors, including VEGF, TNFα, IL8, and fibroblast growth factor-2 (FGF2). Moreover, TAM secrete proteases for the liberation of matrix sequestered

growth factors and for the degradation of extracellular matrix and basement membrane, thus promoting sprouting and expansion of the vasculature and invasive motility of tumor cells.

TAM have been shown to promote tumor angiogenesis mainly by secretion of matrix metalloproteinase 9 (MMP9) which activates matrix-sequestered latent forms of VEGF-A. In the HPV16/E2 transgenic mouse model of cervical carcinogenesis, tumor-infiltrating macrophages provide the majority of MMP9 required for the onset of angiogenesis (Giraudo et al., 2004). Yet, the targeted reduction of intratumoral macrophage levels in CC chemokine receptor-2 (CCR2)-deficient mice is compensated for by the infiltration of MMP9-expressing neutrophils (Pahler et al., 2008). In a syngeneic mouse model of glioblastoma, hypoxia inducible factor 1-α (HIF1α) is critical for the induction of VEGF expression in tumor cells and the concomitant recruitment of MMP9-expressing myelomonocytic cells from the bone marrow (Du et al., 2008). Thereby, the local expression of the cytokine stromal derived factor-1 (SDF1 = CXCL12) contributes to the recruitment and positioning of bone marrow-derived cells in the glioblastoma model. CXCR4, the cognate receptor of CXCL12 is expressed on the majority of $CD45^+$ myelomonocytic cells that are mobilized from the bone marrow. Myeloid cells and their secretion of MMP9 also play an important role in the growth of tumors in pre-irradiated stroma, particularly in supporting vasculogenesis, i.e. the formation of blood vessels by circulating endothelial precursor cells (Ahn and Brown, 2008). Importantly, in all these models, MMP9 is not exclusively provided by myelomonocytic cells, but also by other tumor-infiltrating cells, tumor cells themselves, pericytes or fibroblasts, suggesting that myelomonocytic cells as the major source of MMP9 can be replaced by other cell types to promote tumor angiogenesis and growth. Hence, from a clinical perspective, targeting stroma-derived enzymes might be superior to targeting cell types.

The critical function of TAM has also been documented in the MMTV-PyMT transgenic mouse model of breast cancer. Crossing PyMT breast cancer mice with macrophage-deficient $CSF1^{op/op}$ mice suppressed tumor angiogenesis, tumor progression and lung metastasis, while primary tumor growth remained largely unaffected (Lin et al., 2006; Lin et al., 2001). Transgenic expression of VEGF-A in tumor cells of composite $CSF1^{op/op}$;MMTV-PyMT mice restored the angiogenic switch and tumor progression, indicating that the bioavailability of VEGF-A was a critical factor for tumor progression and suggesting that VEGF-A was produced by TAM (Lin et al., 2007). Similarly, ablating TAM using liposome-encapsulated clodronate significantly reduced tumor angiogenesis and growth of *subcutaneously* transplanted cancer cells in mice (Zeisberger et al., 2006). Moreover, antibody-mediated inhibition of $\alpha_4\beta_1$ integrin in the syngeneic murine Lewis Lung Carcinoma (LLC) model lead to decreased myeloid cell recruitment and resulted in impaired angiogenesis and tumor growth (Jin et al., 2006).

Monocytes called TEM, for *T*ie2-*E*xpressing *M*onocytes, constitute a minor proportion of tumor-infiltrating myeloid $CD11b^+$ cells, yet they seem to be a crucial pro-angiogenic driving force:

firstly, co-injection of tumor cells with tumor-derived TEM but not with $Tie2^-/CD11b^+$ myeloid cells stimulated angiogenesis in growing tumors. Secondly, specific ablation of Tie2-expressing bone marrow cells resulted in markedly impaired tumor angiogenesis (De Palma et al., 2005). $Tie2^+$ monocytes have also been found in human blood; these cells respond *in vitro* to hypoxia and angiopoietin-2, a pro-angiogenic ligand for Tie2, by the upregulated expression of Tie2 and CXCR4 and the down-regulation of TNFα and IL12 (Murdoch et al., 2007). This observation supports the concept of tumors skewing macrophages into a pro-angiogenic, M2-polarized phenotype. Notably, the upregulation of Tie2 on tumor-infiltrating monocytes relative to blood monocytes has also been observed in human cancer patients (Venneri et al., 2007).

VEGFR1, a receptor for VEGF-A and PlGF, is expressed on a subset of mobilized myeloid cells, found in blood and tumors of tumor-bearing mice and cancer patients (Kusmartsev et al., 2008). The abundance of $VEGFR1^+$ cells correlates with tumor size in mice, and they are found at high levels in patients with renal cell carcinoma, a cancer with particularly high levels of circulating VEGF-A, suggesting a stimulating effect of systemic VEGF-A on VEGFR1-mediated bone marrow myelopoiesis. VEGFR1 cells have also been shown to colonize and prepare the “premetastatic niche” in lungs prior to the appearance of metastatic tumors cells (Kaplan et al., 2005). Presumably, VEGF-A, TNFα, and transforming growth factor-β (TGFβ) released by tumor cells induce the expression of the myeloid cell attractant proteins S100A8 and S100A9 in lung endothelial cells (Hiratsuka et al., 2006).

Myeloid cells can also stimulate angiogenesis in a non-tumorigenic environment with high expression of VEGF-A. Notably, myeloid cells from organs, to which they were recruited by organ-specific over-expression of VEGF-A, were even more potent than recombinant VEGF-A in inducing endothelial sprouting (Grunewald et al., 2006). The critical role of VEGFR1 tyrosine kinase activity in VEGF-A-mediated macrophage recruitment has also been demonstrated by the transplantation of VEGFR1 tyrosine kinase deficient (*Vegfr1* $tk^{-/-}$) bone marrow cells into mice over-expressing VEGF-A in the ear skin. Macrophage recruitment, lymphangiogenesis, as well as angiogenesis, were significantly decreased, when bone marrow cells from *Vegfr1* $tk^{-/-}$-mice were transplanted as compared from wild-type mice (Murakami et al., 2008). However, in another tumor-free model system, mobilization of immature myeloid $CD11b^+/Gr1^+$ cells from the bone marrow depended rather on VEGFR2 signaling than on VEGFR1 signaling as shown in mice injected with either VEGFR1 or VEGFR2-specific VEGF-A mutants (Huang et al., 2007). These results suggest that VEGFR2 signaling is more important for mobilization and expansion of BMDC, whereas VEGFR1 signaling is more important for recruitment to and positioning at angiogenic sites.

A number of studies have suggested that macrophages are also important for lymphangiogenesis. In human cervical cancers, peritumoral lymphatic vessel density correlated

with the abundance of TAM that expressed VEGF-C and VEGF-D, the main mitogenic growth factors for lymphatic endothelial cells (Schoppmann et al., 2002). In a model of carcinomatous peritonitis, TAM were found to produce VEGF-C and VEGF-D, thus stimulating the expansion of lymphatic vessels in the diaphragm after *intraperitoneal* injection of tumor cells into mice. The lymphangiogenic phenotype was attenuated by treatment with the Cox2 inhibitor Etodolac, presumably via reduced VEGF-C expression in TAM (Iwata et al., 2007). A similar expression of VEGFs by $CD11b^+/LYVE\text{-}1^+$ macrophages has been observed in a model of non-productive dysfunctional lymphangiogenesis in the diaphragm (Jeon et al., 2008). In a corneal vascularization model, VEGF-A and PlGF stimulated lymphangiogenesis via recruitment of macrophages, and this recruitment was impaired, concomitantly with lymphangiogenesis, when VEGF-A and PlGF were neutralized by soluble VEGF receptor (Cursiefen et al., 2004).

The lymphangiogenic factor VEGF-C is often provided by tumor-recruited macrophages, and macrophage mobilization and homing might result from VEGFR1 activation by its ligands VEGF-A and PlGF. Consistent with this notion, strategies targeting VEGFR1, the common receptor for VEGF-A and PlGF, have been proven successful in reducing tumor angiogenesis and lymphangiogenesis in different pre-clinical cancer models (Fischer et al., 2007). However, a formal proof for the specific delivery of various VEGF family members by tumor infiltrating cells, for example by cell type-specific ablation of these growth factors, is still lacking.

1.4.2.2. Myeloid-derived suppressor cells (MDSC)

MDSC are cells closely related to TAM, however they show an incomplete differentiation along the myeloid axis and cannot be definitely attributed to either the monocytic or the granulocytic lineage. In mice, MDSC are characterized by simultaneous expression of Gr1 (a granulocyte marker) and CD11b (a myeloid cell marker), and their abundance can increase in spleen and peripheral blood in tumor-bearing animals. Importantly, MDSC have the ability to suppress T cell activation *in vitro* and they may overlap functionally (and from their ontogeny) with TAM once recruited to the tumor site (Sica and Bronte, 2007). Subcutaneous co-injection of syngenic tumor cells and isolated MDSC (from spleen of tumor bearing animals) into mice revealed that MDSC directly promoted tumor angiogenesis and tumor growth (Yang et al., 2004). Interestingly, MDSC isolated from tumor-free mice rather repressed than supported tumor growth in these studies, indicating that myeloid cells were already partially polarized before entering the tumor site. Again, MMP9 expression by MDSC was shown to be a critical feature, and one might speculate whether MDSC become *bona fide* TAM upon entering the tumor microenvironment. Reducing the levels of MDSC by either treatment of mice with the chemotherapeutic gemcitabine or by interfering with the (tumor-produced) Kit ligand/c-Kit receptor axis reversed the immune

tolerance of advanced tumors and impaired tumor growth and angiogenesis (Pan et al., 2008; Suzuki et al., 2005). MDSC were found *in vitro* to promote an $IL12^{low}$ M2 state of macrophages and, conversely, were stimulated by macrophages to express high levels of IL10. High levels of IL10 induced immunotolerance by blocking dendritic cell (DC) maturation, and reduced levels of IL12 were insufficient to activate natural killer cells. Similarly, gemcitabine treatment of mice transplanted with metastatic 4T1 breast cancer cells lowered peripheral MDSC levels and slightly increased animal survival (Sinha et al., 2007). When 4T1 cells were transplanted into $IL4R\alpha^{-/-}$ mice, in which macrophages can hardly be skewed into a M2 state by IL4 or IL13, gemcitabine treatment resulted in steady-state levels of MDSC and tumor rejection in almost all treated animals.

An important signaling pathway involved in establishing an immune-privileged, pro-angiogenic tumor microenvironment involves signal transducer and activator of transcription 3 (STAT3) signaling. Many tumor types display constitutively activated STAT3 in tumor and stroma cells. In tumor cells, activated STAT3 promotes tumor cell survival but also represses expression of Th1 immuno-stimulatory molecules, such as IL12 and interferons. On the other hand, STAT3 induces expression of immuno-suppressive factors like IL10, VEGF and IL23 (Kortylewski and Yu, 2008). IL10 itself is a canonical activator of STAT3 signaling, implying a positive feedback loop, and VEGF is one of the most potent pro-angiogenic growth factors. Tumor transplantation studies employing deletion of STAT3 in the hematopoietic system resulted in highly activated dendritic cells, lower levels of regulatory T cells but higher levels of cytotoxic intratumoral T cells. Moreover an enhanced anti-tumor activity of natural killer cells and $Gr1^{+}/CD11b^{+}$ neutrophils has been observed, the latter being reminiscent of MDSC (Kortylewski et al., 2005). A recent study also suggests a crucial role of activated STAT3 in TAM and MDSC for promoting tumor angiogenesis. TAM or MDSC isolated out of tumors from STAT3-deficient mice were markedly less potent in inducing endothelial tube formation *in vitro* as compared to STAT3 wildtype cells, concomitant with markedly reduced expression levels of the proangiogenic factors VEGF, bFGF, IL1β, MMP9 and CCL2 (Kujawski et al., 2008).

1.4.2.3. Neutrophils

In the *simian virus 40* large T antigen-driven transgenic mouse model of insulinoma (Rip1Tag2), antibody depletion experiments revealed that neutrophils were critical players for initiating the angiogenic switch during tumorigenesis, and loss of neutrophils could not be compensated by other inflammatory cells (Nozawa et al., 2006). Consistent with this notion, function blocking antibodies against VEGFR1 expressed on tumor infiltrating monocytes and MDSC did not affect Rip1Tag2 tumorigenesis, also indicating that neutrophil recruitment is

independent of VEGFR1 signaling (Casanovas et al., 2005). Conversely, ablation of MMP9-producing macrophages in the HPV16/E2 transgenic mouse model of cervical carcinogenesis can be compensated by neutrophils (Pahler et al., 2008). Antibody-mediated neutralization of Bv8, a neutrophil-derived soluble mediator of tumor angiogenesis and a regulator of myeloid cell mobilization, revealed that early inhibition of Bv8 impaired the angiogenic switch in emerging tumors but did not have an effect when applied at later stages of tumor growth in the Rip1Tag2 model (Shojaei et al., 2008; Shojaei et al., 2007b).

1.4.2.4. Mast cells

In a transgenic mouse model of pancreatic β-cell carcinogenesis, where a Tamoxifen-inducible version of the oncoprotein c-Myc induces metastatic insulinoma, infiltration of mast cells around neoplastic islets of Langerhans has been observed (Soucek et al., 2007). Mast cell function was shown to be essential for the later stages of tumor expansion, since ablation of mast cells provoked increased tumor cell apoptosis and reduced vascular expansion. The authors speculate whether CCL2 and CCL5 could be responsible for mast cell infiltration, as these chemokines are immediate targets of induced c-Myc expression. In the HPV16/E2 transgenic mouse model of squamous cell carcinoma (SCC) of the skin, mast cells were also important for the initial angiogenic switch by providing MMP9 proteolytic activity, and MMP9-deficiency severely impaired keratinocyte hyperproliferation and the incidence of invasive tumors (Coussens et al., 1999; Coussens et al., 2000). In this model, attraction of mast cells and neutrophils to the pre-neoplastic sites was dependent on tumor-specific, B cell-derived immunoglobulin deposits in the epidermis, implying humoral factors in promoting tumor angiogenesis (de Visser et al., 2005).

D6, a scavenger receptor for CC chemokines mainly expressed on lymphatic endothelial cells, was shown to modulate mast cell (and T cell) infiltration in a model of chemically induced skin carcinogenesis (Nibbs et al., 2007). Tumor growth was accelerated in D6-deficient mice concomitant with increased mast cell and T cell infiltration, whereas tumor growth was delayed in mice over-expressing D6 in keratinocytes. These results indicate an important role of CC chemokines in setting up a pro-inflammatory milieu for the recruitment of pro-angiogenic mast cells.

Endostatin, an anti-angiogenic fragment of Collagen XIII, inhibited lymphangiogenesis by reducing infiltration of VEGF-C-expressing mast cells into chemically induced SCC, whereas macrophage recruitment was neither impaired nor did macrophages produce VEGF-C in this experimental setting (Brideau et al., 2007).

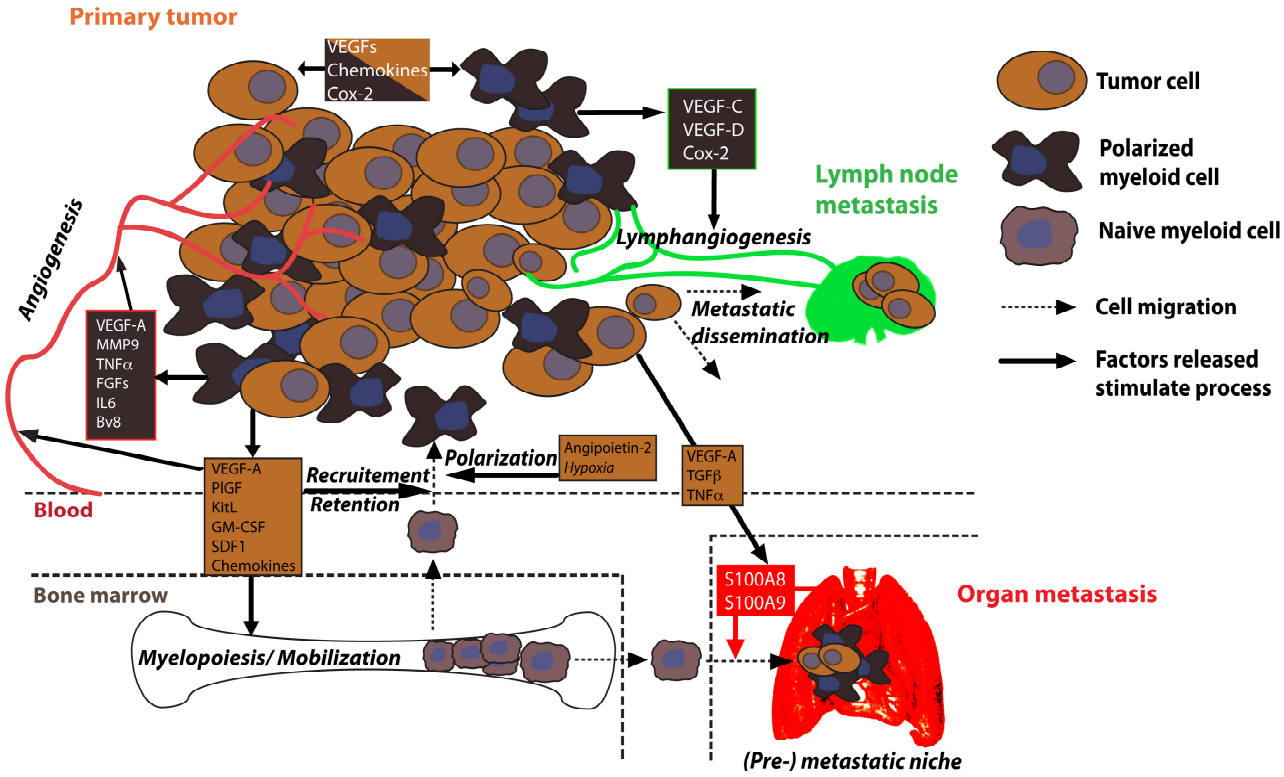

Figure 8. Schematic representation of the interplay between cancer cells and inflammatory, bone marrow-derived cells and their contribution to tumor angiogenesis, lymphangiogenesis and metastasis. See text for details.

1.4.3. Myeloid-endothelial plasticity

The idea that vasculogenesis occurs in adults, and not exclusively during embryonic development, was prompted by the finding that bone marrow-derived cells could integrate into growing blood vessel, cells that were called by their marker profile rather than by their functionality *E*ndothelial *P*rogenitor *C*ells (EPC). The initial descriptions of EPC were based on the phenotypical characterization of $CD34^+$ cells isolated from blood and cultured in pro-angiogenic conditions (Asahara et al., 1997). Yet, overlapping marker profiles obscure the discrimination between haematopoietic and endothelial progenitor cells, and humans and mice seem to have largely different pools of endothelial and hematopoietic stem cells, rendering it difficult to interpret results obtained from injecting human cells into immune-compromised mice. In addition, different mouse strains exhibit highly variable responses to hypoxia and thus varying levels of EPC-like cells (Li et al., 2008; Shaked et al., 2005). EPC characteristics are now generally thought to reside within the $CD14^+/CD34^{low}$-monocytic fraction of peripheral (human) blood (Romagnani et al., 2005).

The remarkable plasticity of monocytic cells has been illustrated by the generation of cells with mesenchymal marker expression (osteoblasts, skeletal myoblasts, chondrocytes, and adipocytes) from $CD14^+$ peripheral blood cells (Kuwana et al., 2003). More important in the context of angiogenesis, cells derived from myeloid progenitors have been found to integrate into the portal veins of either bone marrow-transplanted or parabiotic mice (Bailey et al., 2006). Moreover,

vascular leukocytes carrying a mixed leukocyte/endothelial cell $CD45^+$/VE-$Cadherin^+$ marker profile have been isolated from human ovarian tumors (Conejo-Garcia et al., 2005; Coukos et al., 2005). They may have a dendritic cell precursor phenotype, however, their functional significance and existence beyond ovarian cancer has not been addressed yet.

Recent reports have investigated the contribution of BMDC to blood vessel formation in tumors *in vivo*, coming to conflicting results, even though similar experimental approaches have been used. In one report, up to 30% incorporation of BMDC into tumor neo-vessels was observed, particularly during early tumor growth of LLC cells and in the MMTV-PyMT transgenic model of breast cancer (Nolan et al., 2007). Such incorporation was subsequently shown to play a critical role in promoting the angiogenic switch of lung metastases (Gao et al., 2008). In contrast, other recent reports did not find any integration of BMDC into tumor vessels in a variety of orthotopic transplantation and transgenic cancer models (De Palma et al., 2005; Purhonen et al., 2008). These contradictory results might be explained by differences between the tumor models used and by varying times of analysis during tumor progression. For example, whereas LLC cells employed infiltrating $CD11b^+$/$Gr1^+$ BMDC to overcome VEGF-A inhibition, B16F1 cells exhibited minimal infiltration of $CD11b^+$/$Gr1^+$ cells and were highly sensitive to VEGF-A inhibition (Shojaei et al., 2007a).

In contrast to the discrepancies in EPC and myeloid-lineage cells contributing to and incorporating into blood endothelia, several reports have documented the potential of inflammatory $CD11b^+$ cells to integrate into lymphatic vessels under acute tissue inflammation stress. Myeloid cells, present in the murine inflamed conjunctiva, can express the lymphatic endothelial-specific marker VEGFR3 and can integrate into lymphatic structures that develop in mouse cornea transplants (Hamrah et al., 2003; Maruyama et al., 2005). Another study, employing a cornea angiogenesis model and a syngeneic fibrosarcoma transplantation model, have also revealed the incorporation of BMDC in newly formed lymphatic vessels (Religa et al., 2005). Notably, decreased macrophage numbers resulted in reduced lymphangiogenesis and impaired wound healing in diabetic mice (Maruyama et al., 2007). In another inflammatory condition, the rejection of human kidney transplants, the increased numbers of lymphatic vessels within the rejected organs contain host-derived lymphatic endothelial cells, suggesting the existence of lymphatic endothelial progenitor cells (Kerjaschki et al., 2006). However, the contribution of BMDC to tumor lymphangiogenesis is also controversial. For example, transplantation of LLC or B16F1 melanoma cells in syngeneic mice has not revealed any integration of BMDC into newly formed lymphatic vessels (He et al., 2004).

1.4.4. Perspectives for therapy

The tight coupling of inflammation to the development and progression of most cancers, especially by promoting angiogenesis, opens attractive therapeutic options for targeting cancer via its inflammatory stroma. In recent years, many strategies have aimed at restoring the immunological response against tumor antigens or specific tumor stroma antigens, such as surface molecules expressed by activated tumor endothelium. These approaches have involved overcoming the tumors' immunological anergy, e.g. by decreasing the activity or abundance of immunosuppressor cells or by actively targeting T cell responses to tumor cells or the tumor vasculature. Another avenue towards this goal is to force TAMs back into a M1 state, thus favoring anti-tumor immune responses. Indeed, a preclinical study in mice succeeded in debulking large tumors by a combinatorial treatment with CpG (an activator of Toll-like receptors) and with anti–IL10R antibody, shown to be mediated by an interplay of activated TAM, dendritic cells and cytotoxic T cells (Guiducci et al., 2005).

Several molecular targets which are either expressed by the tumor cells or by the tumor stroma and which are known to promote tumor angiogenesis and tumor progression by supporting inflammatory reactions include Cox-2, CXCR4, MMP, the angiogenic growth factors VEGF-A and PlGF, as well as pro-tumorigenic, M2-type TAM.

Antibodies against VEGF and PlGF

Bevacizumab is a neutralizing antibody against VEGF-A that is now increasingly used in the treatment of a variety of cancer types by directly targeting ongoing tumor angiogenesis. Such treatment has also been found to reduce the levels of circulating immature myeloid cells (iMC), reminiscent of MDSC, in a short term treatment of colorectal cancer patients (Osada et al., 2008). This study suggests that blocking VEGF-A signaling not only blocks tumor angiogenesis but also represses VEGF-A's inhibitory effects on dendritic cell maturation and mobilization of iMC. However, studies in mouse models, as well as the moderate effect of VEGF inhibition in human cancer treatment, suggest that many tumor types activate compensatory angiogenesis programs upon VEGF-A depletion, for example by over-expressing other angiogenic factors, such as FGFs, angiopoietins and PlGF (Casanovas et al., 2005; Fischer et al., 2007). Ongoing clinical and preclinical approaches aimed at targeting the VEGF signaling system include the antibody-mediated neutralization of the activities of PlGF and of neuropilins, co-receptors for VEGF binding and signaling.

PlGF exerts an important function in attracting cells of the immune system to tumor sites via binding to VEGFR1 expressed by the recruited cells. In mouse tumor models, neutralizing antibodies against PlGF reduced tumor vascularization with an efficacy comparable to anti-

VEGFR2 antibodies, an effect that was based on both the direct inhibition of angiogenesis and a reduction of macrophage infiltration into tumors (Fischer et al., 2007). Notably, PlGF seemed to be required exclusively for pathological angiogenesis and was dispensable for physiological angiogenesis and the homeostasis of normal vessels. A phase I clinical trial with the anti-PlGF antibody TB-403 has recently been completed without revealing any toxicity in healthy individuals.

CXCR4 inhibitors

The CXCR4 inhibitor AMD3100 has been successfully employed to augment $CD34^+$ stem cell mobilization upon G-CSF treatment in non-Hodgkin's lymphoma, Hodgkin's disease and multiple myeloma patients prior to autologous stem cell transplantation (Calandra et al., 2008). CXCR4, the bona fide receptor for CXCL12 (SDF1), has been shown to be critical for cancer cell migration, angiogenesis and the positioning and recruitment of pro-angiogenic, myelomonocytic cells. Clinical trials involving the novel CXCR4 inhibitor MSX-122 for the treatment of solid tumors have started only recently.

Trabectedin

Trabectedin, a small chemical entity originally discovered in a Carribean marine tunicate, is a minor groove DNA binder which disrupts cell cycle progression and cell proliferation. It has been approved for the treatment of soft tissue sarcomas refractory to standard chemotherapy regimen (Grosso et al., 2007). It is also under investigation in phase II clinical studies for ovarian cancer and breast cancer (Krasner et al., 2007; Zelek et al., 2006). Intriguingly, human monocytes were particularly sensitive to trabectedin-induced apoptosis as compared to lymphocytes, and in treated patients monocyte counts were reduced and their ability to differentiate into macrophages was impaired. In parallel, freshly isolated TAM or ovarian tumor cells from patient treated with trabectedin expressed lower levels of IL6 and CCL2, the latter being one of the most potent monocyte-attractant chemokines (Allavena et al., 2005). Based on these observations, it is tempting to speculate that trabectedin-treatment not only affects tumor cells but also immunomodulatory functions. The lack of efficacy in trabectedin-treated colorectal cancer (CRC) patients could originate from the fact that in CRC, unlike in most other cancer types, macrophage infiltration usually is a favorable prognostic marker, and trabectedin-treatment might interfere with anti-tumoral TAM (Forssell et al., 2007; Paz-Ares et al., 2007).

Cox-2 inhibitors

Meta-analysis of case control or cohort studies showed a slight but significant risk reduction for the development of breast cancer for woman regularly taking aspirin or other non-steroidal, anti-inflammatory drugs (NSAIDs) (Gonzalez-Perez et al., 2003; Harris et al., 2003; Khuder and Mutgi, 2001). Clinical trials with specific Cox-2 inhibitors documented a significant reduction in adenoma formation in patients at high risk for CRC (Baron et al., 2006; Bertagnolli et al., 2006). However, other clinical trials failed to show a benefit of including Cox-2 inhibitors to standard chemo- or radiotherapeutic regimens, e.g. in advanced pancreatic adenocarcinoma or in cervical cancer (Dragovich et al., 2008; Gaffney et al., 2007). In addition, due to an increased risk of cardiovascular complications, the clinical trials in colorectal cancer patients had to be terminated prematurely. A recent study in which CRC patients have been treated with NSAID three days before surgery, showed an increased tumor infiltration of immune cells indicative for an anti-tumor T cell response, suggesting that prostaglandins mediated immunological tolerance in CRC (Lonnroth et al., 2008).

Inhibitors of matrix metalloproteases (MMP)

Based on the observation that MMP are involved in many processes underlying the regulation of tumor angiogenesis and tumor progression, they might be ideal targets for therapeutic intervention (Noel et al., 2008). However, clinical phase III trials with MMP inhibitors (MMPI) have failed to demonstrate a beneficial effect in patients with advanced cancers (Coussens et al., 2002; Overall and Kleifeld, 2006b). One explanation for such disappointment may be attributable to the use of broad-spectrum inhibitors, which not only block pro-tumorigenic MMP but also repress MMP whose functions may be anti-tumorigenic. From a scientific perspective, the problems to successfully translate preclinical studies to human cancer patients reach beyond species differences. Most likely, the early time point of intervention in animal models fundamentally alters the response to MMP inhibition as compared to the clinical trials in which late stage tumors have been treated. In some clinical trials, patients treated with MMPI fared even worse highlighting the need to develop more specific MMPI (Fingleton, 2003; Overall and Kleifeld, 2006a).

The amino-bisphosphonate zoledronic acid (ZA) inhibits MMP9 activity in preclinicial studies in a mouse cervical cancer model (Giraudo et al., 2004) and is already clinically approved to treat bone metastasis by blocking osteoclastic activity (Rosen et al., 2003). Direct targeting of pro-angiogenic pathways has been recently tested by metronomic (intermittent administration at low dosage) treatment with ZA in a clinical phase I study in patients with advanced solid tumors, resulting in reduced serum levels of VEGF-A (Santini et al., 2007). Moreover, liposomal delivery of the non-amino-bisphosphonate clodronate depleted macrophages in the synovial fluid of

rheumatoid arthritis patients and ablated macrophages and repressed tumor angiogenesis in mouse tumor transplantation models (Barrera et al., 2000; Zeisberger et al., 2006). However, this approach has not been tested in cancer patients yet.

Thalidomide

Thalidomide and its derivative lenalidomide belong to a class of immuno-modulatory drugs and are now approved for treatment of multiple myeloma in combination with dexamethasone (Palumbo et al., 2008). Immuno-modulatory effects include activation of cytotoxic T and NK cells, potentially through upregulation of IL2. Thalidomide's reported anti-angiogenic activities have also set the stage for clinical trials in solid tumors, including prostate cancer and renal cell carcinoma, however with moderate success (Amato et al., 2008; Pacheco et al., 2007; Romero et al., 2007). A direct anti-angiogenic effect of this class of drugs has been proposed, and a recent report has demonstrated inhibitory effects on endothelial sprout formation induced by hypoxia or VEGF (Lu et al., 2008).

1.4.5. Conclusions

Malignant cancers have evolved in a way that they have not only adapted to grow in a growth-restraining environment but they also skew their stroma to support their growth and their metastatic dissemination in the body. A general theme in the activities of inflammatory stroma cells is the enhancement of tumor angiogenesis and the suppression of T cell responses. Understanding these events on a cellular and molecular level will allow the design of novel therapeutic approaches that a) target the compensatory functions of tumor-infiltrating leukocytes under anti-angiogenic treatment regimen and b) support strategies that aim to boost the endogenous immune system, for example by re-activating dendritic cell function and adaptive immunity. To successfully translate these insights from the bench to the bed-side, more experimental work in early-to-intermediate stage tumor models is required, as most of the inflammatory events investigated thus far occur mainly in the early phases of tumor progression, whereas clinically manifested cancers are treated rather at advanced stages.

Tumor model	Immune cells	Experimental modulation	MVD	TV	TP	Additional parameters (change to control/ wildtype)	Ref
tg: K14-HPV16/E2 SCC	Mϕ	Bisphosphate inhibition of Mϕ	↓	↓	↓		[1]
tg: K14-HPV16/E2 SCC	Mϕ, Neutrophils	Breeding in $CCR2^{-/-}$ mice	↔	↔	↓	itMMP9$^+$ Mϕ ↓, itMMP9$^+$ Neutrophils↑	[2]
tt: glioblastoma, BMT	BMDC	Hif1α-deficient glioblastoma cells				itMMP9$^+$ BMDC↓, VEGF-A↓, SDF-1↓, perivascular invasion↑	[3]
tt: breast Ca, BMT	CD11b$^+$ BMDC	IR of tumors or pre-IR of tumor bed, MMP9-deficient host and/or bone marrow donor	↓	↓		itMMP9$^+$ BMDC↑ (IR vs. non-IR); TV↓ MVD↓ in $MMP9^{-/-}$ animals, but TV↔ & MVD↔ with $MMP9^{+/+}$ BM	[4]
tg: PyMT breast Ca	Mϕ	breeding in Mϕ-deficient $CSF1^{op/op}$ mice		↔	↓	itMϕ↓, Lung metastasis↓; rescue by tg MMTV-CSF1	[5]
tg: PyMT breast Ca	Mϕ	breeding in Mϕ-deficient $CSF1^{op/op}$ mice	↓			correlation of itMϕ, malignant transition and angiogenic switch; rescue by tg MMTV-VEGF-A	[6, 7]
tt: glioblastoma tt: N202, breast Ca	TEM	TEM ablation in transplanted BM	↓	↓		TEM but not CD11b$^+$Tie2$^-$ myeloid cells isolated from tumors stimulate angiogenesis when co-injected with tumor cells	[8]
tt: Lewis Lung Ca tt: B16 melanoma	VEGFR1$^+$ BMDC	anti-VEGFR1 Ab, anti-Integrinα_4 Ab, specific VEGFR1$^+$ cells vs. VEGFR1$^-$ BMT				reduced or abolished lung metastases	[9]
tt: F9 teratocarcinoma tt: A673 rhabdomyosarcoma	Mϕ	Mϕ-ablation by liposome-encapsulated clodronate	↓	↓		itMϕ ↓; MVD correlation with itMϕ	[10]
tt: Lewis Lung Ca	Mϕ	anti-Integrinα_4 Ab	↓	↓		itMϕ ↓	[11]
tt: OCUM2 gastric Ca	Mϕ	Cyclooxygenase-2 inhibition		↓		LVD↓, LNM↓, VEGF-C↓	[12]
tt: Panc02 pancreas Ca tt: CT26 colon Ca	Mϕ	anti-PlGF Ab, liposome-encapsulated clodronate Mϕ ablation	↓	↓		BMC↓, EC apoptosis↑; itMϕ ↓, LNM↓, LVD↓, VEGF-C↓	[13]
tt: MC26 colon Ca tt: Lewis Lung Ca	MDSC	co-injection of MC26 with splenic Gr1$^+$CD11b$^+$ MDSC from tumor bearing mice	↑	↑		hypoxia↓, tumor cell apoptosis↓, pericyte coverage↑, effects not seen with MDSC from non-turmor bearing mice	[14]
tt: MCA26 colon Ca	MDSC	sKitL-deficient colon cancer cells; anti-cKit Ab	↓			blood MDSC↓, tumor T cell proliferative capacity↑, itMDSC↓	[15]
tt: A673 rhabdomyosarcoma tt: HM7 colon Ca	MDSC	anti-Bv8 Ab	↓	↓		blood MDSC↓, itMDSC↓, enhancement of anti-VEGF and Cisplatin treatment	[16]
tg: Rip1Tag2 insulinoma	Neutrophils	anti-Gr1 Ab		↔	↓	itMMP9$^+$ Neutrophils↓, ligated VEGFR2↓	[17]
tg: K14-HPV16 SCC	Granulocytes, MC, B cells	breeding in $Rag1^{-/-}$ mice (no adaptive immunity)		↓	↓	itMC↓, itGranulocytes↓, itMMP2 and MMP9 activity↓, keratinocyte proliferation↓; rescue by B cell transfer or serum injection isolated from K14-HPV-16 wt tumor bearing mice	[18]
tg: pIns-mycER^{TAM} inducible insulinoma	MC	inhibition of MC degranulation by cromolyn, breeding in MC-deficient $Kit^{W\text{-}sh/W\text{-}sh}$ mice	↓			tumor cell proliferation↔, EC proliferation↓, tumor cell apoptosis↑, hypoxia↑	[19]
cc: SCC	MC	tg K14-endostatin mice	↓	↔	↓	itMC↓, TI↔, LVD↓, LNM↓; VEGFR3↓, VEGF-C↓	[20]
tt: B16 melanoma tt: MB49 bladder Ca	Neutrophils, DC, NK, TC	hematopoietic deletion of STAT3 in Mx1-Cre;$STAT3^{loxP/loxP}$ mice, STAT3 inhibition by CPA7		↓		DC activation↑, cytolytic activity of neutrophils and NK cells↑, itTC↑ itT_{reg}↓	[21]

Table 1. The function of inflammatory cells in mouse models of tumor angiogenesis.

Abbreviations: ↓: reduced, ↑: increased, ↔: unchanged, Ab: antibody, BMC: blood monocyte count, BM: bone marrow, BMDC: bone marrow derived cell, BMT: bone marrow transplantation, Ca: carcinoma, cc: chemical carcinogenesis, DC: dendritic cell, EC: endothelial cell, IR: irradiation, it: intratumoral, LNM: lymph node metastasis, LVD: lymphatic vessel density, Mϕ: macrophage, MC: mast cell, MVD: microvessel density, NK: natural killer cell, SCC: squamous cell

carcinoma, TEM: Tie2 expressing monocycte, tg: transgenic, TC: T cell, T_{reg}: regulatory T cell, tt: tumor transplantation, TP: tumor progression, TV: tumor volume, TI: tumor incidence, wt: wild-type

References: [1]: (Giraudo et al., 2004), [2]: (Pahler et al., 2008), [3]: (Du et al., 2008), [4]: (Ahn and Brown, 2008), [5]: (Lin et al., 2001), [6]: (Lin et al., 2007), [7]: (Lin et al., 2006), [8]: (De Palma et al., 2005), [9]: (Kaplan et al., 2005), [10]: (Zeisberger et al., 2006), [11]: (Jin et al., 2006), [12]: (Iwata et al., 2007), [13]: (Fischer et al., 2007), [14]: (Yang et al., 2004), [15]: (Pan et al., 2008), [16]: (Shojaei et al., 2007b), [17]: (Nozawa et al., 2006), [18]: (de Visser et al., 2005), [19]: (Soucek et al., 2007), [20]: (Brideau et al., 2007), [21]: (Kortylewski et al., 2005)

2. Aim of the study

The critical importance of the tumor stroma during carcinogenesis has only been appreciated during the last decade. Immune cells, mainly derived from the bone marrow, are an important component of the tumor stroma and immune cell infiltration into tumors is often indicative for pro-tumorigenic inflammation.

The objective of the studies presented here was to define the functional role of bone marrow-derived cells in the processes of angiogenesis and lymphangiogenesis in the Rip1Tag2 carcinogenesis models. I analyzed the spatial and temporal interaction of bone marrow-derived cells with the tumor by employing lineage tracing strategies, including bone-marrow transplantation and Cre/Lox technology. High-resolution confocal microscopy and flow cytometry allowed me to gain insight into the dynamics of the tumor stroma composition and the interactions between tumor and stroma cells.

I particular, I set out to investigate the following research aims:

Aim 1: What is the extent and significance of bone marrow-derived immune cell infiltration into tumors of Rip1Tag2 mice?

Aim 2: What is the importance of bone-marrow derived cells in supporting the growth of either tumor, endothelial or lymphendothelial cells via paracrine actions using loss-of-function approaches?

Aim 3: What is the range of non-hematopoietic phenotypes that bone marrow-derived cells can acquire in tumors?

A better understanding of tumor – stroma interactions holds strong promise to funnel into the development of novel strategies for the treatment of cancer. Bone marrow-derived cells as crucial components of growing cancers might be an attractive target of intervention in order to prevent metastasis and resistance to therapy.

3. Materials and Methods

Specific Materials and Methods are described in the chapters "4.2. Myeloid cells contribute to tumor lymphangiogenesis" and "4.4. Improved mouse model of pancreatic β-cell carcinogenesis."

Chemicals

General chemicals used were all purchased from SIGMA-ALDRICH (Buchs, Switzerland) unless otherwise stated.

Laboratory mice/ mouse strains

Animals were fed regular laboratory chow (M/R Extrudat 3436EX.F12, Kliba Navag) and water *ad libitum* and were housed in a 12 h day and night cycle. Animals were kept under *specified pathogen-free* conditions and regularly checked for pathogens. All animal experiments described were approved by the Cantonal Veterinary office Basel-Stadt and covered by the licenses 1878 (organ biopsies), 1907 (tumor transplantation), 1908 (pharmacological treatments including ClodroLip and Luciferin injections), 2137 (bone marrow transplantations).

Tissue processing for histology

For organ biopsies, mice were euthanized by cervical dislocation and organs quickly removed. Organs were either fixed at 4° C in 4% phosphate buffered paraformaldehyde (PFA) for 12 hours and then embedded in paraffin after ethanol/xylene dehydration; alternatively organs were fixed at 4°C in 4% PFA for 2h, and cryo-preserved for 10 hours in 20% sucrose in PBS prior to embedding in OCT freezing matrix. Occasionally, organs were frozen without prior fixation in OCT freezing matrix. Paraffin slides were cut 5μm thick and rehydrated according to standard protocols. For immunohistochemical (IHC) stainings of PFA fixed, paraffin embedded specimens, antigen epitopes were retrieved by boiling slides in 10mM Na-Citrate buffer (pH6.0) for 10' in a microwave oven, endogenous peroxidase was quenched by treatment with 3% H_2O_2 for 10 minutes. Cryosections were cut 7μm thick, postfixed for 5' in either 4% PFA or 70% ethanol and dried for 30' prior to rehydration in PBS.

Toluidine blue staining for Mast cells

Deparaffinize and rehydrate PFA fixed/ paraffin embedded organ sections. Stain Toluidene Blue working solution (0.1% (w/v) Toluidine Blue O, 0.9% (w/v) NaCl, 7% ethanol (v/v)) for 2 minutes, rinse in ddH_20 3x, dehydrate quickly thought 95% and absolute ethanol, clear in xylene.

Mast cells should stain red-purple (metachromatic staining) and the background stain blue (orthochromatic staining).

Antibodies

Antibodies used are specified under the respective manuscripts.

Fluorescence activated cell sorting (FACS)

All FACS analyses were performed on a Becton Dickinson FACSCanto II Flow Cytometer using FACS DIVA software (Becton Dickinson, Allschwil, Switzerland).

Oligonucleotides

Oligonucleotides used for cloning and/ or quantitative real-time PCR (qPCR) are described in the respective manuscripts. qPCR primers were designed using Universal ProbeLibrary Assay Design Center (http://www.roche-applied-science.com/sis/rtpcr/upl/acenter.jsp?id=030000) or by PrimerExpress 1.5 (Applied Biosystems).

4. Results

4.1. Infiltration of immune cells into tumors of Rip1Tag2 mice

In order to assess the infiltration of immune cells into Rip1Tag2 tumors, we set out to quantify the infiltration by immune cells using immunofluorescence/ histology and flow cytometry. The following markers were used to describe the tumors "infiltrome".

CD45: pan leukocyte marker
CD3ε: pan T-cell marker
CD19: pan B-cell marker
CD11b: marker for all myeloid cells (including macrophages, monocytes and granulocytes)
F4/80: phagocytic macrophage marker
Gr-1: granulocyte marker
Toluidine blue staining: mast cell

As can be seen in Figure 9, a robust infiltration of immune cells is evident in tumors of Rip1Tag2 mice. $CD45^+$ cells constitute about 9.8% of the tumors total cell number. Myeloid cells ($CD11b^+$) constitute 5.8% of the cells in the tumors and are the largest sub-type of infiltrating immune cells. T-cells (CD3) contribute 3.4% of cells. B cells were hardly found in Rip1Tag2 tumors, indicating that blood (which contains 5-10% B cells) is not a major contaminant of tumor cell preparations for FACS analysis. The myeloid cells further split into monocytes/ macrophages ($CD11b^+/F4/80^+$) and granulocytes ($CD11b^+/Gr\text{-}1^+$), which each constitute 1-2% of cells as analyzed by FACS.

In contrast to histological analyses, where small tumor foci (< 1mm) can be analyzed, FACS analyses can only be done with macroscopic tumors (> 1.5mm). Therefore, one cannot directly compare the results obtained by histology and by FACS. Amazingly, whereas in FACS CD11b gave an excellent signal for cell preparations from tumors, in histology CD11b was hardly detected at intra-tumoral locations (but clearly extratumoral). In contrast, cells positive for F4/80, a marker for differentiated phagocytic macrophages, were much more abundant in histology than when analyzed by FACS. This could be due to the different processing techniques, which unfold different epitopes recognized by the respective antibodies.

Even though T cells were quite abundant in macroscopic tumors when analyzed by FACS, similarly to CD11b, we could not detect CD3ε positive cells in tumors by histology, whereas in lymph nodes of the very same section, CD3ε positive cells were clearly detectable. It has

previously been shown that the adaptive immune system does not play a major role in tumorigenesis of Rip1Tag2 mice, as crossing of Rip1Tag2 mice with Rag1$^{-/-}$ mice, lacking adaptive immunity, did not impair tumorigenesis markedly (Casanovas et al., 2005).

Mast cells, identified via a red-purple staining after Toluidine blue stain, were never detected by histology within tumors and were only rarely found in connective tissue (inset in Figure 9). Mast cell infiltration has been identified as an important determinant in the establishment of tumor vasculature in a c-Myc induced insulinoma model (Soucek et al., 2007). Fundamental differences in the cytokines produced by the neoplastic lesions might be one reason for the differential infiltration by mast cells between Rip1Tag2 and c-Myc induced insulinomas.

As myeloid cells represent the most abundant immune cell compartment in Rip1Tag2 tumors, we set out to characterize in further detail the contribution of this immune cell compartment to tumorigenesis in Rip1Tag2 mice.

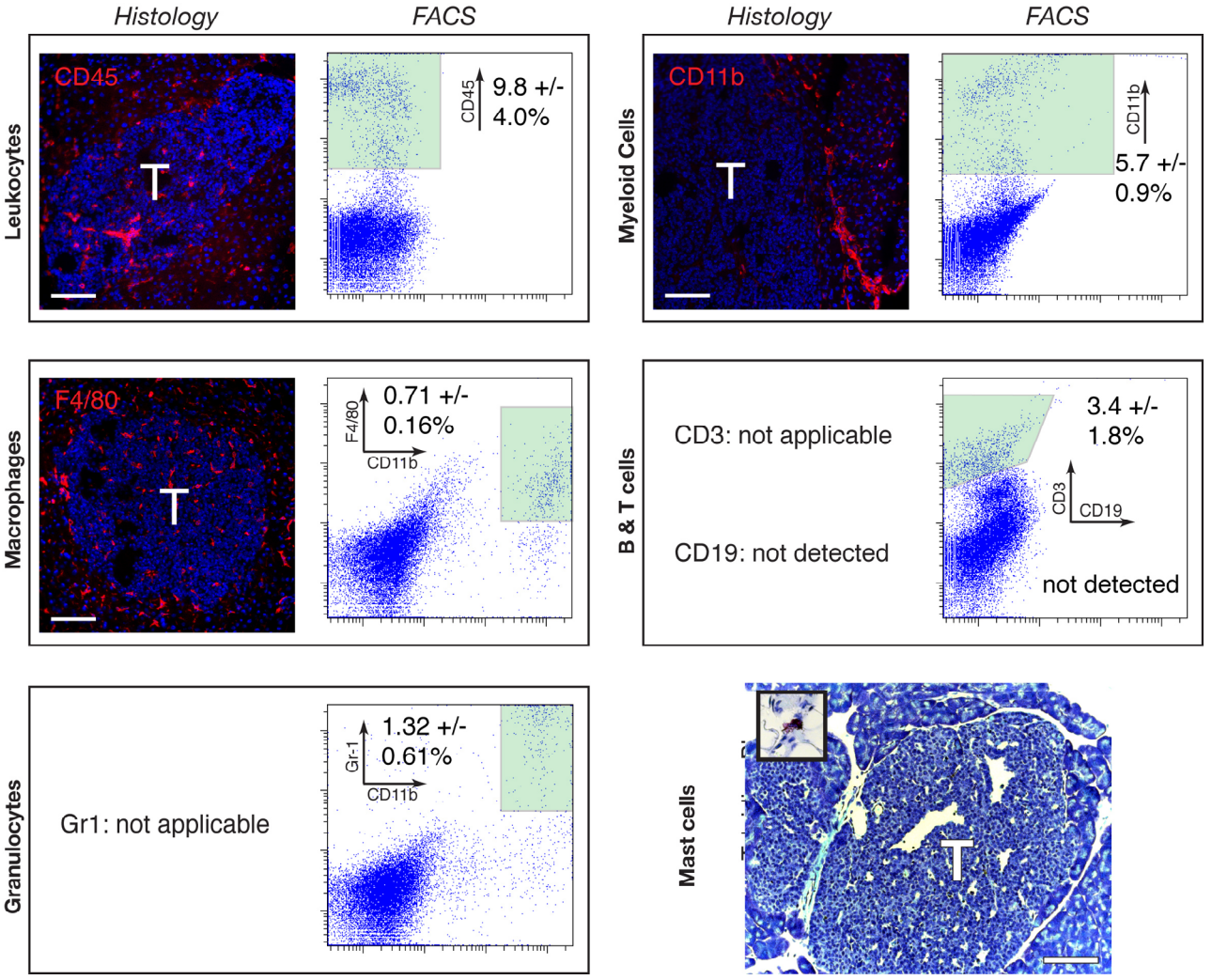

Figure 9. The immune cell infiltration into tumors of Rip1Tag2 was studied by histology and/ or flow cytometry. Pancreata of 12-13 week old tumor mice were either analyzed via immuno-fluorescent staining of tissue sections or tumor single cell preparations (obtained as described under 4.2.5.) were analyzed by FACS. CD11b^{+} myeloid cells constitute the most abundant immune cell type found in Rip1Tag2 tumors. Mast cells, identified by toluidine blue staining, were not found in tumors but only in connective tissue (inset). Arrows in FACS dot plot indicate the marker used in the respective axis. Numbers shown are the mean +/- standard deviation of 6 tumors analyzed (from 3 different mice), as found in the green shaded area. T: tumor. Scale bar: 100μm.

4.2. Myeloid cells contribute to tumor lymphangiogenesis

Adrian Zumsteg[1,5], Vanessa Baeriswyl[1,5], Natsuko Imaizumi[2], Reto Schwendener[3], Curzio Rüegg[2], and Gerhard Christofori[1,4]

[1]Institute of Biochemistry and Genetics, Department of Biomedicine, University of Basel, Switzerland.

[2]Centre Pluridisciplinaire d'Oncologie, Lausanne Cancer Center, Epalinges, Switzerland.

[3]Institute for Molecular Cancer Research, University of Zürich, Zürich, Switzerland.

[4]Corresponding Author:

Gerhard Christofori
Institute of Biochemistry and Genetics
Department of Clinical Biological Sciences
University of Basel
Center of Biomedicine
Mattenstrasse 28
4058 Basel
Switzerland
Tel. +41 61 267 35 64
Fax. +41 61 267 35 66
e-mail: Gerhard.christofori@unibas.ch

[5]These authors contributed equally to this work.

Running title: Myeloid cells and lymphangiogenesis

Keywords: angiogenesis, bone marrow cells, lymphangiogenesis, macrophages, myeloid cells, tumorigenesis

4.2.1. Abstract

The formation of new blood vessels (angiogenesis) and lymphatic vessels (lymphangiogenesis) promotes tumor outgrowth and metastasis. Previously, it has been demonstrated that bone marrow-derived cells (BMDC) can contribute to tumor angiogenesis. However, the role of BMDC in lymphangiogenesis has largely remained elusive. Here, we demonstrate by bone marrow transplantation/reconstitution and genetic lineage tracing experiments that BMDC integrate into tumor-associated lymphatic vessels in the Rip1Tag2 mouse model of insulinoma and in the TRAMP-C1 prostate cancer cell transplantation model. The results indicate that bone marrow-derived, integrated cells originate from the myelomonocytic lineage. Conversely, pharmacological depletion of tumor-associated macrophages reduces lymphangiogenesis. No cell fusion events are detected by genetic tracing experiments. Rather, the phenotypic transition of myeloid cells into lymphatic endothelial cells is recapitulated in an *in vitro* tube formation assay. The data indicate that myeloid cells can trans-differentiate into lymphatic endothelial cells and thus contribute to tumor lymphangiogenesis.

4.2.2. Introduction

In the adult, the vascular network is usually expanded and remodeled by sprouting and proliferation of endothelial cells from pre-existing blood and lymphatic vessels, processes called angiogenesis and lymphangiogenesis, respectively. In addition to tissue resident cell types, several studies have demonstrated that BMDC are recruited to angiogenic sites to support the establishment of new vessels (De Palma et al., 2005; Grunewald et al., 2006; Lyden et al., 2001). BMDC are typically sub-classified into haematopoietic progenitor cells (HPC) and endothelial progenitors cells (EPC). In various tumor models, HPC have been shown to contribute to blood vessel angiogenesis by secreting angiogenic factors and proteases required for the activation of latent forms of angiogenic factors (Coussens et al., 2000; Cursiefen et al., 2004). HPC have also been implicated in the preparation of a pre-metastatic niche in organs that are colonized by disseminating cancer cells (Kaplan et al., 2005). EPC on the other hand have been shown to directly integrate into growing blood vessel walls, however, to varying extents, ranging from 0 to 50% and thus raising questions about their functional contribution to blood vessel angiogenesis in various physiological and pathological conditions (De Palma et al., 2005; Garcia-Barros et al., 2003). Recently, it has been reported that also cells of the myeloid lineage are able to differentiate into *bona fide* blood endothelial cells (Bailey et al., 2006).

Only few studies have addressed the role of BMDC in lymphangiogenesis. Haematopoietic stem cells have recently been shown to contribute to normal lymphatic endothelium in liver,

stomach and intestine under physiological conditions (Jiang et al., 2008). More specifically, myeloid cells present in the murine inflamed conjunctiva have been found to express the lymphatic endothelial specific marker VEGFR3 and to integrate into lymphatic structures that develop in mouse cornea transplants (Hamrah et al., 2003; Maruyama et al., 2005). During the rejection of human kidney transplants, another inflammatory process, lymphatic vessels within the rejected organs contained host-derived lymphatic endothelial cells, suggesting the existence of lymphatic endothelial progenitor cells (Kerjaschki et al., 2006). Experiments employing a cornea angiogenesis model and a syngeneic fibrosarcoma transplantation model have also revealed the incorporation of BMDC in newly formed lymphatic vessels (Religa et al., 2005). Finally, decreased macrophage numbers appear to cause reduced lymphangiogenesis and impaired wound healing in diabetic mice (Maruyama et al., 2007). However, the contribution of BMDC to tumor lymphangiogenesis is controversial. Transplantation of Lewis Lung Carcinoma or B16-F1 melanoma cells in syngeneic mice has not revealed any integration of BMDC into newly formed lymphatic vessels (He et al., 2004). In contrast, employing two different murine tumor models and an *in vitro* differentiation assay, we demonstrate here that cells derived from the myeloid lineage physically contribute to tumor lymph*vasculogenesis.*

4.2.3. Results

BMDC integrate into tumor lymphatics

We have employed the Rip1Tag2 (RT2) mouse model of multistage pancreatic β-cell carcinogenesis to investigate the contribution of BMDC to tumor angiogenesis and lymphangiogenesis (Hanahan, 1985). RT2 transgenic mice recapitulate hallmarks of tumor progression, including the regulated onset of tumor angiogenesis, the functional contribution of tumor-infiltrating immune cells to a pro-angiogenic tumor microenvironment, and the transition from adenoma to carcinoma (Bergers et al., 2000; Nozawa et al., 2006; Perl et al., 1998). When crossed to Rip1VEGF-C (VC) or Rip1VEGF-A (VA) mice, double-transgenic RT2;VC mice develop tumors with high peritumoral lymphangiogenesis and lymph node metastasis (Mandriota et al., 2001), whereas double-transgenic RT2;VA mice exhibit an earlier onset of tumor angiogenesis and accelerated tumor growth in the absence of any lymphangiogenesis and metastasis (Gannon et al., 2002).

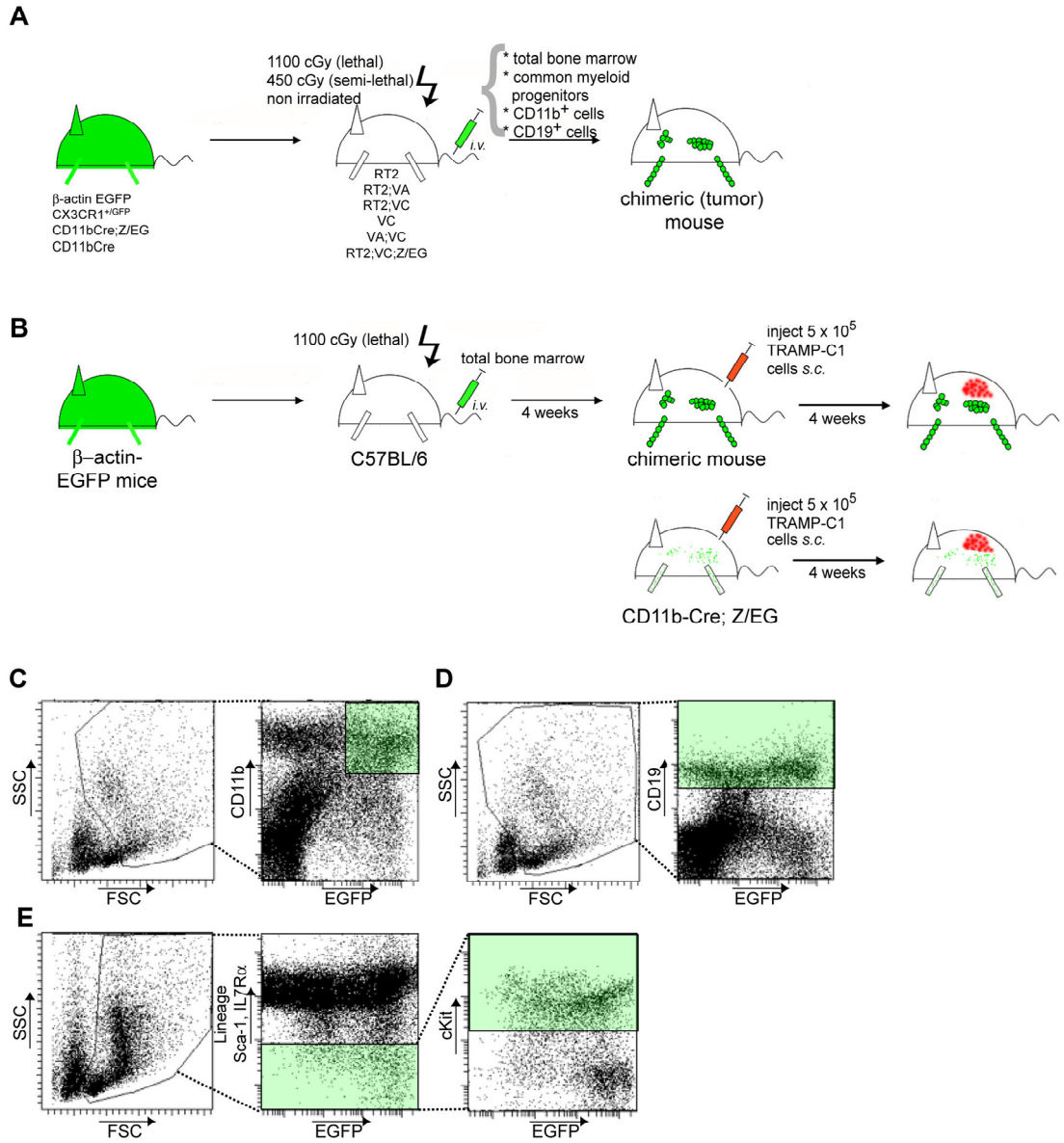

Figure 10. Bone marrow transplantation strategies. (**A**) For total bone marrow transplantations, 5 x 10^6 T cell-depleted total bone marrow cells from donor mice were injected *i.v.* into lethally irradiated (2 x 550 cGy) mice, as indicated. Semi-lethally irradiated (450 cGy) mice were injected with FACS-sorted 4 x 10^5 $CD11b^+$ myeloid cells, 4 x 10^5 $CD19b^+$ B-cells or 4 x 10^4 common myeloid progenitors (CMP) cells. 4 x 10^5 $CD11b^+$ myeloid cells were also transferred into non-irradiated mice. After 3-8 weeks mice were sacrificed, engraftment of transplanted bone marrow was evaluated by FACS and pancreata were analyzed by histology for the presence of bone marrow-derived cells at the tumor site. (**B**) Schematic illustration of syngeneic TRAMP-C1 tumor experiments. 5x10^5 TRAMP-C1 cells were injected into the flank of either C57BL/6 previously reconstituted with bone marrow of b-actin-GFP transgenic mice or bone marrow of double-transgenic CD11b-Cre;Z/EG mice, and tumors were allowed to grow for 3 to 4 weeks. FACS analysis was used to assess bone marrow reconstitution or Cre recombinase-mediated GFP expression, respectively. Histological sections from TRAMP-C1 tumors were analyzed by immunofluorescence for the presence of GFP^+ cells. (**C-E**) Flow cytometry-based strategy for cell sorting. (**C**) Within a scatter gate excluding lymphocytes, $CD11b^{high}$/ GFP^{high} cells were isolated by FACS. (**D**) $CD19^+$ was used as marker for the isolation of B lymphocytes. (**E**) CMP cells were sorted as lin^-/ $Sca\text{-}1^-$/ $IL7Ra^-$/ $cKit^+$ as described in Methods.

To investigate whether BMDC integrate into tumor blood and lymphatic vasculature in the RT2 model, lethally irradiated RT2, RT2;VA and RT2;VC mice were transplanted with bone marrow isolated from actin-GFP transgenic mice (Figure 10A). FACS analysis of peripheral blood (PB) showed efficient hematopoietic reconstitution with more than 90% chimerism (data not shown).

Immunofluorescence analysis of tumor sections revealed that the proportion of GFP$^+$ tumor-infiltrating BMDC was invariant in the range of 3.5% of total cellularity, independent of the transplantation of single transgenic RT2 mice or double-transgenic mice expressing either VEGF-A or C (Figure 11). Increased serum levels of these growth factors are thought to mediate mobilization and recruitment of BMDC to sites of neo-angiogenesis as shown for VEGF-A (Grunewald et al., 2006; Hattori et al., 2001). Yet, despite the high expression of the angiogenic factors by tumor cells of double-transgenic RT2;VA and RT2;VC mice, specific ELISA analysis did not reveal any of these growth factors in the serum of these mice, suggesting that they are locally sequestered and are not affecting the recruitment of BMDC (data not shown). From the GFP$^+$ BMDC within the tumors, approximately 80% were F4/80$^+$ macrophages (Figure 11). Immunofluorescence co-staining for F4/80 and the hyaluronan receptor LYVE-1 identified LYVE-1$^+$ macrophages in the tumor periphery with relatively large size compared to intra-tumoral macrophages (data not shown) (Cho et al., 2007; Schledzewski et al., 2006). In contrast, Podoplanin or Prox-1 were not expressed by tumor-associated macrophages (TAM). These observations instructed us to carefully differentiate between tumor lymphatic endothelium, defined as a continuous LYVE-1$^+$/Prox-1$^+$/Podoplanin$^+$ and CD31$^+$ vessel lining, and isolated, peritumoral LYVE-1$^+$ macrophages.

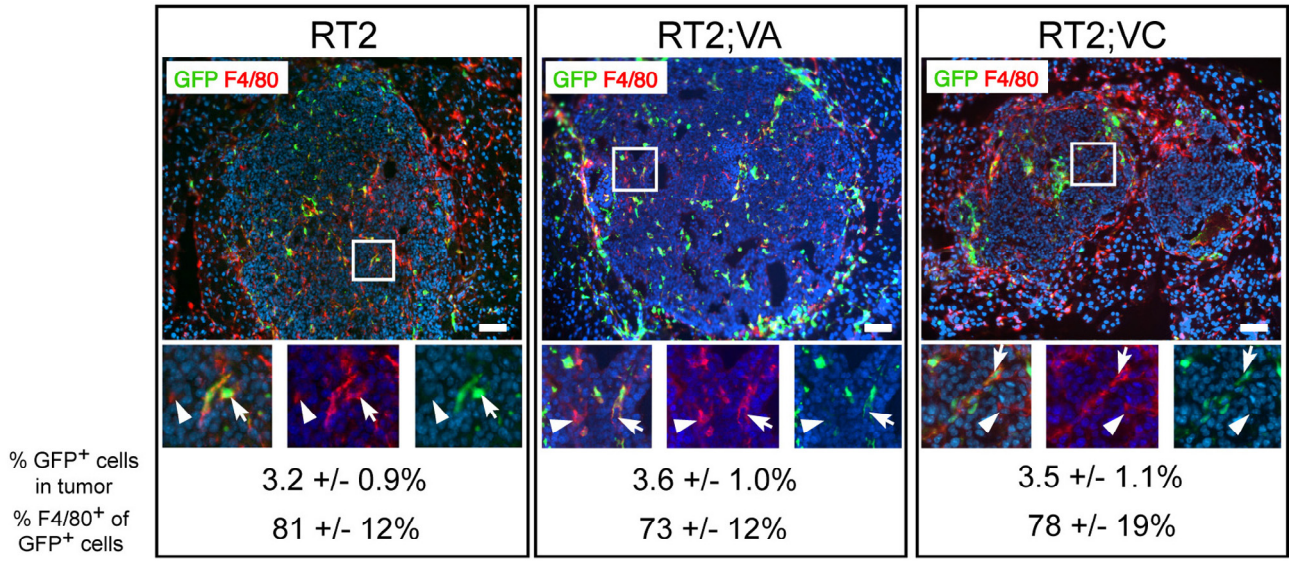

Figure 11. Infiltration of transplanted BMDC in RT2 tumors. Lethally irradiated RT2, RT2;VA and RT2;VC mice were transplanted with GFP-labeled bone marrow, as indicated. No significant differences could be observed in tumor infiltrating bone marrow-derived cells between the different angiogenic factor-expressing tumors. Approximately 3-3.5% of tumor-constituting cells were GFP$^+$ (green) and thus bone marrow-derived, and approximately 80% of GFP$^+$ cells co-expressed the monocyte/macrophage marker F4/80 (red). White rectangles indicate area of higher magnification shown below, with merge picture on the left, F4/80 in the middle, and GFP on the right. F4/80$^+$ macrophages are either donor-derived (co-expressing GFP, indicated by arrows) or host-derived (no GFP expression, arrowheads). 3 mice per genotype with 16-29 tumors each were analyzed. DAPI was used for nuclear counterstaining (blue). Scale bar: 50 μm.

To assess the potential contribution of BMDC to intra-tumoral blood vessels, confocal microscopy and subsequent 3D reconstitution analysis were performed on pancreatic sections of

transplanted RT2 and RT2;VA mice stained for the endothelial marker CD31 and for GFP. Bone marrow-derived, GFP^+ cells were mainly found in close proximity of blood vessels (Figure 12, arrow heads). In very rare cases (< 0.4% of blood endothelial cells; Figure 12, arrow), $GFP^+/CD31^+$ double-positive cells could be observed, indicating that in the Rip1Tag2 model the direct incorporation of BMDC into the blood vasculature is negligible.

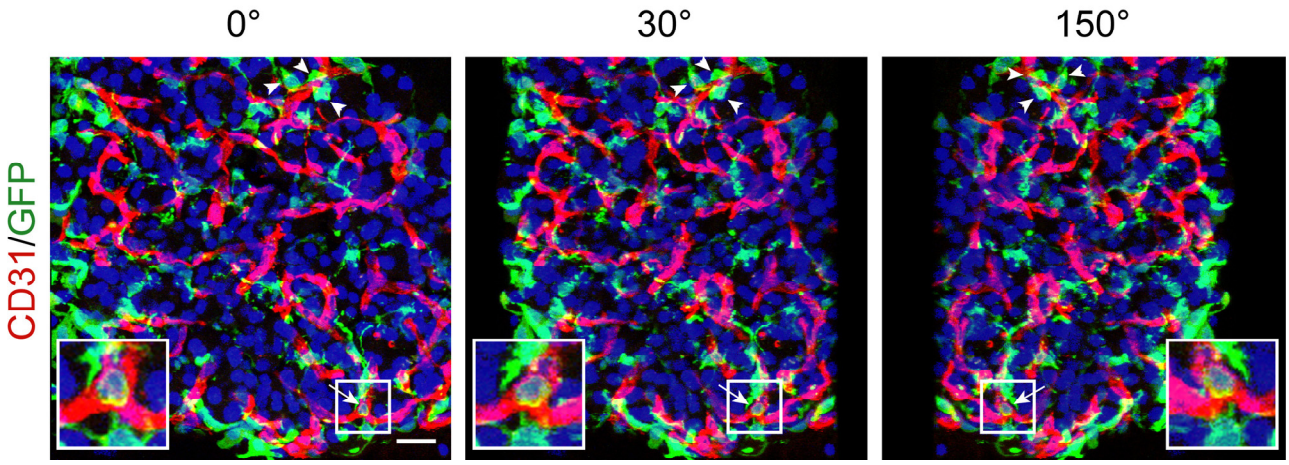

Figure 12. Rare integration of BMDC into blood vessels of RT2 tumors. 20 μm tumor sections of RT2 (3 mice) and RT2;VA (2 mice) mice transplanted with GFP-labeled bone marrow were stained for the endothelial marker CD31 (red) and GFP (green) and analyzed by confocal microscopy and subsequent 3D reconstitution. Different angles of a representative 3D reconstituted tumor section are shown. As indicated by arrowheads, GFP^+ cells were mainly found in close proximity of blood vessels. As indicated by the arrow, cells co-expressing GFP and CD31 were rarely detected in this experimental setting (7 $CD31^+/GFP^+$ cells out of 2141 $CD31^+$ cells). Insets represent magnifications of a rare GFP/CD31 double-positive cell. DAPI stains nuclei (blue). Scale bar: 20 μm.

In contrast, BMDC had incorporated into lymphatic vessels surrounding VEGF-C-expressing β cell tumors of transplanted RT2;VC mice. Pancreatic sections from these mice were stained for the three lymphatic markers Podoplanin, Prox-1 and LYVE-1 and for GFP. Confocal imaging revealed that 3% of $Podoplanin^+$ tumor lymphatic endothelial cells (TLEC) as well as 3.5% of $Prox\text{-}1^+$ or $LYVE\text{-}1^+$ TLEC co-expressed GFP, indicating that about 3.3% of tumor-surrounding lymphatic endothelial cells are derived from the bone marrow (Figure 13A). Routine laser scanning confocal microscopy analysis on 7-20 μm thick sections with subsequent 3D reconstitution enabled us to exclude false double-positive cells, as shown in supplemental videos 1 & 2 (on attached CD). Furthermore, VE-cadherin, an endothelial-specific adherens junction molecule, reported to connect lymphatic endothelial cells in lymphatic vessels (Baluk et al., 2007), was expressed on host as well as on bone marrow-derived TLEC, further demonstrating a functional integration of BMDC into tumor lymphatic vasculature (Figure 14). Note that in contrast to blood endothelial cells, where VE-cadherin usually clusters at cell-cell junctions (Figure 14, arrows), VE-cadherin staining on lymphatic endothelium is found to be more homogenously distributed throughout the lymphatic endothelial cell membranes.

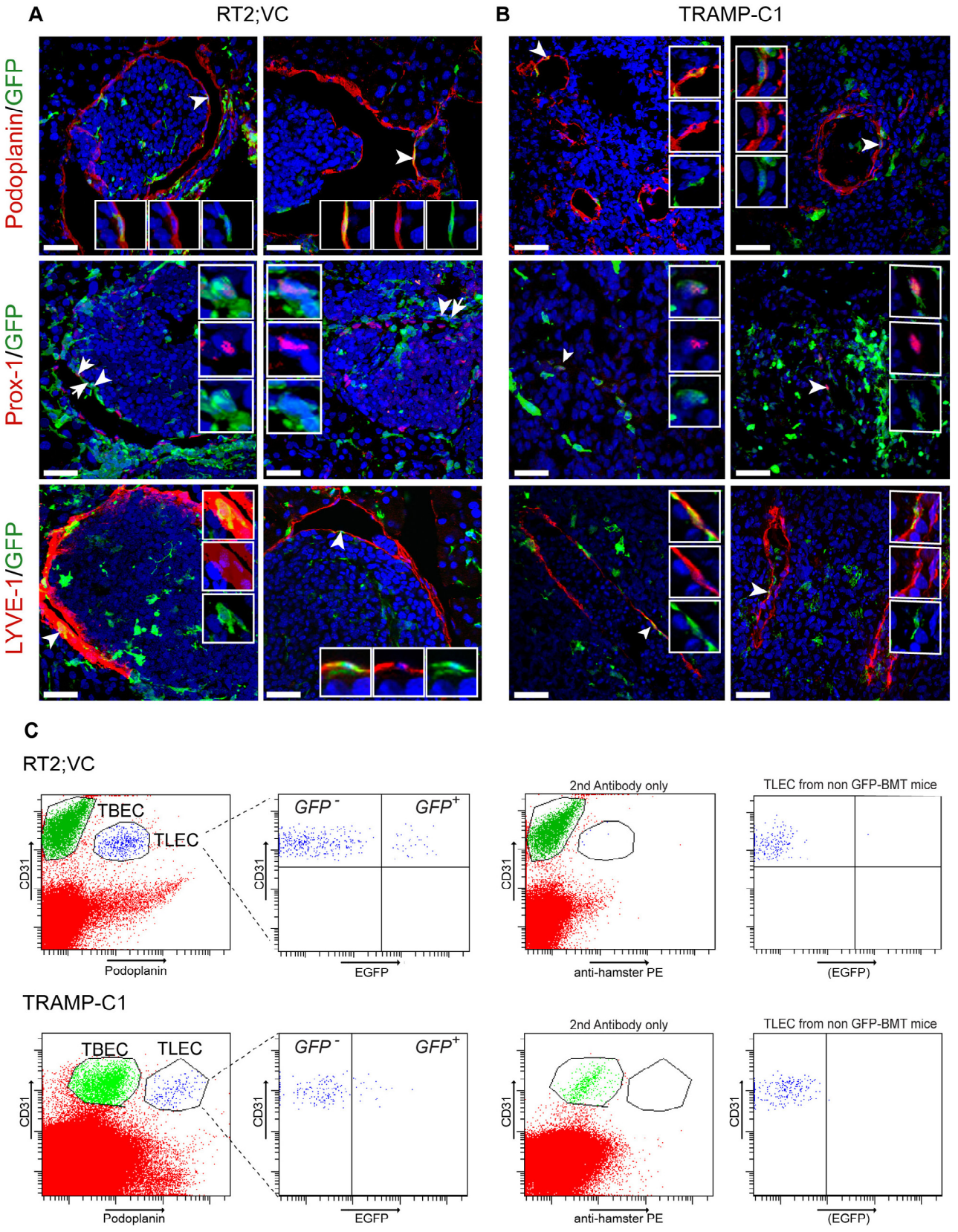

Figure 13. BMDC integrate into tumor-associated lymphatic vessels. (**A**) Lethally irradiated RT2;VC mice (5 mice) were reconstituted with GFP-labeled bone marrow. 7-20 μm histological pancreatic sections were stained for the lymphatic markers Podoplanin, Prox-1, LYVE-1 and for GFP as indicated and analyzed by confocal microscopy and subsequent 3D reconstitution. Two representative tumor sections per lymphatic marker are shown. 3% of Podoplanin$^+$ TLEC (7 Podoplanin$^+$/GFP$^+$ cells out of 227 Podoplanin$^+$ cells) as well as 3.5% of Prox-1$^+$ or LYVE-1$^+$ TLEC (14 Prox-1$^+$/GFP$^+$ cells out of 400 Prox-1$^+$ cells and 17 LYVE-1$^+$/GFP$^+$ cells out of 485 LYVE-1$^+$ cells) are bone marrow-derived. (**B**) TRAMP-C1 tumors were subcutaneously implanted in C57BL/6 mice (4 mice) previously reconstituted with GFP-labeled

bone marrow. 7μm histological tumor sections were stained as in (A). 4.1% of Podoplanin$^+$ TLEC (14 Podoplanin$^+$/GFP$^+$ cells out of 334 Podoplanin$^+$ cells) as well as about 2.8% of LYVE-1$^+$ TLEC (11 LYVE-1$^+$/GFP$^+$ cells out of 395 LYVE-1$^+$ cells) are bone marrow-derived. Arrows indicate double-positive cells and arrowheads indicate double-positive cells shown in inset magnifications. Insets show merged and individual channels. DAPI stains nuclei (blue). Scale bars: 40 μm. (**C**) Tumors of GFP-labeled bone marrow-transplanted RT2;VC mice or TRAMP-C1 tumors grown in GFP-labeled bone marrow-transplanted C57BL/6 mice were enzymatically digested (3 mice each). Single cell suspensions were stained for the pan-endothelial marker CD31 and the lymphatic endothelial marker Podoplanin and analyzed by FACS (left panels). 9.4 +/- 4.1% (RT2;VC) and 10 +/- 4.6% (TRAMP-C1) of CD31$^+$/ Podoplanin$^+$ TLEC were GFP$^+$, indicating their bone marrow origin (middle left panels). As control, the anti-Podoplanin antibody was omitted resulting in no separation between TLEC and TBEC (middle right panels). Furthermore, similar analysis of tumors grown in non-transplanted mice showed no GFP$^+$ cells within the TLEC population (right panels).

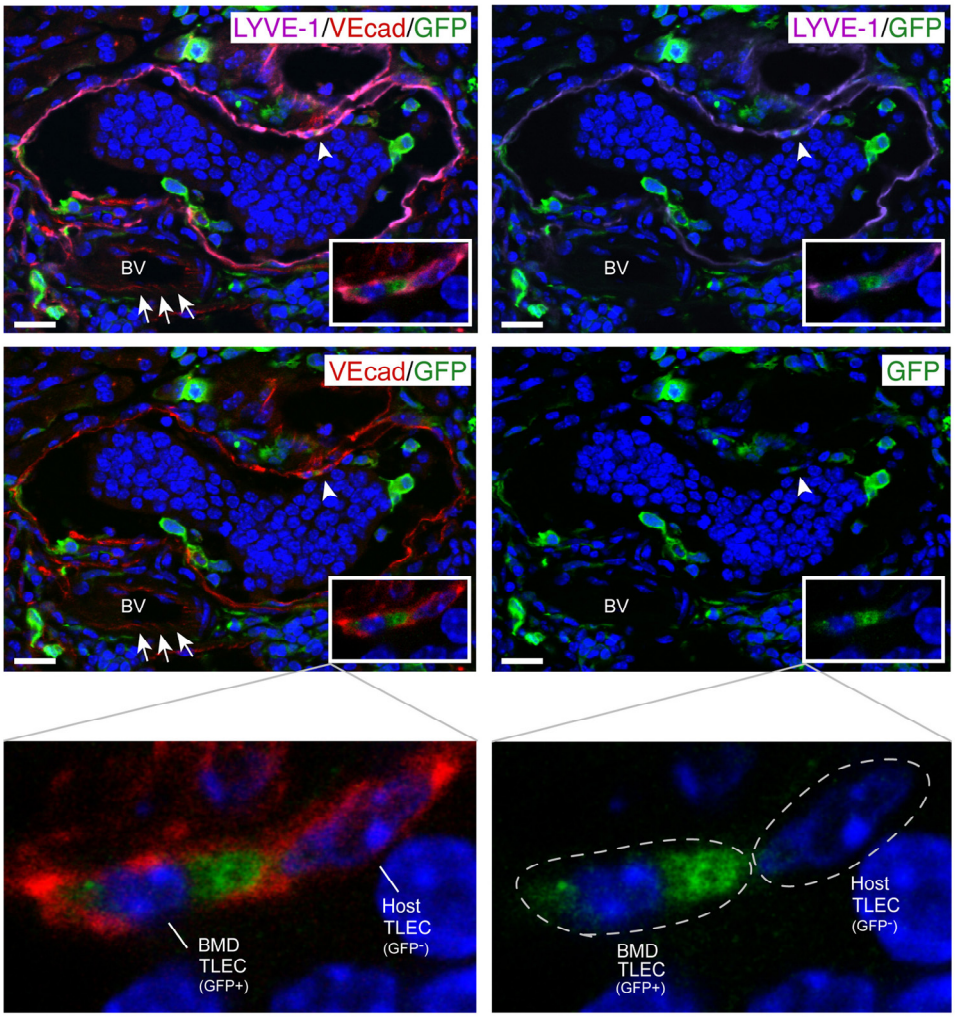

Figure 14. BMDC integrated into tumor lymphatics express VE-cadherin. A representative tumor section from RT2;VC mice previously reconstituted with GFP-labeled bone marrow was stained for the lymphatic marker LYVE-1 (purple), for the cell junction molecule VE-cadherin (red), and for GFP (green) and analyzed by confocal microscopy and subsequent 3D reconstitution. As indicated by arrowheads and shown magnified in insets, VE-cadherin expression, indicative for homophilic cell-cell contact, is observed between bone marrow-derived (BMD TLEC) and host-derived TLEC (Host TLEC). Note the continuous VE-cadherin staining between lymphatic endothelial cells in contrast to the cell-cell contact restricted staining of blood endothelial cells depicted by arrows. DAPI was used for nuclear counterstaining (blue). BV: blood vessel. Scale bars: 20 μm.

To expand the significance of the findings in the RT2 insulinoma model as well as to test whether the observed integration of BMDC occurred also in the absence of artificially expressed VEGF-C, we employed the TRAMP-C1 murine prostate adenocarcinoma cell line previously shown to induce robust tumor lymphangiogenesis upon transplantation into syngeneic C57BL/6 mice (Gingrich et al., 1996; Ozerdem, 2006). TRAMP-C1 cells were subcutaneously injected into one flank of C57BL/6 mice that had been previously reconstituted with GFP$^+$-labeled bone marrow (Figure 13B). In the resulting tumors, the number and morphology of BMDC that had integrated in tumor lymphatic vessels were comparable to the results obtained with RT2;VC mice. GFP$^+$ cells were detected in lymphatic vessels staining for LYVE-1 and Podoplanin (Figure 13B) and

constituted 2.8% of LYVE-1$^+$ and 4.1% of Podoplanin$^+$ cells within lymphatic vessel structures. GFP expression was also detected in Prox-1$^+$ TLEC, however to a lower extent as compared to LYVE-1 or Podoplanin. This might be explained by the fact that overall only a subset of LYVE-1$^+$ TLEC express Prox-1 (data not shown).

To validate the results of the confocal microscopical analysis, single cell suspensions of tumors obtained from GFP$^+$ bone marrow-transplanted or control non-transplanted mice were analyzed by FACS for the presence of GFP$^+$ TLEC (Figure 13C). TLEC were identified by co-expression of CD31 and Podoplanin (Figure 13C, left panels). Indeed, 9.4 +/- 4.1% and 10 +/- 4.6% of TLEC in tumors from RT2;VC and TRAMP-C1 mice , respectively, were GFP$^+$, confirming the results obtained by confocal immunofluorescence microscopy analysis. As expected, GFP$^+$ TLEC were not observed in non-transplanted mice, documenting the specificity of the FACS analysis (Figure 13C, right panels). In order to exclude the detection of false positive signals by cell duplets containing GFP$^+$ BMDC and Podoplanin$^+$ TLEC that would appear as CD31$^+$/Podoplanin$^+$/GFP$^+$ triple-positive cells, such events were rigidly excluded by forward scatter pulse width (data not shown).

To investigate whether BMDC integration into newly formed lymphatic structures occurred only in a tumor microenvironment, non tumor-bearing, single-transgenic VC mice were transplanted with GFP-labeled bone marrow. Notably, no GFP$^+$ cells were found incorporated into the lymphatic vessels surrounding normal islets of Langerhans in these mice (Mandriota et al., 2001) (Figure 15). Increasing the levels of VEGF-A by transgenic expression of VEGF-A in VA;VC double transgenic mice also did not provoke an integration of BMDC into the lymphatic vasculature surrounding the islets (Figure 15). These results demonstrate the ability of BMDC to incorporate into actively growing lymphatic vessels, yet only in a tumor microenvironment.

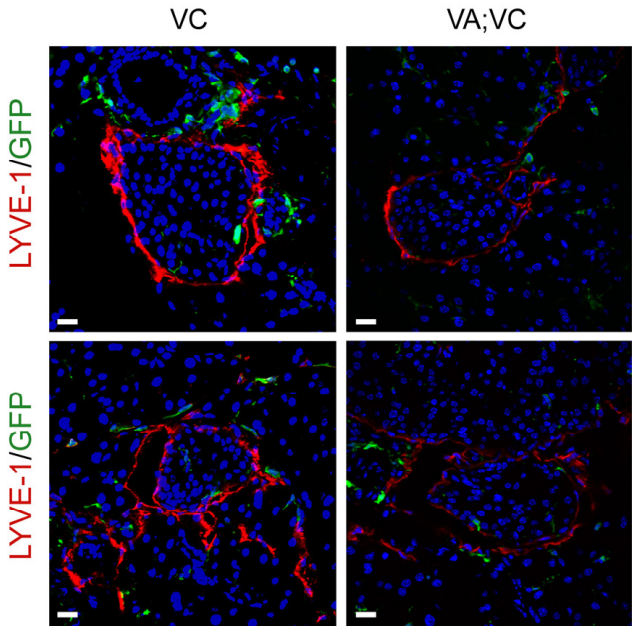

Figure 15. BMDC do not integrate into lymphatic vessels surrounding normal islets. VC mice (2 mice) or VA;VC (2 mice) were transplanted with GFP-labeled bone marrow. Pancreatic sections of transplanted mice were stained for the lymphatic markers LYVE-1 (red) and GFP (green) and analyzed by confocal microscopy. Two representative tumor sections per experiment are shown. No GFP$^+$ cells were found integrated into islet surrounding lymphatic structures, indicating that BMDC did not contribute to *de novo* lymphangiogenesis under non-tumorigenic conditions. DAPI stains nuclei (blue). Scale bar: 20 μm.

Integrated BMDC are of myeloid origin

To investigate whether BMDC contributing to tumor lymphangiogenesis express macrophage markers, pancreatic sections of transplanted RT2;VC mice were stained for the lymphatic marker LYVE-1, the macrophage marker F4/80 and GFP (Figure 16A). Triple-positive GFP$^+$/LYVE-1$^+$/F4/80$^+$ cells were readily observed in lymphatic vessels surrounding the tumors. Interestingly, not all BMDC that had integrated into the lymphatic vasculature expressed F4/80, suggesting that macrophages physically contributed to tumor lymphatics but eventually lost their macrophage features upon integration, as previously reported (Maruyama et al., 2007).

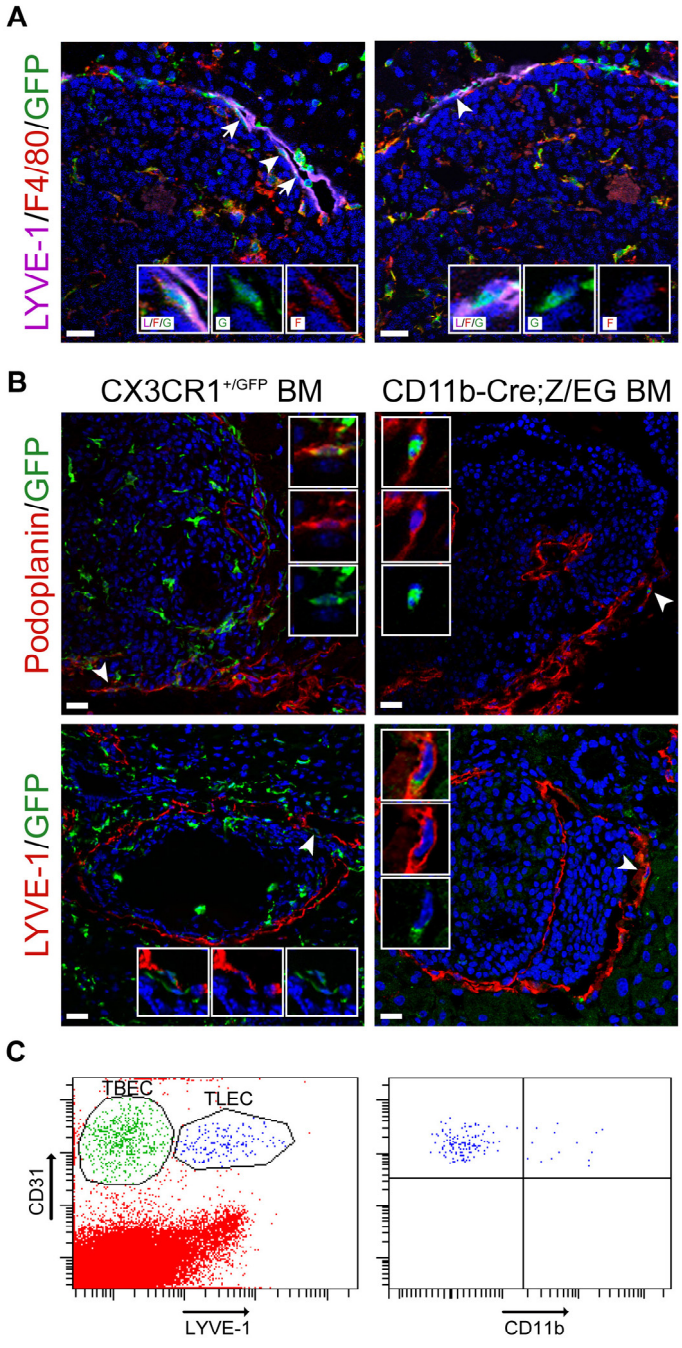

Figure 16. Myeloid origin of bone marrow-derived TLEC. (**A**) 20 μm histological pancreatic sections of GFP-labeled bone marrow-transplanted RT2;VC mice were stained for the lymphatic marker LYVE-1 (purple), for the monocyte/macrophage marker F4/80 (red), and for GFP (green) as indicated and analyzed by confocal microscopy and subsequent 3D reconstitution. Two representative tumor sections are shown. Left panel: BMDC that have integrated into tumor lymphatics express the macrophage marker F4/80. Arrows indicate triple positive cells and the arrowhead indicate a triple-positive cell shown in inset magnifications. Right panel: not all integrated cells express F4/80. The arrowhead indicates an integrated cell (LYVE-1$^+$/GFP$^+$) that does not express F4/80. Inset magnifications of this double-positive cell are shown. Insets show merged and individual channels. (**B**) 7-20 μm histological pancreatic sections of RT2;VC mice transplanted with bone marrow isolated from either CX3CR1$^{+/GFP}$ (2 mice) or CD11bCre;Z/EG mice (3 mice) were stained for the lymphatic markers Podoplanin or LYVE-1 (red) as well as for GFP (green) and analyzed by confocal microscopy. Two representative tumor sections per lymphatic marker are shown. In both transplantation settings, myeloid cells were found integrated into the lymphatic vasculature surrounding the tumors. Arrowheads indicate double-positive cells shown in inset magnifications (first inset: merged channels, second and third insets: red and green channel, respectively). DAPI stains nuclei (blue). Scale bars: 20 μm. (**C**) Tumors of RT2;VC mice were enzymatically digested. Single cell suspension was stained for the pan-endothelial marker CD31, the lymphatic endothelial marker LYVE-1 and the myeloid marker CD11b and analyzed by FACS (left panel). 6.2 +/- 4.5% of CD31$^+$/ LYVE-1$^+$ TLEC co-expressed CD11b (right panel).

To assess whether cells of the myeloid lineage were able to incorporate into tumor lymphatic vessels, we performed cell lineage tracing experiments. First, lethally irradiated RT2;VC mice were transplanted with bone marrow isolated from either CX3CR1$^{+/GFP}$ knock-in mice or CD11b-Cre;Z/EG double-transgenic mice. In CX3CR1$^{+/GFP}$ mice, the coding region for EGFP had been inserted in the *CX3CR1* gene, a receptor expressed mainly by monocytes and to a minor extent by a subset of lymphocytes, resulting in monocyte-specific GFP expression (Jung et al., 2000) (Figure 17A). The Z/EG transgene contains, under the control of an ubiquitous promoter, a *lacZ* gene/stop cassette flanked by loxP recombination sites and followed by the coding region for EGFP (Novak et al., 2000). When crossed to CD11b-Cre mice, expressing Cre recombinase under the control of the myeloid specific CD11b promoter, Cre-mediated excision of the *lacZ* gene/stop cassette induced permanent GFP expression exclusively in cells having passed through a CD11b-expressing, myeloid stage (Ferron and Vacher, 2005). Pancreatic sections of transplanted RT2;VC were stained for the lymphatic markers Podoplanin or LYVE-1 and for GFP, and double-positive cells were scored. In both transplantation settings, GFP$^+$ cells were found integrated into the tumor lymphatic vasculature, demonstrating that cells of the myeloid lineage physically contributed to tumor lymphangiogenesis (Figure 16B). In addition, FACS analysis of tumors from non-transplanted RT2;VC mice revealed that some *bona fide* CD31$^+$/ LYVE-1$^+$ TLEC express the myeloid marker CD11b (Figure 16C), again confirming the microscopical analysis and indicating that during active tumor lymphangiogenesis TLEC may express a myeloid marker.

To test whether CD11b$^+$ cells indeed integrated into tumor lymphatics without prior bone marrow transplantation, TRAMP-C1 cells were transplanted in CD11b-Cre;Z/EG mice (Figure 10B). Specific Cre-mediated recombination within the myeloid lineage of these mice was confirmed by FACS analysis of peripheral blood cells (Figure 17B). In the resulting tumors, GFP$^+$ cells were found incorporated into LYVE-1$^+$ and Podoplanin$^+$ lymphatic vessels (Figure 18A). Triple staining for LYVE-1, Prox-1 and GFP further showed that formerly myeloid cells simultaneously expressed two lymphatic markers (Figure 18B, arrowhead), demonstrating their differentiation towards a lymphatic endothelial phenotype. These experiments also revealed that integration occurred independently of prior irradiation, which had been previously reported to increase macrophage infiltration in human cancer (McDonnell et al., 2003). No GFP$^+$ cells were found incorporated into lymphatic vessels of tumor-free skin or intestine (data not shown), further highlighting the critical role of the tumor environment in stimulating integration.

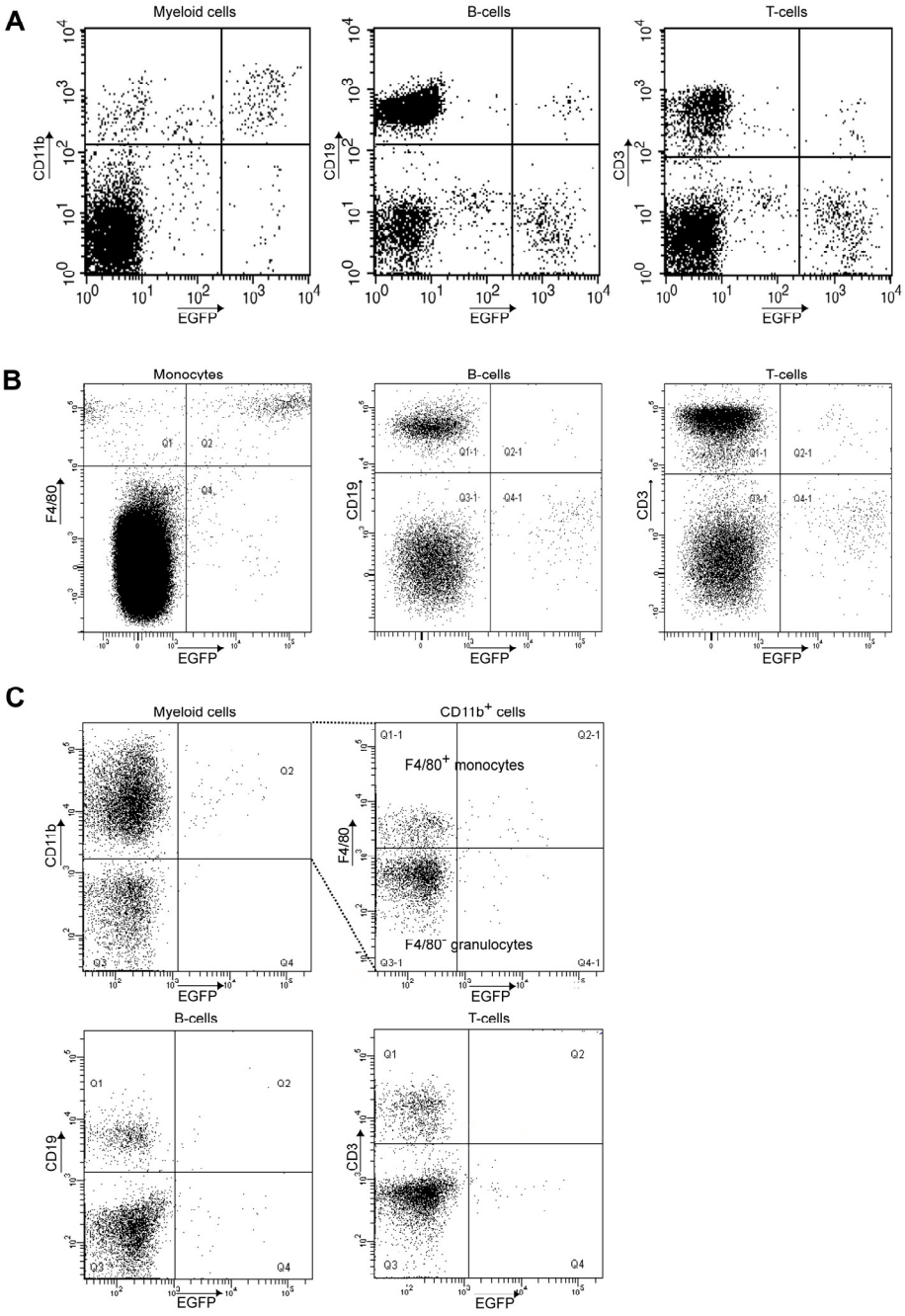

Figure 17. FACS analysis of the lineage tracing experiments. (**A**) FACS analysis of peripheral bood cells from a representative RT2;VC mouse reconstituted with bone marrow isolated from CX3CR1$^{+/GFP}$ mice indicates GFP expression mainly in CD11b^{+} cells. A minor fraction of CD19^{+} B-cells and CD3^{+} T-cells also expressed GFP. (**B**) FACS analysis of peripheral blood cells from CD11b-Cre;Z/EG mice transplanted with TRAMP-C1 tumors indicates effective Cre-mediated recombination and subsequent expression of GFP predominantly in F4/80^{+} monocytes and to lesser extent in B or T lymphocytes. (**C**) FACS analysis of peripheral blood cells from RT2;VC mice reconstituted with common myeloid progenitor (CMP) cells indicates that GFP^{+} cells are present within the CD11b^{+}/F4/80^{+} monocyte fraction and the CD11b^{+}/F4/80^{-} granulocyte fraction but not in B or T lymphocytes.

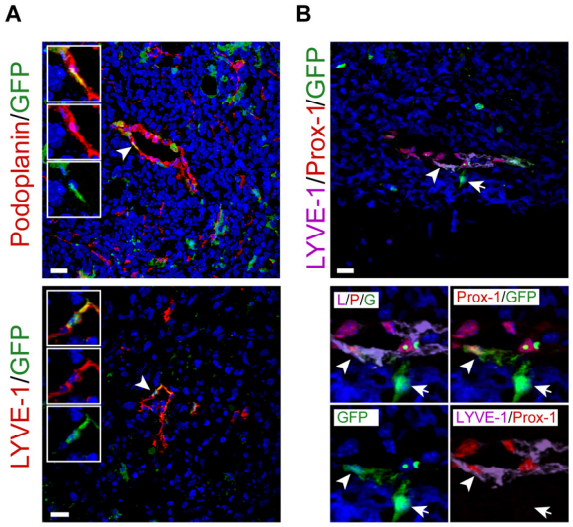

Figure 18. CD11b^{+} lineage tracing shows myeloid origin TLEC in a bone marrow transplantation-independent setting. TRAMP-C1 tumors were grown subcutaneously in CD11b-Cre;Z/EG mice (3 mice). In these mice, cells that have passed through a CD11b^{+} myeloid lineage express GFP. (**A**) GFP^{+} cells with typical lymphatic extended morphology were identified in Podoplanin and LYVE-1-immunoreactive lymphatic vessels. Arrowheads indicate double-positive cells shown in inset magnifications (first inset: merged channels, second and third insets: red and green channel, respectively). (**B**) Triple stain revealed co-expression of LYVE-1 and Prox-1 on myeloid derived GFP^{+} cells integrated into lymphatic vessels (arrowhead). The lower panel represents a magnification of the relevant region with individual channels combined. Note that GFP^{+} cells not connected to vascular structures do express neither LYVE-1 nor Prox-1 (arrow). DAPI stains nuclei (blue). Scale bars: 20 μm.

In a second series of lineage tracing experiments, FACS-sorted CD11b$^+$ myeloid cells from actin-GFP transgenic mice (Figure 10C) were *i.v.* injected into semi-lethally RT2;VC mice. 3 weeks after injection, adoptively transferred GFP$^+$ cells were observed integrated into tumor lymphatics, identified by LYVE-1 or Prox-1 expression. Notably, adoptive transfer of CD11b$^+$/GFP$^+$ cells into non-irradiated RT2;VC mice gave similar results (Figure 19A), indicating that reconstitution of the haematopoietic system by stem cells is not a prerequisite for BMDC contribution to tumor lymphangiogenesis. To assess whether common myeloid progenitor cells (CMP) (Akashi et al., 2000) provide the cells that incorporate into tumor lymphatics, FACS-sorted CMP cells (lin$^-$/Sca-1$^-$ /IL7Rα^-/cKit$^+$/GFP$^+$; Figure 10E) were adoptively transferred into semi-lethally irradiated RT2;VC mice. FACS analysis of peripheral blood cells three weeks after transplantation revealed that the transferred CMP cells contributed to the generation of CD11b$^+$/F4/80$^+$ monocytes and CD11b$^+$/F4/80$^-$ granulocytes but not to CD19$^+$ B lymphocytes or CD3$^+$ T lymphocytes (Figure 17C). Also here, GFP$^+$ cells were found integrated into tumor-associated lymphatic endothelium, detected by LYVE-1 or Podoplanin expression (Figure 19B). In contrast, adoptive transfer of FACS-sorted CD19$^+$/GFP$^+$ B cells (Figure 10D) did not result in any incorporation of these cells into tumor lymphatic vessels (Figure 20), underscoring the exclusive ability of myeloid cells to contribute to tumor lymphangiogenesis and excluding the possibility that minor contaminations of haematopoietic stem cells in the FACS-sorted fractions may have contributed to the GFP$^+$ cells that incorporated into tumor lymphatics.

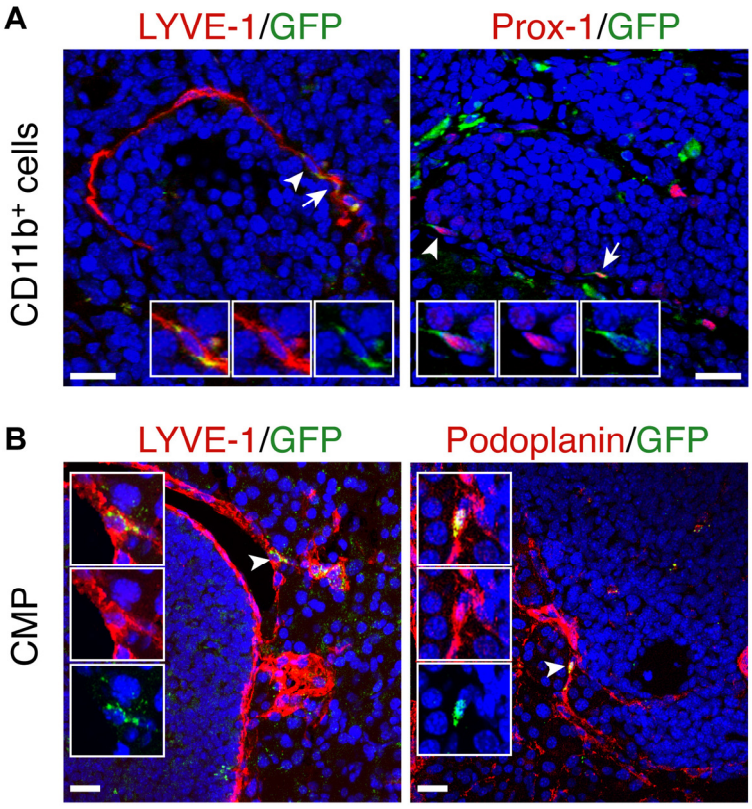

Figure 19. Adoptive transfer of myeloid lineage cells. (**A**) CD11b$^+$ myeloid cells integrate into tumor-associated lymphatic vessels. FACS-sorted CD11b$^+$/GFP$^+$ cells were adoptively transferred into non-irradiated RT2;VC mice (3 mice). 7-20 μm histological pancreatic sections of transplanted mice were stained for the lymphatic markers LYVE-1 and Prox-1 (red) and for GFP (green) and analyzed by confocal microscopy. Representative tumor sections are shown. Arrows indicate double-positive cells and arrowheads indicate double-positive cells shown in inset magnifications (first inset: merged channels, second and third insets: red and green channel, respectively). (**B**) Common myeloid progenitor (CMP) cells integrate into tumor-associated lymphatic vessels. FACS-sorted lin$^-$/Sca-1$^-$/IL7Ra$^-$/cKit$^+$ CMP cells were adoptively transferred into semi-lethally irradiated RT2;VC mice. Histological sections of tumors of the transplanted mice were stained for LYVE-1 or Podoplanin (red) and for GFP (green) and analyzed as in (**A**). Arrowheads indicate cells double-positive for GFP and LYVE-1 or Podoplanin shown in inset magnifications (first inset: merged channels, second and third insets: red and green channel, respectively). DAPI stains nuclei (blue). Scale bar: 20 μm.

In order to assess potential fusion events between bone marrow-derived cells and pre-existing lymphatic endothelial cells, lethally irradiated triple-transgenic RT2;VC;Z/EG mice were transplanted with bone marrow isolated from CD11b-Cre mice. Fusion of $CD11b^+$ BMDC, expressing the Cre recombinase, with host (tumor lymphatic endothelial) cells would result in GFP expression from the recombined Z/EG locus. Seven weeks after transplantation, no GFP^+ cells were detected in or around lymphangiogenic insulinomas, indicating that Cre-expressing, bone marrow-derived myeloid cells had not fused with RT2;VC;Z/EG lymphatic endothelial cells or any other host cell (data not shown).

These results demonstrate that cells found integrated into growing tumor lymphatic vessels can have a myeloid origin and that bone marrow-derived lymphatic progenitor cells are at least in part derived from the already myeloid-committed haematopoietic lineage.

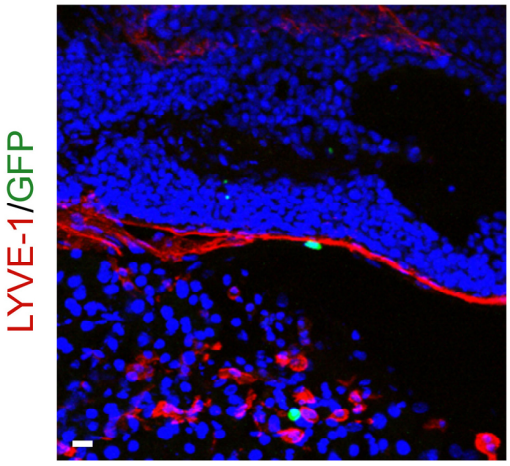

Figure 20. $CD19^+$ B lymphocytes do not integrate into tumor-associated lymphatics. FACS sorted $CD19^+/GFP^+$ cells were adoptively transferred into semi-lethally irradiated RT2;VC mice (2 mice). 3 weeks after transfer, mice were sacrificed and tumor sections were stained for the lymphatic marker LYVE-1 (red) and for GFP (green) and analyzed by confocal microscopy. No GFP^+ cells co-expressing LYVE-1 could be observed. DAPI was used for nuclear counterstaining (blue). Scale bar: 20 μm.

Depletion of macrophages

To assess the functional contribution of macrophages to tumor lymphangiogenesis, RT2;VC mice were treated with liposome-encapsulated Clodronate (ClodroLip) or PBS as vehicle-control for four weeks to ablate TAM (Van Rooijen, 1989; Van Rooijen and Sanders, 1994). Successful macrophage depletion was achieved as shown by reduced F4/80 immuno-reactivity in ClodroLip treated mice (Figure 21A). Peri-tumoral lymphatic vessel density (LVD) was significantly decreased in ClodroLip vs. PBS treated mice (Figure 21B; treated: median 70%, mean: 61% vs. control: median 90%, mean 74.9%; $P < 0.01$). In contrast to a recent study where ClodroLip reduced tumor growth of xenotransplants in immuno-compromised mice (Zeisberger et al., 2006), average tumor volume, tumor incidence and blood vessel density were not significantly reduced in our experiments (Figure 22). To evaluate the amount of VEGF-C and VEGF-D provided by TAM, $CD11b^+$ cells were isolated from RT2 or RT2;VC tumors and mRNA levels were assessed by quantitative PCR and compared to levels in total RT2 tumors. The expression of endogenous

murine VEGF-C and D in tumors (not considering the high levels of transgenic human VEGF-C expression in RT2;VC mice) was higher than in TAM (Figure 21). From these results we conclude that macrophages contribute to tumor lymphangiogenesis in RT2;VC mice by processes other than the secretion of the main lymphangiogenic factors.

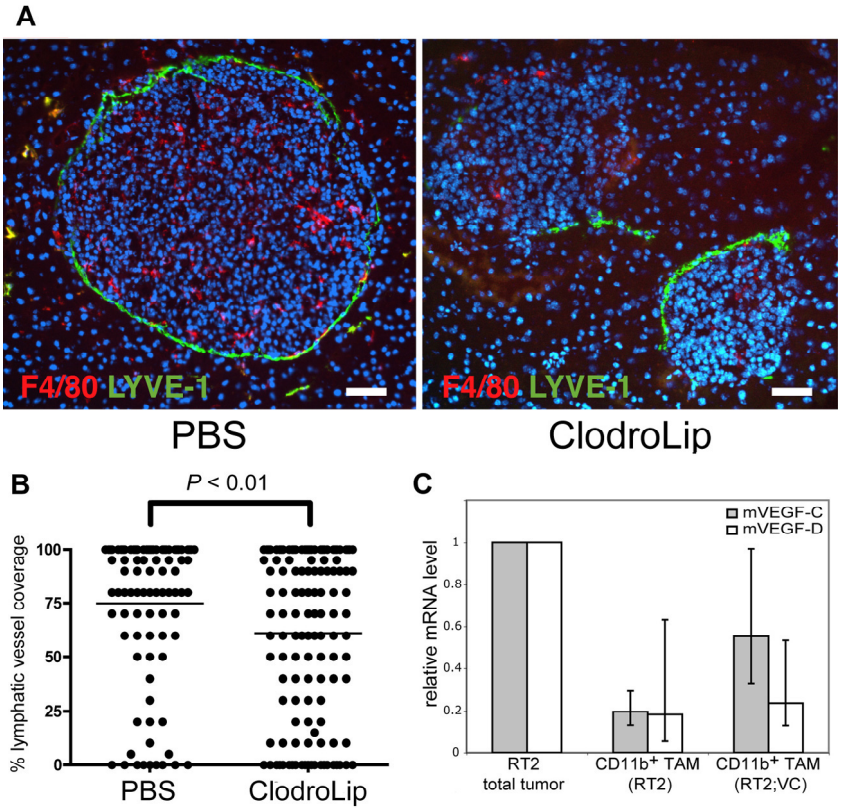

Figure 21. Depletion of macrophages reduces peritumoral lymphatic vessel density. (**A**) RT2;VC mice were treated with liposome-encapsulated Clodronate (ClodroLip). Pancreatic sections representing a total of 5 PBS vehicle control-treated mice (97 tumors) and 6 ClodroLip-treated (132 tumors) mice were analyzed. Successful depletion of intra- and extra-tumoral macrophages in ClodroLip-treated mice is illustrated by the reduction of F4/80 immunoreactivity (red). Co-staining with the lymphatic endothelial marker LYVE-1 (green) reveals a reduced coverage of tumors by lymphatic vessels in ClodroLip-treated mice vs. in PBS-treated mice. DAPI was used for nuclear counterstaining (blue). T: tumor. Scale bar: 50 μm. (**B**) Tumors of ClodroLip and control-treated mice were analyzed by immunofluorescence staining with antibodies against LYVE-1 for the extent of lymphatic vasculature surrounding the perimeter of the tumors. Tumors of control-treated mice were surrounded by 90% or more with lymphatic vessels (median 90%, mean 74.9%), whereas tumors of ClodroLip-treated mice had significantly lower coverage (median 70%, mean 61.1%; $P < 0.01$, Mann-Whitney test). (**C**) Tumor-associated $CD11b^+$ macrophages (TAM) were isolated from tumors of RT2 or RT2;VC mice by flow cytometry, and mRNA levels for murine VEGF-C and VEGF-D were quantified using real-time PCR and compared to levels in total tumors. Shown is the result of three independent TAM isolations.

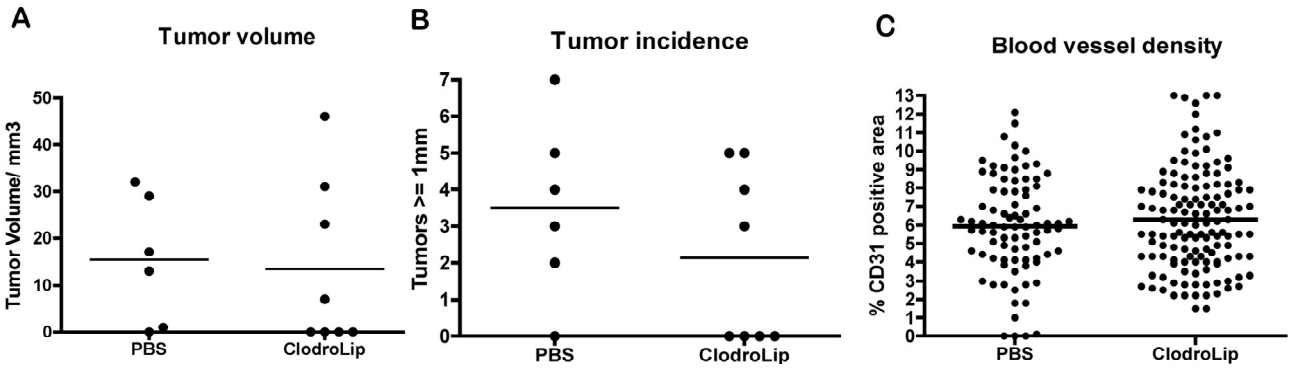

Figure 22. Macrophage depletion does not affect tumor growth. RT2;VC mice were treated for 4 weeks either with PBS (vehicle control) or with ClodroLip as described in Methods in order to deplete intra- and peritumoral macrophages. Tumor volume has been determined as the total volume of tumors per mouse (A), tumor incidence is the number of tumors larger than 1mm per mouse (B), and blood vessel density is the % area fraction of CD31 staining, as determined using ImageJ image analysis software (C). None of these parameters was significantly altered between ClodroLip- and control-treated mice.

Macrophages form lymphatic-like structures *in vitro*

We next investigated whether bone marrow-derived macrophages had an intrinsic capability to form lymphatic vessel-like structures. Employing a well-established protocol of *in vitro* macrophage differentiation (Gatfield and Pieters, 2000), bone marrow cells were cultured for 7 days in 30% M-CSF-containing medium to induce the specific differentiation of progenitor cells into non-activated macrophages. Flow cytometric analysis confirmed the macrophage identity ($CD11b^+$/ $F4/80^+$) of these cells (Figure 23A). The bone marrow-derived-macrophages were then activated with LPS and seeded on Matrigel to monitor differentiation and tube formation. After two days in a defined endothelial cell-specific medium, macrophages associated in clumps, before forming tube-like structures with increasing connections between days 3 and 15 (Figure 23A). Confocal immunofluorescence microscopy analysis at day 12 revealed that these tube-like structures stained positively for the lymphatic marker Podoplanin. Notably, only macrophages that had formed tube-like structures and not single isolated cells expressed the lymphatic marker (Figure 23B). Furthermore, quantitative PCR analysis of mRNA from macrophages isolated either before or after the tube formation process revealed a marked up-regulation of the lymphatic markers LYVE-1, Prox-1, VEGFR3, Foxc2 and Foxc1 as well as a down-regulation of the hematopoietic/monocytic markers CD45 and CX3CR1 during tube formation. Exclusion of individual growth factors revealed the requirement of FGF-2 for tube formation (Figure 23C), whereas the other supplemental growth factors (VEGF-A, IGF-1, EGF, hydrocortisone) were dispensable. Notably, mRNA levels of FGF receptors-1 and 2 increased during tube formation (Figure 23C).

In order to assess the capacity of myeloid cells to integrate into lymphatic structures *in vitro*, GFP-labeled macrophages were generated as described above from bone marrow of actin-GFP transgenic mice and subsequently cultured on Matrigel alone or in combination with SV40 T antigen-immortalized murine lymphatic endothelial cells (SV-LEC) (Ando et al., 2005). Five days later, the cultures were stained for Podoplanin. Cultured SV-LEC formed tube-like structures positive for Podoplanin expression (Figure 23D/1), and cultured *in vitro* activated macrophages were positive for GFP (Figure 23D/2). In mixed cultures, bone marrow-derived macrophages lined up with SV-LEC, incorporating into tube-like structures and expressed Podoplanin (Figure 23D/3-6). Interestingly, GFP^+ macrophages were predominantly located at the tips and at branch points of growing tube-like structures (Figure 23D/3-6) and seemed to guide SV-LEC to form a new sprout as observed by time-lapse video microscopy (Figure 24, supplemental video 3, on CD). These results demonstrate that bone marrow-derived macrophages have the ability to form lymphatic tube-like structures as well as to incorporate into lymphatic structures *in vitro* and suggest a role of these cells in lymphatic endothelial cell sprouting *in vitro*.

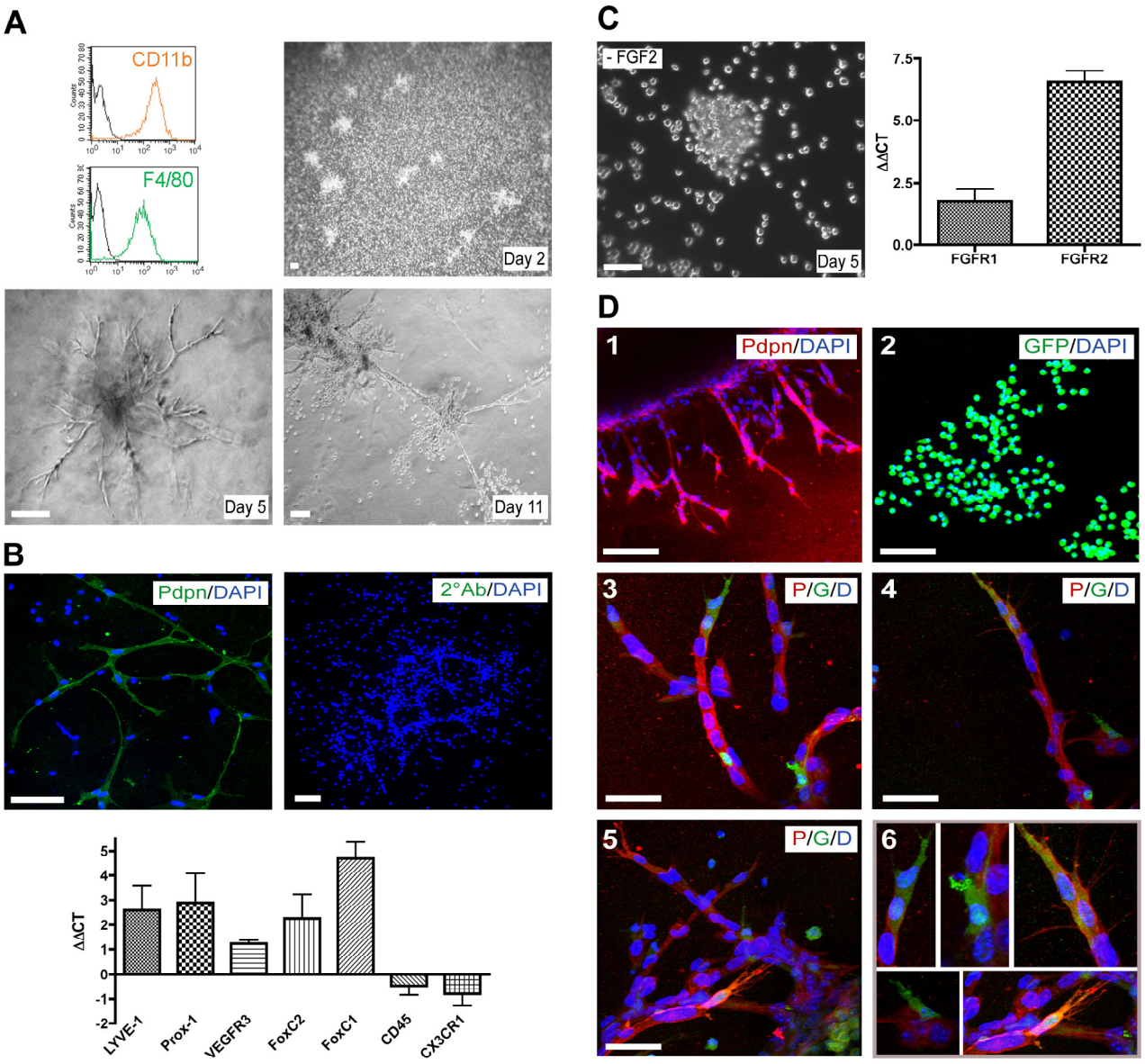

Figure 23. Bone marrow-derived-macrophages form lymphatic-like structures *in vitro.* (**A**) *In vitro* generated macrophages showed a specific marker expression profile ($CD11b^+$/ $F4/80^+$) (upper left panel). Tube formation on Matrigel was monitored by phase-contrast microscopy. At day 2, macrophages formed clusters. Between days 3 and 15, they developed into tube-like structures with numbers of branches increasing over time. Scale bar: 100 μm. (**B**) Immunofluorescence staining against Podoplanin (Pdpn) revealed that macrophages having formed tube like structures express Podoplanin whereas single cells do not. Staining of the tubular structures in the absence of any primary antibody was used as a control (2°Ab). DAPI stains nuclei (blue). Scale bar: 100 μm. Quantitative PCR analysis revealed that upon tube formation, macrophages up-regulate the expression of lymphatic markers (LYVE-1, Prox-1, VEGFR3, Foxc2, Foxc1) and down-regulate hematopoietic/myeloid markers (CD45, CX3CR1). ΔΔCT corresponds to the difference between the normalized CT values of macrophages forming tubes (day 8) and macrophages not having formed tubes yet (day 1). (**C**) FGF-2 is required for macrophage tube formation as its specific exclusion from culture medium abrogated this process (left panel). Furthermore, analysis of mRNA levels revealed up-regulation of FGF receptors -1 and -2 during tube formation. (**D**) Immortalized $Podoplanin^+$ murine lymphatic endothelial cells (SV-LEC) (panel 1), GFP-labeled bone marrow-derived-macrophages (panel 2), and mixed cultures of macrophages and SV-LEC (panels 3-6) were seeded in Matrigel. At day 5, cells were stained for Podoplanin (red) and analyzed by confocal microscopy. Mixed cultures demonstrate that bone marrow-derived macrophages contribute to SV-LEC-mediated tube formation: GFP^+ cells (green) are found integrated into $Podoplanin^+$ tube-like structures. Note the preferential integration of bone marrow-derived macrophages at the tips and branch points of sprouting tube-like structures formed by SV-LEC (magnified in panel 6). DAPI stains nuclei (blue). Scale bars: 100 μm (panels 1 and 2) and 50 μm (panels 3 to 6).

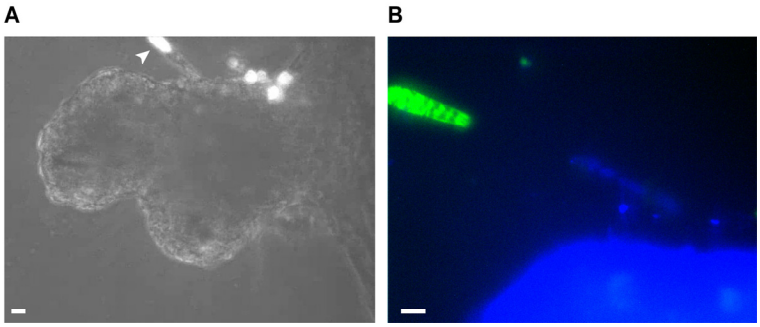

Figure 24. Macrophages initiate lymphatic endothelial cell tube formation in an *in vitro* co-culture system. (**A**) Phase contrast microscopy of SV40 large T antigen-immortalized lymphatic endothelial cells (SV-LEC) co-cultured with GFP^+ macrophages in Matrigel. GFP^+ macrophages are detected by their bright signal in phase-contrast microscopy. As an initial step, SV-LEC associate into compact cell aggregates with concomitant recruitment of macrophages. As indicated by an arrowhead, after 1 day, GFP^+ macrophages could be observed leading outgrowing SV-LEC tubes. (**B**) Immunofluorescence microscopy of a magnification of the same field depicted in (**A**) showing the tube-leading GFP^+ macrophage followed by four Hoechst-stained SV-LEC. Scale bars: 10 μm.

Supplemental videos

Supplemental video 1

3D reconstitution of a 20μm tissue section of a tumor, derived from a RT2;VC mouse transplanted with GFP labeled bone marrow. The arrow indicates a GFP^+ cell (green) integrated in the $Podoplanin^+$ (red) lymphatic vessel. The arrowhead indicates a GFP^+ cell not completely integrated (noticeable only at certain angles). Ex: exocrine pancreas, L: lymphatic vessel lumen, T: tumor.

Supplemental video 2

3D reconstitution of a 7μm tissue section of a TRAMP-C1 tumor, grown in a GFP-labeled bone marrow-transplanted C57BL/6 mouse. The arrow indicates a GFP^+ cell (green) integrated in the $Podoplanin^+$ (red) lymphatic vessel.

Supplemental video 3

Macrophages initiate lymphatic endothelial cell tube formation in *in vitro* co-culture. Time-lapse video microscopy after 24h co-culture of SV-LEC and GFP^+ macrophages on Matrigel. GFP^+ macrophages were distinguished from SV-LEC by their bright signal in phase-contrast. The movie shows a GFP^+ macrophage located at the rim of SV-LEC compact structure initiating outgrowth of a tube-like structure. As also visible in Figure S7, the SV-LEC follow the tube-leading macrophage in the newly forming tube-like structure.

4.2.4. Discussion

Research on BMDC in patho-physiological processes, such as atherosclerosis, limb/heart ischemia and cancer, has in the past mainly focused on the importance of haematopoietic cells in promoting or attenuating inflammation, in clearing cancer cells, or in inducing immunological tolerance to neoplastic lesions. However, recent findings indicate that the bone marrow is also a rich source of progenitor cells with mesenchymal and endothelial potential (Bertolini et al., 2006; Gregory et al., 2005). In the case of endothelial progenitor cells, the lineage relationship to the haematopoietic system is not clear. While some experiments suggest the existence of an adult haemangioblast, a progenitor cell of both haematopoietic and endothelial lineage (Pelosi et al., 2002), others support a pathway of differentiation of myeloid cells to endothelial cells (Bailey et al., 2006; Loomans et al., 2006).

Here, we have used bone marrow transplantation experiments in two different mouse models of carcinogenesis to demonstrate that BMDC significantly contribute to tumor lymphangiogenesis, but rarely integrate into tumor blood vessels. About 3% of lymphatic endothelial cells in the periphery of lymphangiogenic tumors are of bone marrow origin, a contribution comparable to findings in rejected human kidney transplants (Kerjaschki et al., 2006) and in liver, stomach and intestine of HSC transplanted mice (Jiang et al., 2008). Moreover, we have performed lineage tracing experiments to obtain insights into the ontogeny of bone marrow-derived TLEC. First, transplantations of FACS-sorted bone marrow fractions representing different haematopoietic lineages or of total bone marrow expressing GFP under a myeloid specific promoter indicate that integrated BMDC are derived from the myeloid lineage. Second, genetic tagging of myeloid cells with GFP confirms this notion; cells that have passed through the myeloid linage are found integrated into the lymphatic vasculature surrounding tumors. Third, depletion of tissue macrophages using ClodroLip significantly reduces peri-tumoral lymphatic vessel density, demonstrating a functional role of macrophages in tumor lymphangiogenesis. In order to directly assess whether macrophage depletion would abolish BMDC integration into tumor lymphatic vessels, we have combined bone marrow transplantation and ClodroLip treatments, yet due to a high mortality rates we had to terminate these experiments. Fourth, the contribution of macrophages to lymphatic structures is recapitulated in an experimental *in vitro* system.

Taken together, our results from experiments *in vivo* and *in vitro* demonstrate that cells of the myeloid lineage physically contribute to tumor lymphangiogenesis. We therefore propose a model in which lymphatic vessel growth not only relies on the proliferation, migration and sprouting of pre-existing lymphatic endothelial cells but also depends on the trans-differentiation of cells of the myeloid lineage into lymphatic endothelial cells. The existence of specific lymphatic progenitor cells (LPC), distinct from haematopoietic as well as blood endothelial progenitor cells, has not been established. Based on a number of control experiments, such as the transplantation of FACS-

sorted $CD19^+$ B-cells or the adoptive transfer of $CD11b^+$ myeloid cells into non-irradiated recipients, we exclude the possibility that FACS-sorted cell fractions may have contained haematopoietic stem cells that also reconstitute potential LPC. Rather, our data indicate a myeloid origin of cells that trans-differentiate into lymphatic endothelial cells, thus supporting the notion that LPC reside at least partially within an already committed haematopoietic lineage.

BMDC integration into newly formed lymphatic vessels has been shown to take place mainly under inflammatory or wound healing conditions (Kerjaschki et al., 2006; Maruyama et al., 2007; Maruyama et al., 2005). Our results support this notion, since transplanted, non-tumor bearing mice did not show any BMDC integration into lymphatic vessels. In support, normal tissue lymphatics of TRAMP-C1 tumor-bearing CD11b-Cre;Z/EG mice did not show any incorporation of myeloid-derived cells. In summary, we demonstrate here that in the inflammatory context of tumor growth, cells of the myeloid lineage participate in tumor lymphangiogenesis. Since tumor lymphatic vessels provide a route for metastatic dissemination, understanding the functional role of bone marrow-derived tumor lymphatic endothelial cells seems warranted.

4.2.5. Materials and Methods

Mouse strains

Generation and phenotypic characterization of Rip1Tag2, Rip1VEGF-A and Rip1VEGF-C mice have been described previously (Gannon et al., 2002; Hanahan, 1985; Mandriota et al., 2001). C57BL/6-Tg(ACTB-EGFP)mice (Okabe et al., 1997) and Z/EG mice (Novak et al., 2000) were provided by K. Hafen (University of Basel). CD11b-Cre mice (Ferron and Vacher, 2005) and CX3CR1$^{+/GFP}$ mice (Jung et al., 2000) were obtained from J. Vacher (University of Montreal) and C. Rüegg (CePO Lausanne), respectively. All experiments involving mice were performed in accordance with the guidelines of the Swiss Federal Veterinary Office (SFVO) and the regulations of the Cantonal Veterinary Office of Basel-Stadt.

Total bone marrow transplantations

Bone marrow cells were extracted under sterile conditions from femurs and tibiae from donor mice indicated in Figure 1. After T cell depletion (Benard et al., 2006), 5 x 10^6 cells were injected in the tail vein of lethally irradiated (2 x 550 cGy) 6 week old mice which were sacrificed for further analysis 5 to 7 weeks after transplantation.

TRAMP-C1 subcutanous tumor model

5x10^5 TRAMP-C1 cells (Foster et al., 1997) (provided by N. Greenberg, FHCRC, Seattle) were injected into the flank of either GFP-labeled bone marrow transplanted C57BL/6 mice (4 weeks after transplantation) or CD11b-Cre;Z/EG mice and grown for 3 to 4 weeks.

Flow cytometric analysis

Cells were washed in PBS supplemented with 5% FBS, Fc-blocked with a monoclonal antibody against mouse CD16/CD32 (Clone 2.4G2, Pharmingen), and stained with directly-labeled monoclonal antibodies against mouse CD19 (Clone MB19-1, eBioscience), CD3 (Clone 145-2C11, eBioscience), CD11b (Clone M1/70.15, CALTAG), F4/80 (Clone CI:A3-1, Serotec), LYVE-1 (Clone ALY7, CliniSciences), CD31 (Clone 390, eBioscience). Podoplanin expression was revealed by hamster anti-mouse Podoplanin (Clone 8.1.1), followed by biotinylated anti-hamster-IgG antibody and streptavidin-PE (eBioscience). Stained cells were analyzed on a FACSCanto II using DIVA software (Becton Dickinson). Dead cells were excluded by a combination of light scatter and PI fluorescence. Cell duplets were excluded by forward scatter pulse width. Peripheral blood mononuclear cells were isolated by Ficoll–Histopaque (SIGMA) density-gradient centrifugation. Bone marrow cells were extracted from mouse femurs and tibiae by flushing. Tumor single cell

suspensions were obtained by digestion for 45 minutes at 37° C using the following digestion buffers: TRAMP-C1: HEPES buffered saline, 0.1mg/ml DNaseI (Roche), 1mg/ml collagenase I (SIGMA); RT2: DMEM, 5% NU serum (Becton Dickinson), 0.2mg/ml DNaseI, 1.2U/ml DispaseII (Roche Applied Science).

$CD11b^+$ and CMP cell sorting and adoptive transfer

Bone marrow cells were extracted from femurs and tibiae of female C57BL/6-Tg(ACTB-EGFP) mice, washed in PBS/ 2% BSA, Fc blocked and stained with a phycoerythrin (PE)-conjugated monoclonal antibody against mouse CD11b (CALTAG) or, for CMP isolation, lineage markers, CD3, CD4 (Clone GK1.5), CD8 (Clone 53-6.7), Ter119 (Clone TER-119), B220 (Clone RA3-6B2), CD19, Gr-1 (Clone RB6-8C5), Sca-1 (Clone D7), IL7Ra (Clone A7R34) and Allophycocyanin-labeled anti-cKit (Clone 2B8) (all from eBioscience). $CD11b^+$ GFP^+ or CMP (lineage$^-$/ Sca-1$^-$/ IL7Ra$^-$/ cKit$^+$) cells were sorted on a FACSAria (Becton Dickinson) with a purity > 98%. 4 x 10^5 $CD11b^+$ or 4 x 10^4 CMP were injected in the tail vein of semi-lethally (450 cGy) or non irradiated 9 week old RT2;VC mice, which were sacrificed 3 weeks after transplantation.

Histological analysis

7 or 20 μm cryosections from pancreata or TRAMP-C1 tumors were prepared and stained as described (Bailey et al., 2006). When required, PBS/0.2% Triton-X-100 was used for permeabilization. The following primary antibodies were used: rat anti-mouse LYVE-1 (Clone ALY-7, MBL, Japan), rabbit anti-mouse LYVE-1 (Reliatech, Germany), rabbit anti-mouse Prox-1 (K. Alitalo, University of Helsinki), goat anti-human Prox-1 (R&D Systems), rabbit anti-Podoplanin (D. Kerjaschki, Medical University Vienna), hamster anti-mouse Podoplanin (Clone 8.1.1), rat anti-mouse VE-Cadherin hybridoma supernatant (Clone B14, E. Dejana, University of Milano), rat anti-mouse F4/80 (Clone CI:A3-1, Serotec), rat anti-mouse CD11b (Clone M1/70.15, Serotec) and rat anti-mouse CD31 (Clone MEC 13.3, Pharmingen). Alexa Fluor 488-, 568- and 633-labeled secondary antibodies (Molecular Probes) were used. Alexa Fluor 488-conjugated rabbit anti-GFP antibody (Molecular Probes) was employed for the detection of GFP. DAPI (SIGMA) was used for nuclear counterstaining. Sections were analyzed on a Nikon Diaphot 300 immunofluorescence microscope (Nikon) using Openlab 3.1.7. software (Improvision) or with a LSM 510 Meta confocal microscope using LSM software for 2D and 3D analysis (Zeiss). Videos were created using Imaris 6.1.1 software (Bitplane Scientific Solutions, Zurich, Switzerland).

ClodroLip-mediated macrophage depletion

Eight week old RT2;VC mice were injected *i.p.* every 4 days for 4 weeks with 80mg/kg body weight (first injection) or 40mg/kg body weight (following injections) ClodroLip or with an equal

volume of PBS as control. 2 days after the last injection, mice were sacrificed, pancreata were embedded in OCT and snap frozen in liquid nitrogen. Tumor macrophage depletion and tumor lymphatic vessel coverage were determined by immunofluorescence stainings with anti-F4/80 antibodies and anti-LYVE-1 antibodies, respectively, and ImageJ software (http://rsb.info.nih.gov/ij/). Statistical analysis and graphs were performed with GraphPad Prism software (GraphPad Software Inc.). Non-parametric Mann-Whitney tests were used to compare tumor lymphatic vessel coverage of treated versus control mice.

Isolation of tumor associated macrophages

Single cell suspensions of tumors from 13-14 week old RT2 or RT2;VC mice were obtained as described above, washed in FACS buffer (PBS/ 2% BSA/ 5mM EDTA) and stained with anti-CD11b-PE. 20'000 – 50'000 $CD11b^+$ cells were sorted on a FACSAria directly into TRIZOL reagent (Invitrogen).

Quantitative real time RT–PCR

Total RNA was prepared using TRIZOL, and reverse transcribed with random hexamer primers using M-MLV reverse transcriptase (SIGMA). cDNA was quantified on a ABI Prism 7000 light cycler (Applied Biosystems) using SYBR green PCR MasterMix (Fermentas) using the following primers: mVEGFC: fwd: 5'-AGCAGCCACAAACACCTTCTT-3', rev: 5'-TCAAACAACGTCTTGCTGAGG-3'; mVEGFD: fwd: 5'-GCACCTCCTACATCTCCAAACAG-3', rev: 5'-GGCAAGCACTTACAACCCGTAT-3'; mFGFR1: fwd: 5'-TGTTTGACCGGATCTACACACA-3', rev: 5'-CTCCCACAAGAGCACTCCAA-3'; mFGFR2: fwd: 5'-TCGCATTGGAGGCTATAAGG-3', rev: 5'-CGGGACCACACTTTCCATAA-3'; mLYVE-1: fwd: 5'-GGTGTCCTGATTTGGAATGC-3', rev: 5'-AGGAGTTAACCCAGGTGTCG -3'; mProx-1: fwd: 5'-AAGAGAGAGAGAAAGAGAGAGAGTGG-3', rev: 5'-TGGGCACAGCTCAAGAATC-3'; mVEGFR3: fwd: 5'-CGTGTGTGAAGTGCAGGATAGG-3', rev: 5'-TCACTCACGTTCACCAGGAGGT-3'; mFoxC1: fwd: 5'-GCTTTCCTGCTCATTCGTCTT-3', rev: 5'-AAATATCTTACAGGTGAGAGGCAAG-3'; mFoxC2: fwd: 5'-GACCCTAGCTCGCTGACG-3', rev: 5'-CACCAGCCCTTCCGAGT-3'; mCD45: fwd: 5'-CAAAAGCAGATCGTCCGGA-3', rev: 5'-TGTCGGCCGGGAGGTT-3'; mCX3CR1: fwd: 5'-AAGTTCCCTTCCCATCTGCT-3', rev: 5'-CAAAATTCTCTAGATCCAGTTCAGG-3'; mRPL19: fwd: 5'-ATCCGCAAGCCTGTGACTGT-3', rev: 5'-TCGGGCCAGGGTGTTTTT-3'. Ct values were normalized against ribosomal protein L19 (RPL19).

Tube formation assay using bone marrow-derived-macrophages

Bone marrow cells were extracted from femurs and tibiae of C57BL/6 or C57BL/6-Tg(ACTB-EGFP) mice and cultured on Teflon plates for 7 days in DMEM supplemented with 10%

FBS, 2 mM glutamine, 100 units/ml penicillin and 30% L929 cell conditioned media containing M-CSF. Bone marrow-derived-macrophages were collected with PBS/ 1 mM EDTA. Matrigel (Becton Dickinson) was mixed 1:1 with endothelial cell medium (EGM-2 MV, Cambrex) and allowed to solidify for 1 hour at 37°C in 8-chamber slides. 2-3 x 10^5 bone marrow-derived macrophages or immortalized lymphatic endothelial cells (SV-LEC) or a mixture of each 1.5 x 10^5 cells each in EGM-2 MV supplemented with 1 μg/ml LPS were seeded on the polymerized matrigel and tube formation was monitored up to 20 days. Immunofluorescence staining of tube-like structures was performed as described (Debnath et al., 2003). For time-lapse video microscopy, Hoechst labeled SV-LEC and GFP^+ macrophages were co-cultured as described above and pictures were taken every 10 minutes for a period of 12 hours using a Zeiss Axiovert 35M microscope (Zeiss), Princeton Instruments CCD camera and Metamorph Imaging software (Universal Imaging Corporation).

Acknowledgements

We would like to thank F. Lehembre and M. Cabrita for critical comments on the manuscript. We are grateful to K. Alitalo, D. Kerjaschki, A. Rolink, K. Hafen, E. Dejana, and J. Vacher for advice, reagents and mice, and H. Antoniadis, U. Schmieder, K. Strittmatter and R. Jost for technical support. This work was supported by the EU-FP6 framework programme LYMPHANGIOGENOMICS LSHG-CT-2004-503573 (GC), the National Centre of Competence in Research (NCCR) Molecular Oncology of the Swiss National Science Foundation (GC and CR), and a Comprehensive Cancer Research Project (CCRP) of the Swiss Cancer League (GC and CR).

4.3. Depletion of macrophages in Rip1Tag2/ NCAM$^{+/-}$ mice reduces blood vessel density but not lymphangiogenesis

Tumors in Rip1Tag2 mice/ NCAM$^{+/-}$ mice have previously been shown to metastasize to regional lymph nodes by a "passive" mechanism, by which tumor disaggregation facilitates spreading of tumor cells to the pancreatic lymph nodes (Perl et al., 1999). This lympho-genic spreading of tumor cell clusters might be supported by ongoing lymphangiogenesis in NCAM-deficient Rip1Tag2 tumors (Crnic et al., 2004), where tumor cell clusters within lymphatic vessels were detected. In order to evaluate the role of macrophages on tumor lymphangiogenesis and angiogenesis, we treated Rip1Tag2;NCAM$^{+/-}$ mice using ClodroLip in to deplete the macrophages. Analysis of immune cell infiltration by FACS, similar to section 4.1., did not reveal differences in the overall infiltration between Rip1Tag2 and Rip1Tag2;NCAM$^{+/-}$ for CD11b^{+}, F4/80^{+} or Gr-1^{+} myeloid cells (data not shown). This indicates, that NCAM-deficiency does not trigger a differential immune cell infiltration.

Macrophage depletion was performed with using Clodronate liposomes as described in section 4.2.5., starting at ten weeks of age and giving 4 supplementary doses over 3 weeks until analysis (Figure 25A). Body weight was monitored and it was detected that ClodroLip treatment resulted in body weight loss, which could lead up to 30% body weight loss upon ClodoLip treatment (Figure 25B). At analysis, tumor volume but not incidence of ClodroLip-treated mice was moderately reduced as compared to PBS treatment (Figure 25C). When we analyzed macrophage infiltration by immunofluorescence for F4/80, we detected a highly significant reduction of macrophages in tumors (Figure 25D). Interestingly, F4/80/ LYVE-1 double-positive macrophages, usually found around the tumor and in the exocrine pancreas (arrowheads in Figure 25D, left panel), were completely absent in ClodroLip-treated animals. This suggests a high phagocytotic activity of those cells and a good penetration of the ClodroLip into the exocrine pancreas. We then analyzed the tumor microvessel and lymphatic vessel density using CD31 and LYVE-1, respectively (Figure 26A). CD31 immunoreactivity was measured by either quantifying the number of vessels per area or by quantifying the percentage of area occupied by these vessels (Figure 26B). Using both readouts, a significantly lower number of blood vessels was observed in tumors of ClodroLip vs. PBS treated mice. The tumor's lymphatic vessel coverage of the mice in this experiment was very low, and we could not detect differences in the amount of lymphatic structures around the tumors (Figure 26C). To test if the reduced blood vessel density had an effect on proliferation of tumor cells, we stained the sections for the mitotic marker Phospho-Histone H3, indicative of cell division. No difference in proliferation was detected (Figure 26D).

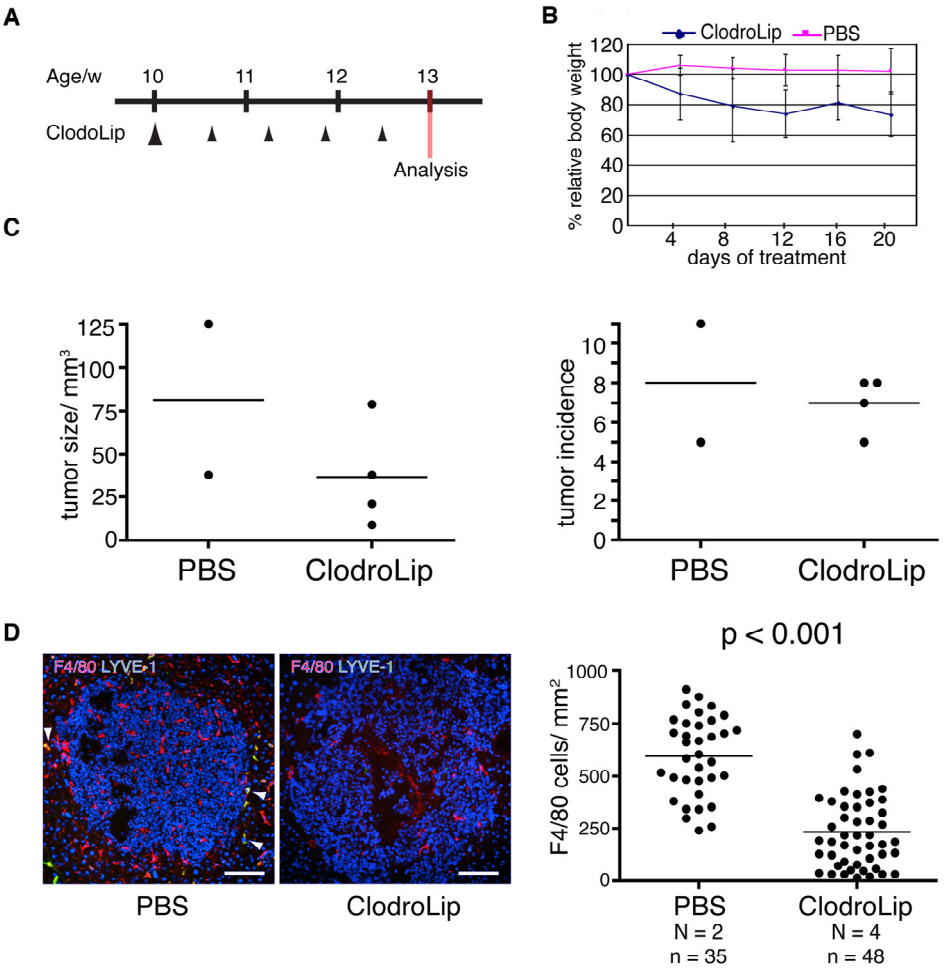

Figure 25. ClodroLip treatment reduces intratumoral macrophages. (**A**) Mice were treated with ClodroLip or PBS by *i.p.* injection starting at 10 weeks age and given four consecutive injections and analyzed at 13 weeks. (**B**) ClodroLip treatment induces body weight loss up to 30% compared to the beginning of the experiment. (**C**) Tumor volume but not incidence is reduced in ClodroLip vs. PBS treated mice (N too low for statistical evaluation). (**D**) ClodroLip treatment efficiently depletes intra- and extratumoral macrophages, as assessed by F4/80 staining. Extratumoral LYVE-1/ F4/80 double positive macrophages (arrowheads) are completely absent in treated mice. Right panel: quantification of intratumoral macrophages (N: number of mice, n: number of tumors). Student's unpaired two-tailed t-test. Scale bar: 100μm.

This section's results contrast with another ClodroLip treatment (presented in "4.2.3. Depletion of macrophages") by the reduced blood vessel density in this experiment, not observed in the other study. In the regimen used in this trial, mice were treated at a later timepoint, and this seems to negatively influence the effect of ClodroLip on the general health status, as evidenced by the reduced body weight. Even though blood vessel density was reduced in tumors of ClodroLip treated mice, other tumor parameters were not or not significantly altered. It seems therefore likely that macrophage function is not essential for angiogenesis and tumor growth in Rip1Tag2 mice. It has been previously shown that neutrophils are important for providing MMP9 and supporting the angiogenic switch in Rip1Tag2 tumors (Nozawa et al., 2006).

As the lymphangiogenesis phenotype of Rip1Tag2;NCAM$^{+/-}$ is very moderate in this experiment, we cannot draw a conclusion on the effects of macrophages on stochastic, endogenous lymphangiogenesis. Correlation analysis performed on Rip1Tag2 and Rip1Tag2;NCAM$^{+/-}$ mice did not show a correlation between intra-tumoral or peripheral macrophage infiltration and either genotype (Rip1Tag2 vs. Rip1Tag2;NCAM$^{+/-}$) or extent of peritumoral lymphangiogenesis (data not shown).

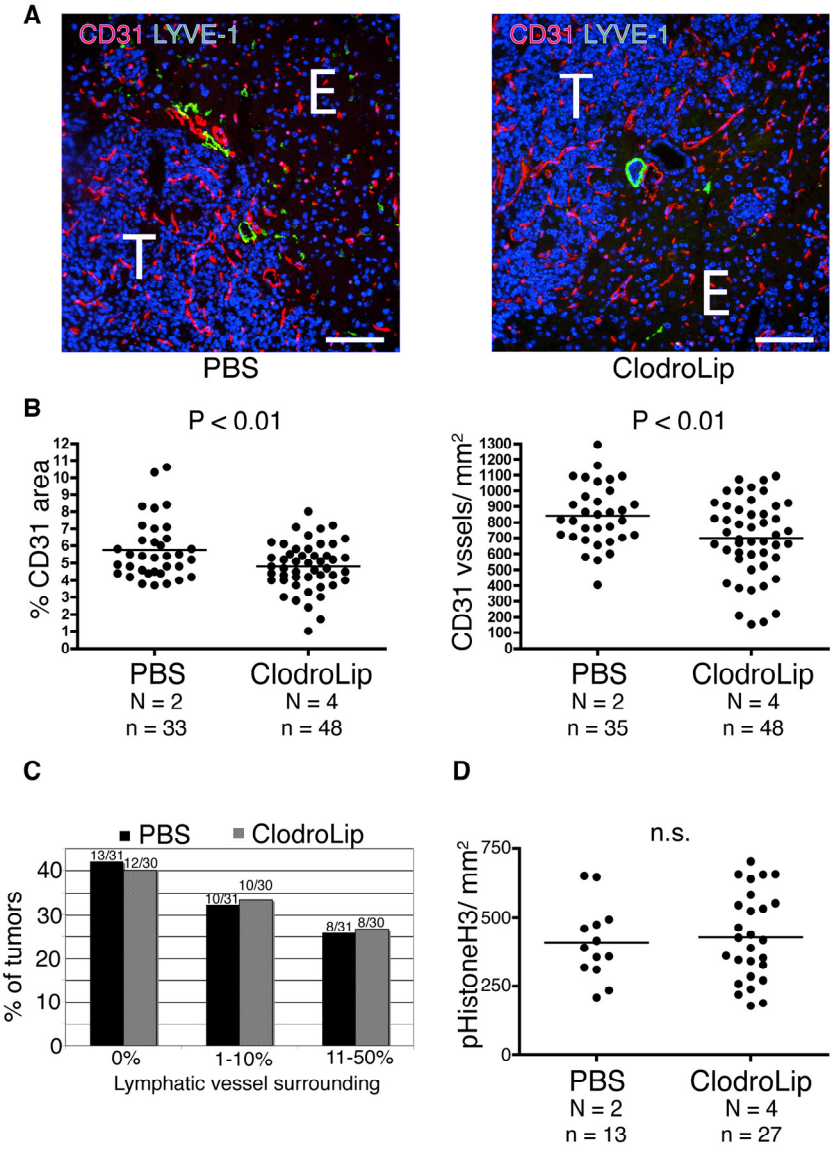

Figure 26. ClodroLip treatment reduces blood vessel density. (**A**) Pancreatic sections were stained for blood vessel marker CD31 and lymphatic vessel marker LYVE-1. (**B**) ClodroLip treatment induces a slight but significant reduction of blood vessel density (left panel: CD31 area fraction, right panel: number of vessels). (**C**) No difference is found in the distribution between not (0% surrounded by LYVE-1 vessels), slightly (1-10% surrounded) or moderately (11-50% surrounded) lymphangiogenic tumors. Numbers above bars indicate tumor in category/ total tumors. (**D**) The reduced blood vessel density does not cause a reduction in mitotic Phospho-Histone H3 positive cells between PBS and ClodroLip treated mice. N: number of mice, n: number of tumors, n.s.: not significant. T: tumor, E: exocrine pancreas. Student's unpaired two-tailed t-test was used in (B) and (D) Scale bar: 100μm.

4.4. Improved mouse model of pancreatic β-cell carcinogenesis

Adrian Zumsteg[1], Karin Strittmatter[1], Daniela Klewe-Nebenius[2], Helena Antoniadis[1] and Gerhard Christofori[1,3]

[1]Institute of Biochemistry and Genetics, Department of Biomedicine, University of Basel, Switzerland.

[2]Transgenic Mouse Core Facility, University of Basel, Switzerland.

[3]Corresponding Author:

Gerhard Christofori
Institute of Biochemistry and Genetics
Department of Clinical Biological Sciences
University of Basel
Center of Biomedicine
Mattenstrasse 28
4058 Basel
Switzerland
Tel. +41 61 267 35 64
Fax. +41 61 267 35 66
e-mail: Gerhard.christofori@unibas.ch

4.4.1. Abstract

By transgenic expression of a bicistronic mRNA in mice under control of the Rat insulin promoter 1, encoding for SV40 large T antigen followed by an internal ribosomal entry site preceding a firefly luciferase gene, we developed a versatile tool to study β-cell carcinogenesis non-invasively by *in vivo* bioluminescence. Numerous tumors of different malignancy stages can be detected in single mice, indicating that this model recapitulates multistage carcinogenesis. In addition, in this mouse strain called *RL-1* (*R*ipTag-IRES-*L*uciferase line *1*), due to the very stringent expression exclusively in the β-cells of Langerhans islets, we could determine micro-metastasis in liver via luciferase expression of metastatic cells. This mouse line will be of value to study tumor-promoting as well as metastasis-related genes when crossed to other transgenic or gene-targeted mice.

4.4.2. Introduction

The first transgenic cancer models in mice have been established around 1984, using simian virus 40 (SV40) derived T antigen oncoproteins, myc, ras and fos, whose expression was driven by tissue specific or viral promoters. This over-expression resulted in brain, mammary, bone, pancreatic acinar cell or endocrine tumors and, in the case of myc over-expressed in B lymphocytes, in lymphoma (Hanahan et al., 2007). In the meantime, a plethora of new murine cancer models have been established, and the range of endogenous tumor models (versus transplantation models) has been expanded by chemical, physical and hormonal induction protocols of cancer. Transgenic and induced cancer models offer the possibility to study tumorigenesis in a fully immune-competent background. This is in contrast to xeno-transplantation studies, in which human cancer cell lines are grafted into immune-compromised mice.

One of the first “oncomice” was the transgenic Rip1Tag2 mouse, recapitulating β-cell carcinogenesis of islets of Langerhans, elicited by rat insulin promoter mediated expression of SV 40 large T antigen (Tag). It has been used widely in cancer research over the last two decades (Hanahan, 1985) and, together with others, has substantially contributed to the concept summarized as “hallmarks of cancer” (Hanahan and Weinberg, 2000). Particularly, a tumors’ requirement for angiogenesis, evasion from apoptosis as well as tissue invasion and metastasis were demonstrated in the Rip1Tag2 model. The onset of angiogenesis, a prerequisite for the growth of macroscopic tumors, is a highly regulated process, which is mainly governed by the expression of pro-angiogenic growth factors including vascular endothelial growth factor A (VEGF-A) and other factors. In models of multi-stage carcinogenesis, angiogenesis is mainly found to occur in mid-stage tumor lesions and results from a shift in the balance of pro- and anti-angiogenic

factors, an emerging imbalance triggered by hypoxia, nutrient deprivation and activation and liberation of matrix sequestered growth factors. Evasion of apoptosis as a critical feature of tumors can be acquired by combined inactivation of cellular apoptosis inducers (e.g. p53 or tumor necrosis factor (TNF) receptor) and over-expression of anti-apoptotic molecules including members of the Bcl-2 family or activation of anti-apoptotic signaling pathways. In the Rip1Tag2 tumor model, over-expression of insulin like growth factor II, normally down-regulated in rodents after birth throughout the body, was shown to be crucial for growth of macroscopic tumors by counteracting apoptosis in tumors (Christofori et al., 1994). Sooner or later, most solid tumors leave the primary tumor site and seed to distant organs, a process called metastasis. Tissue invasion and metastasis are mechanistically closely related, and cellular changes observed in invading tumor cells are often mirrored by the metastasis. Rip1Tag2 mice have been instrumental to define a role for cell-cell adhesion molecules of the immunoglobulin and calcium-dependant cadherin families as well as the role of integrins, which connect cells to the extracellular matrix. Intercrossing Rip1Tag2 mice with transgenic mice that maintain E-cadherin expression in tumor cells results in arrest of tumor development at the adenoma stage, whereas expression of a dominant-negative form of E-cadherin induces early invasion and metastasis (Perl et al., 1998). In the same tumor model, mice develop lymph node metastases when neural cell adhesion molecule (N-CAM), a member of the immunoglobulin CAM, is expressed at reduced levels (Perl et al., 1999). Partial deletion of β_1 integrin in tumor cells in Rip1Tag2 mice leads to increased tumor cell dissemination via the lymphatic system (Kren et al., 2007).

Another critical feature of cancer development, not appreciated in experimental animal studies until the last decade, is the tumors' interaction with the immune system, resulting in recruitment of inflammatory cells that promote tumor growth, angiogenesis and invasion and that help the tumor to evade immune surveillance (reviewed in (Zumsteg and Christofori, 2009)). Rip1Tag2 mice have been used to define critical roles of bone-marrow derived cells by supplying matrix metalloproteinase 9, which can activate matrix sequestered VEGF-A (Bergers et al., 2000; Nozawa et al., 2006).

However, the Rip1Tag2 model has limitations that we thought could be prevented. In contrast to skin, breast or subcutaneously transplanted tumors, the islets of Langerhans form a part of the pancreas, hence are buried in the mouse body, rendering it impossible to monitor tumor growth in longitudinal analyses. Even though many preclinical studies have been undertaken in Rip1Tag2 mice (Schomber et al., 2009; Shojaei et al., 2008; Wicki et al., 2007), the necessity to set a defined endpoint due to unknown tumor growth diminishes the flexibility of this cancer model. Another limitation is the transgene integration site in the Rip1Tag2 mice, which causes aberrant expression in cells of gastrointestinal L cells, giving rise to intestinal neuro-endocrine carcinoid

tumors in some backgrounds, occasionally hampering the analysis of β-cell tumorigenesis (Dietrich et al., 1994; Grant et al., 1991).

By using the same construct originally used to create the Rip1Tag2 mouse, and expanding it by an internal ribosomal entry site (IRES) followed by a luciferase gene, we were able to develop a transgenic carcinogenesis model in which tumor growth can be monitored non-invasively by bioluminescence. The integration site causes an expression highly restricted to β-cells in islets of Langerhans, avoiding secondary tumor development at other sites and allowing immediate detection of metastatic events by analysis of organ lysates due to the expression of luciferase exclusively in metastatic tumor cells in target organs. The different tumor stages, occasional regional lymph node metastasis and the occurrence of distant organ metastasis therefore recapitulate multistage carcinogenesis.

4.4.3. Results

RipTag-IRES-Luciferase mice develop insulinoma

Generation of transgenic RipTag-IRES-Luciferase mice

We sought to create a transgene cassette driving the expression of simian virus 40 (SV40) large T antigen oncoprotein followed by an internal ribosome entry site (IRES) also allowing firefly luciferase expression in a bicistronic manner. To specifically have expression in β-cells of Langerhans islets, the rat insulin promoter 1 (Rip1), derived from the rat insulin II gene, was used. The original pRip1Tag vector (Hanahan, 1985) was modified by introducing an IRES-luciferase cassette between the SV40 large T antigen stop codon and the SV40 polyadenylation signal (Figure 27A). SV40 early region encoding large T antigen contains an intron, an important feature for efficient transgene expression (Le Hir et al., 2003). The construct was transiently transfected into the insulinoma cell line βT2 and luciferase activity above background was detected, indicating the functionality of the IRES element and activity of the promoter (data not shown). The linearized plasmid was used to generate transgenic mice in FVB/N background. White mice were chosen because their lack of melanin expression facilitates the detection of bioluminescence *in vivo.* Three founder lines were obtained, termed RL-1, RL-2 and RL-3. For line RL-1, which was finally propagated, we determined the transgene integration site by linker-mediated PCR and found it to be in the distal H4 region of chromosome 3, 100kb and 500kb away from the next annotated genes, respectively (Figure 27B). This allowed us to design a muliplex PCR discriminating between wildtype or RL-1 transgenic allele (Figure 27C). Mice homozygous for the RL-1 transgene did not

show any abnormalities, indicating negligible distortion of the genomic locus. Nevertheless, all data presented in this publication are derived from heterozygous mice.

We analyzed transgene copy number by quantitative PCR on genomic DNA and found RL-1 mice to have about 8 times more transgene copies than Rip1Tag2 mice, which were reported to have a heterozygous copy number of 5 (per diploid genome); we therefore assume a copy number of around 40 transgene copy numbers (not shown).

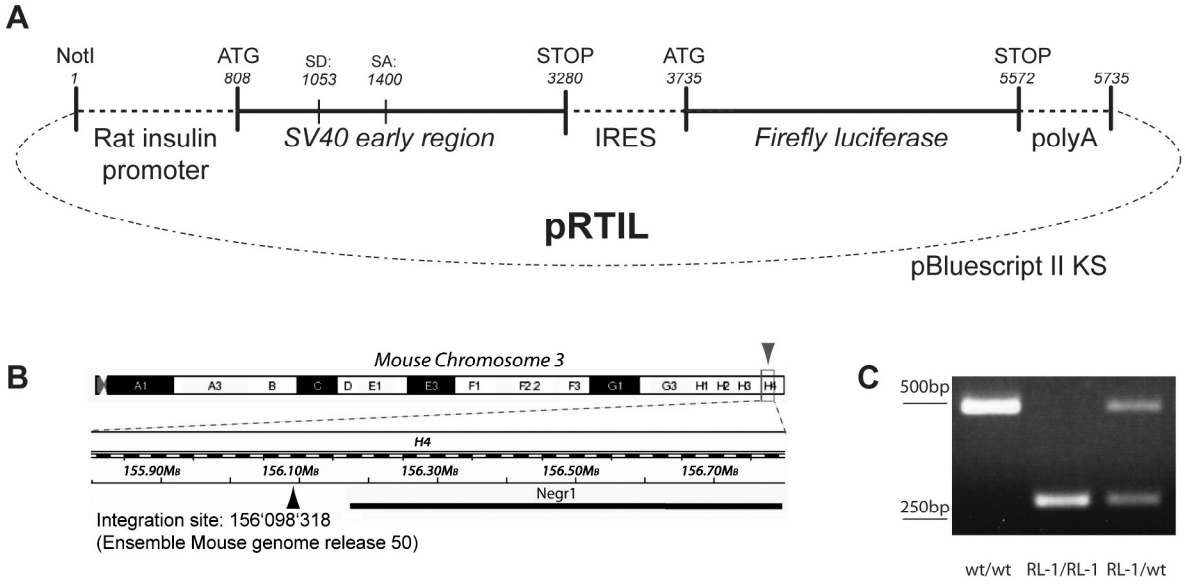

Figure 27. Generation of transgenic Rip-Tag-IRES-Luciferase mouse. (**A**) An IRES-Luciferase cassette was inserted into a modified pRIP1-Tag vector between the SV40 large T antigen STOP codon and the SV40 polyadenylation site as described in Materials and Methods. Notice the intron between splice donor and acceptor (SD and SA) in SV40 early region. NotI linearized pRTIL was used to produce transgenic mice. (**B**) Linker mediated PCR was used to determine transgene integration site in RL-1 mice, which was found to be the distal arm H4 of mouse chromosome 3, about 100kb away from the next protein coding gene. (**C**) Multiplex PCR allowing detection of wt/wt, heterozygous RL-1/wt or homozygous RL-1/RL-1 transgene configuration. IRES: internal ribosomal entry site.

Initial characterization of founder lines by in vivo and ex vivo luciferase bioluminescence

All three transgenic mouse lines develop potentially fatal insulinoma, but in lines RL-2 and -3, only males developed tumors within the observation span (40 weeks), even though the transgene did not integrate in the Y chromosome in either of these lines (autosomal transmission of the transgene). The amount of mRNA coding for large T antigen, isolated out of Langerhans islets from non tumor-bearing mice, indicated a 12 – 20 fold lower expression level in RL-2 and RL-3 mice as compared to RL-1 mice (data not shown). The onset of tumor growth in males from lines RL-2 and RL-3 was after 25 weeks. The lengthy and variable kinetic prompted us not to propagate these lines.

In vivo bioluminescence signals were aberrant in lines RL-2 and -3, whereas in RL-1 line, tumors as small as 2 mm could be detected at the expected site located in the higher peritoneal region. Figure 28A shows tumor bearing mice from all three founder lines which were subjected to *in vivo* bioluminescence measurement, all three mice having tumors of 3-4 mm diameter.

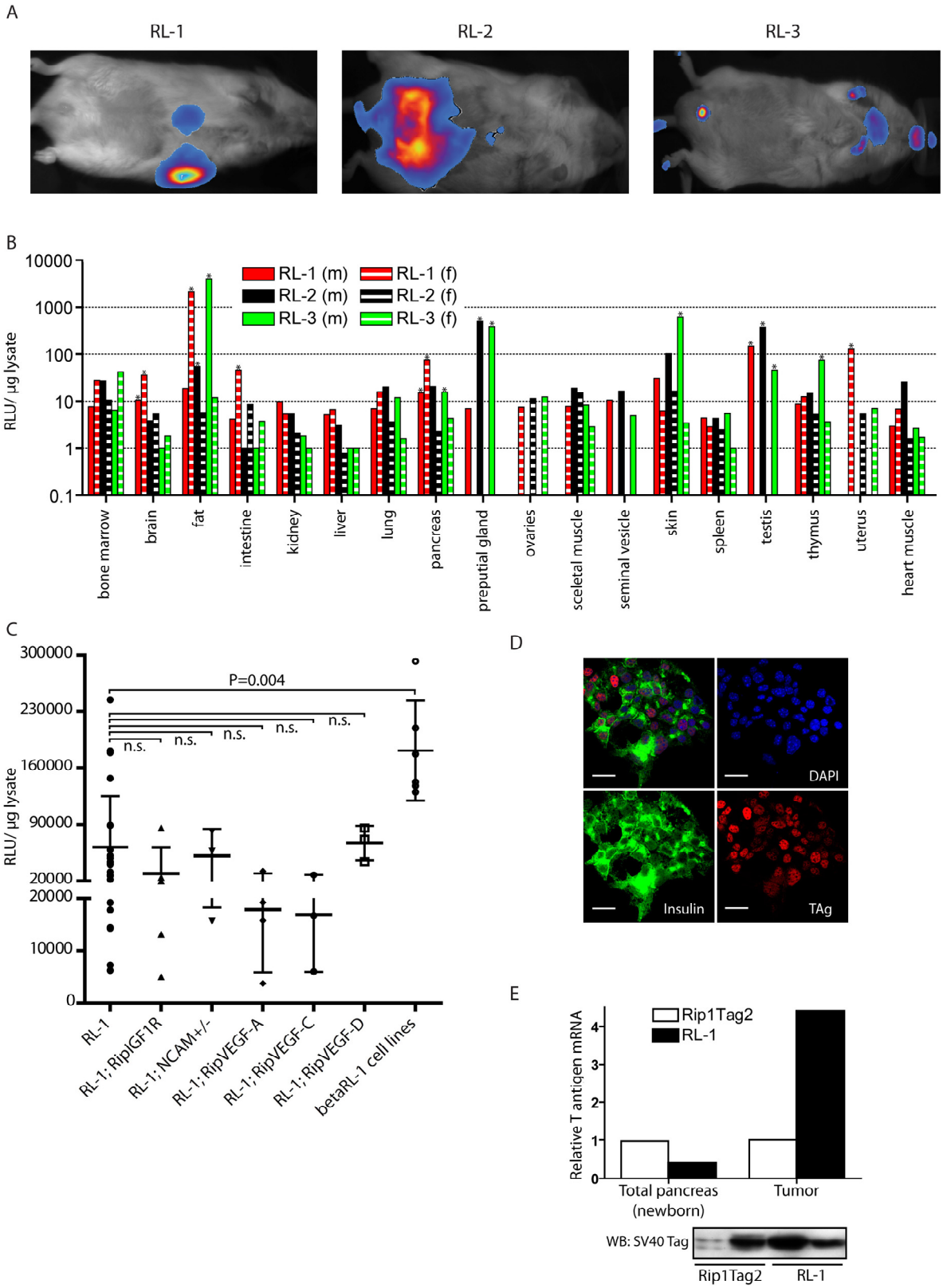

Figure 28. Luciferase expression in organs and tumor lysates. (**A**) *In vivo* luciferase bioluminescence of transgenic mouse lines RL-1, RL-2 and RL-3 allows non-invasive tumor monitoring. All three mice shown have similar insulinoma sizes of 3-4 mm, yet only line RL-1 shows signals restricted to the pancreatic area, located in the higher peritoneal region. Line RL-3 shows detectable luciferase signal in skin devoid of fur. (**B**) *Ex vivo* luciferase values from organ lysates of 6-8 week old tumor free RL mice. Asterisks indicate levels that are at least 3-fold higher than in control organs from non-transgenic mice. Minor leakiness is detected in some organs, including brain, fat, preputial gland, skin, testis and uterus. (**C**) *Ex vivo* luciferase activity of tumor lysates derived from RL-1 or RL-1 composite mice show normalized luciferase values 100 - 10'000 fold higher than from organ lysates (B). Tumors derived from composite mice as

compared to RL1 single transgenic mice do not have significantly different *ex vivo* luciferase activity. Lysates from tumor cell lines derived from RL-1 tumors have a statistically higher luciferase activity *. Shown are individual values, with means +/- SEM. (**D**) betaRL1-223 cell line is 100% positive for insulin and Tag expression, indicating functionality of the insulin promoter and that the normalized luciferase values measured for cell lines in (C) represent the highest range of luciferase expression possible in the RL-1 system. (**E**) Tag is expressed in total pancreas isolated from newborns and in tumors. Top panel: qPCR from mRNA isolated either from pancreas of newborn mice or from tumors, normalized to newborn Rip1Tag2. Bottom panel: Western blot for large T antigen of insulinomas shows a tendency towards higher Tag expression in RL-1 mice. * Unpaired, two-tailed Student's t-test. (m): males, (f): females, scale bar in (D): 20μm.

One big advantage of the luciferase approach is the possibility to track tumor cell dissemination quantitatively by analysis of organ lysates. To evaluate the feasibility of this approach for detecting metastatic events, we analyzed baseline levels of luciferase expression in organs from 6 - 8 week old RL mice. As the mice are tumor-free at this point and no metastases are expected, any detected luciferase activity would be due to leakiness of the rat insulin promoter. The indicated organs were homogenized and luciferase activity analyzed *in vitro*. Generally, luciferase levels were very low in most of the organs analyzed (Figure 28B). Asterisks indicate organs in which the raw values were more than threefold over the blank control, which was considered as aberrant expression. Testes lysates were positive in all mouse lines, indicating baseline activity of the Rip promoter in this organ. Preputial gland was positive in lines RL-2 and RL-3. Skin showed aberrant luciferase expression in males of line RL-3 (Figure 28A, right panel). Fat tissue has aberrant luciferase expression in all founder lines. Brain homogenates showed luciferase expression in line RL-1.

Tumor lysates from RL-1 tumors were found to have very high luciferase expression (Figure 28C), about 3-5 $\log_{10}$ units above levels detected in liver and lung, two potential target organs of insulinoma metastasis. The normalized luciferase activity in tumor lysates of RL-1 mice was relatively variable ranging from 6'000 to 240'000 relative light units (RLU)/ μg lysate with a mean of 62'000. This variability might reflect different degree of down-regulation of insulin expression observed in insulinomas (Figure 32C) as well as different relative proportions of tumor cells constituting the tumor mass.

We then crossed the RL-1 mice to mice expressing tumor "modifier" genes, which are also expressed under the control of rat insulin promoter and had previously been characterized in the Rip1Tag2 tumor model. Vascular endothelial growth factor A (VEGF-A) is one of the most potent pro-angiogenic growth factors and accelerates tumor growth in Rip1Tag2 mice without affecting metastases (Gannon et al., 2002) whereas VEGF-C and VEGF-D promote tumor lymphangiogenesis and lymph node metastases (Kopfstein et al., 2007; Mandriota et al., 2001). Insulin like growth factor receptor 1 (IGF-1R) over-expression was shown to dramatically accelerate tumor growth and progression in Rip1Tag2 mice (Lopez and Hanahan, 2002), whereas neural cell adhesion molecule (NCAM) deficiency was shown to promote lymph node metastases by decreasing tumor - extracellular matrix adhesion and increasing tumor lymphangiogenesis (Crnic et al., 2004; Perl et al., 1999). Tumor lysates derived from these composite mice didn't show

significantly different luciferase values, indicating that expression of the modifier genes didn't lead to a drastically changed tumor/ stroma ratio or perturbation of oncogene expression (Figure 28C). Lysates prepared from two cell lines derived from tumors of RL-1 mice showed luciferase expression in the highest range detected for total tumor lysates, significantly higher than lysates derived from primary tumors of all analyzed genotypes. One of these cell lines is 100% positive for Tag and insulin expression (Figure 28D), indicating that the luciferase activity measured for this cell line denotes the upper limit of luciferase expression in the RL-1 system.

When we analyzed the amount of large T antigen mRNA in RL-1 or Rip1Tag2 from either total pancreas of newborn mice or in tumors, we found in tumors of RL-1 mice four-fold higher transcript levels as compared to Rip1Tag2 mice, findings that were also confirmed by immuno-blotting (Figure 28E). In contrast, at birth, Rip1Tag2 mice have about two-fold more Tag mRNA as RL-1 mice. In addition to T antigen mRNA, lysates from total pancreata from newborn RL-1 mice were also positive for luciferase activity *in vitro,* demonstrating not only transcription but also translation of the bicistronic transgene (not shown).

Bigger but fewer tumors allow RL-1 mice to outlive Rip1Tag2 mice

Rip1Tag2 mice have been classically bred in C57BL/6 background, and the average survival time of these mice is around 12.6 weeks with mice living up to 16 weeks (Lopez and Hanahan, 2002). Average tumor volume of Rip1Tag2 mice at 12 weeks, i.e. shortly prior to average survival time, is around 36 mm^3. In contrast, RL-1 mice have a median survival of 20.7 weeks, with a sex difference showing female RL-1 mice dying earlier than males, with a median survival of 19.4 weeks for female and 22.0 weeks for male mice, respectively (Figure 29A). When we analyzed survival of RL-1 mice in pure FVB/N background vs. C56BL/6 into FVB/N backcross generations 1 - 4, we did not detect differences in survival for single-transgenic RL-1 mice (Figure 29A, right panel). Backcross generations 1 - 4 harbor 50% - 93.75% FVB/N genetic background. These mice were obtained from crossing in of modifier genes present in C57BL/6 background. Hence it is feasible to use the data from composite mice from all backcross generations pooled. When we analyzed survival of RL-1;RipVEGF-C, RL-1;RipVEGF-D and RL-1;$NCAM^{+/-}$ composite transgenic mice, no difference in survival was found. In contrast, transgenic co-expression of VEGF-A or IGF1R under the Rip promoter caused a drastic, highly significant survival reduction in RL-1;RipVEGF-A and RL-1;RipIGF1R mice (Figure 29B, Table 2).

Genotype	*N*	*Median survival/ weeks*	*log-rank vs. RL-1*
RL-1	173	20.7	
RL-1; RipIGF1R	26	11.4	P<0.0001 ***
RL-1; NCAM+/-	16	n.d.	P=0.13
RL-1; RipVEGF-A	26	13.0	P<0.0001 ***
RL-1; RipVEGF-C	15	21.4	P=0.83
RL-1; RipVEGF-D	28	20.7	P=0.76

Table 2. Median survival of RL-1 composite mice as shown in Figure 29. N indicates total number of mice. Survival of RL-1;RipIGF1R and RL-1;RipVEGF-A mice was significantly (***) reduced compared to RL-1 mice, as analyzed by log-rank test. n.d.: not determined

When we analyzed the tumor volumes of RL-1 female vs. male mice, no significant differences could be found in the absolute tumor volumes when mice at age 18 – 20 weeks were analyzed (Figure 29C), with an average tumor volume of 99 +/- 29 mm^3 and 65 +/- 12 mm^3 for females and males, respectively (mean +/- SEM). However, at age 21 – 22 weeks, average tumor size of females dropped to 37 +/- 11 mm^3, whereas males could bear much larger tumors of 233 +/- 33 mm^3 (Figure 29C). This indicates that females alive at this age had a delayed tumor progression, whereas males could still live under massively higher tumor burden. The distribution of tumor burden within mouse groups was not Gaussian, forcing us to use non-parametric Mann-Whitney U test for assessing significance of tumor volume differences. When we analyzed the tumor incidence, i.e. the number of macroscopic tumors per mouse, in average 2.93 +/- 0.21 macroscopic tumors were detected per mouse, independent of sex and early vs. late analysis time span (not shown). As females and males had age-matched similar tumor size at 18 – 20 weeks of age, we compared single RL-1 with composite transgenic mice with data from both sexes combined, however only include data up to the median survival time. Similarly to the survival data and the previously published data on RipVEGF-C, RipVEGF-D and $NCAM^{+/-}$ in Rip1Tag2 mice, no significant changes in tumor volume or incidence were seen when RL-1 mice where compared to RL-1;RipVEGF-C/ RipVEGF-D/ $NCAM^{+/-}$ composite mice (Figure 29C, Table 3). In contrast RL-1;RipIGF1R had bigger and twice as many macroscopic tumors than RL-1 mice (Figure 29C. Table 3), even though they were analyzed at only 9 – 11 weeks of age (vs. 18 – 20 weeks in RL-1 mice), highlighting the role of IGF1R as a tumor progression driver. RL-1;RipVEGF-A double transgenic mice, analyzed prior to median survival time, had statistically significant smaller tumors than RL-1 mice. This is in sharp contrast to the reduced median survival time and suggests that VEGF-A does not play a role in tumor cell transformation, but rather allows rapid growth once an initial, angiogenesis-dependant tumor has formed. In RL-1 mice, the initial formation of angiogenesis-dependent hyperplastic islets seems to be delayed as compared to Rip1Tag2 mice, which can also

be estimated from the reduced tumor incidence, with only 3 macroscopic tumors in RL-1 mice to more than 5 tumors in Rip1Tag2 mice at a much earlier age.

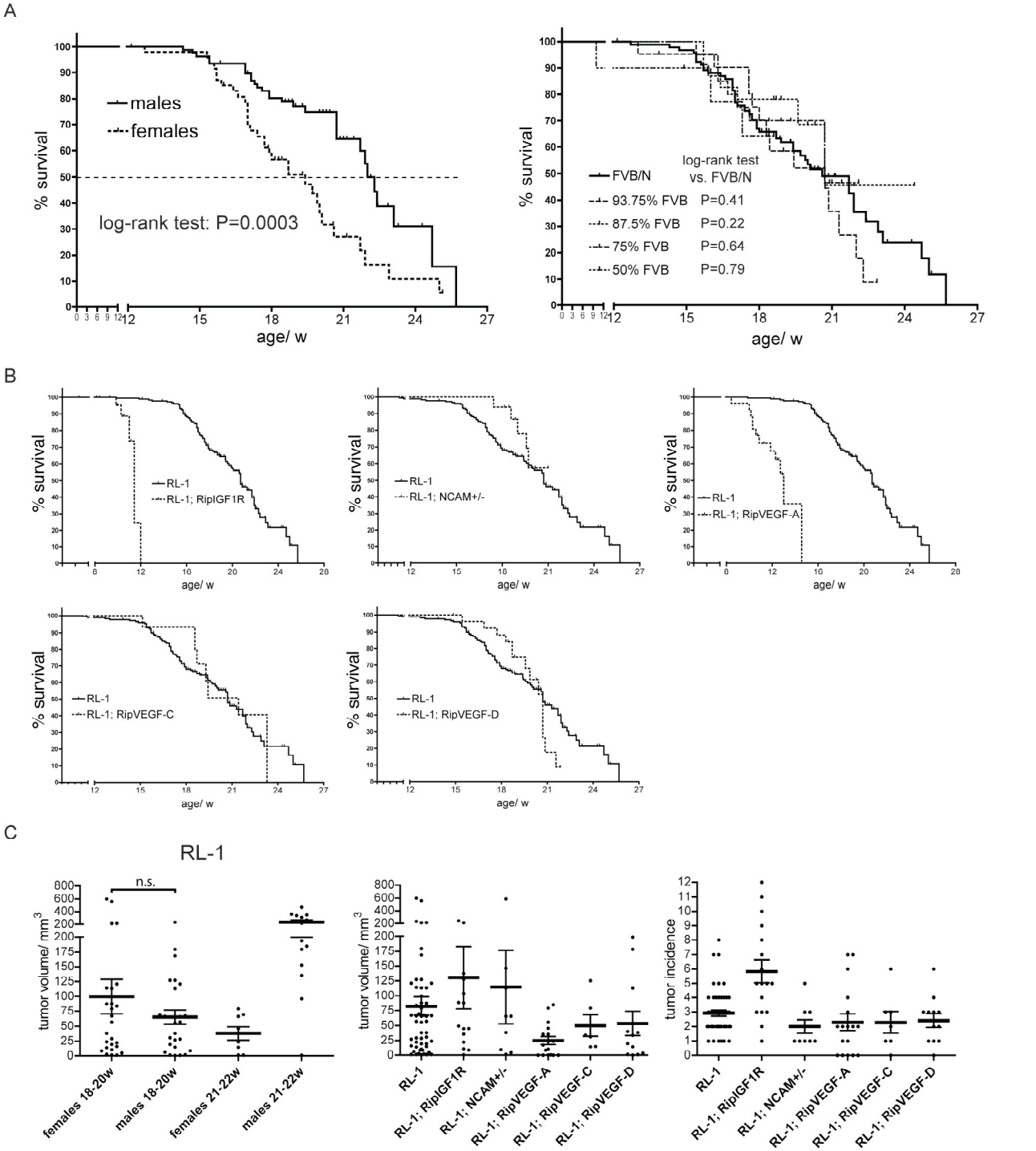

Figure 29. Sex and tumor modifier genes but not genetic background influence survival and tumor size. (**A**) Survival curve of male vs. female RL-1 mice, indicating a significantly reduced survival of female vs. male RL-1 mice (median survival 19.4 vs. 22 weeks, respectively; left panel). In contrast, single transgenic RL-1 mice from different backcross generations from C57BL/6 into FVB/N did not show significantly different survival (right panel). (**B**) Survival of RL-1; RipIGF1R and RL-1;RipVEGF-A composite mice is dramatically reduced as compared to RL-1 single transgenic mice. Neither VEGF-C, VEGF-D over-expression in β-cells nor NCAM heterozygosity impacts survival. See Table 2 for median survival of composite mice. (**C**) RL-1 males and females have similar tumor sizes before week 20, but after week 20 only male mice can support larger tumors whereas female tumor size drops, indicating that those were escapers (left panel). All mice were therefore analyzed prior to their median survival (as determined for both sexes) indicated in Table 3. RL1; RipIGF1R mice had more and bigger tumors than RL-1 mice, whereas RL-1; RipVEGF-C/ RipVEGF-D/ NCAM$^{+/-}$ composite mice did not exhibit differential tumor sizes or incidence. RL1; RipVEGF-A mice had smaller tumors than RL-1 mice prior to median survival. Shown are individual values with means +/- SEM.

Genotype	*N*	*Analysis window/ age in weeks*	*Mean tumor volume/ mm^3 +/- SEM*	*Mean tumor incidence +/- SEM*	*Mann-Whitney test: tumor volume vs. RL-1*	*students t-test: incidence vs. RL-1*
RL-1	54	18-20	82 +/- 16	2.93 +/- 0.21		
RL-1; RipIGF1R	16	9-11	130 +/- 52	5.82 +/- 0.78	P=0.32	P<0.0001***
RL-1; NCAM+/-	9	18-20	115 +/- 61	2.00 +/- 0.47	P=0.99	P=0.09
RL-1; RipVEGF-A	17	11-13	23 +/- 8	2.29 +/- 0.58	P=0.003**	P=0.20
RL-1; RipVEGF-C	6	18-20	50 +/- 18	2.29 +/- 0.75	P=0.81	P=0.31
RL-1; RipVEGF-D	12	18-20	53 +/- 20	2.41 +/- 0.47	P=0.25	P=0.31

Table 3. Tumor volume and incidence of RL-1 and RL-1 composite mice as shown in Figure 29C. N: number of mice analyzed.

Luciferase bioluminescence quantification of tumor growth *in vivo*

As has been observed for tumor lysates, the luciferase activity in tumors has a relatively large spread. Bearing this in mind, we analyzed mice over time up to 4 weeks and analyzed *in vivo* bioluminescence once or twice weekly to estimate relative growth. We found that signal intensity was maximal about 10 minutes after D-luciferin injection and stayed at plateau levels for 20 - 30 minutes (data not shown). As tumors can be located very diversely, especially they can be buried deeper in the mouse and the light path might be longer, it is not possible to compare tumor sizes between mice. However, for individual mice, an increase in luciferase activity can be nicely monitored over time (Figure 30). The fact that RL-1 mice have in average only 3 macroscopic tumors facilitates discrimination of tumor nodules at image analysis. When we analyzed a large cohort of mice, we could nicely detect a threefold increase in average signal intensity over four weeks (Figure 30B), but fluctuations for single mice could be quite high, as can be estimated from the individual curves shown in the right panel.

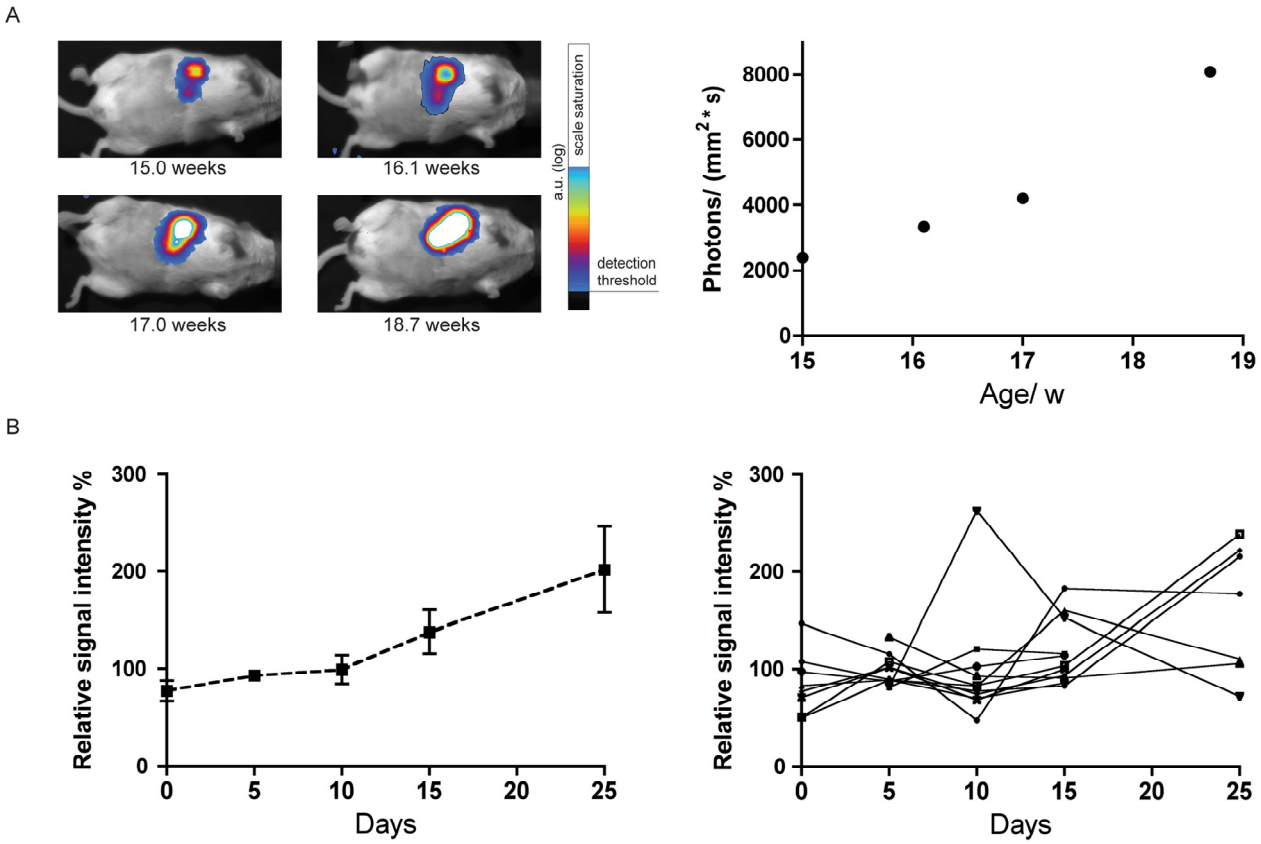

Figure 30. *In vivo* bioluminescence can be used to monitor tumor growth in RL-1 mice. (**A**) Longitudinal analysis of luciferase bioluminescence in a RL-1 mouse over 4 weeks shows increasing light emission over time. The same scale was used for all 4 images causing signal intensities out of scale at age 17 and 18.7 weeks (white central area inside false colored area). Right panel: photon flow quantification of the (false) colored area from left panel. (**B**) Tumor growth in a cohort of 12 mice (average age at first monitoring: 15 weeks) was followed over 25 days by *in vivo* bioluminescence. The signal intensities were normalized for each mouse individually, with 100% representing the geometrical mean of all values obtained per mouse during the 25 days observation period. Shown are means of the 12 mice +/- SEM. Right panel: individual mice normalized luminescence signals used to generate curve in left panel indicate relatively high variability for individual mice. a.u.: arbitrary units.

Insulinomas are hemorrhagic, poorly vascularized and downregulate insulin and E-Cadherin

Hyperplastic and angiogenic islets were detected in RL-1 mice at 7 weeks of age, as detected by BrdU incorporation in islets and hemorrhage, but only after 10 weeks of age macroscopic tumors could be detected. The low abundance of macroscopic tumors in RL-1 mice was also qualitatively confirmed in histology, where only few small to intermediate size lesions apart from the macroscopic tumors were found. We subdivided the identified endocrine tumors into 3 classes: normal/ hyperplastic islets, type 1 and type 2 tumors, with representative pictures shown in Figure 31A. Type 1 tumors show an increased nucleus/ cytoplasm ratio as compared to normal appearing hyperplastic islets and they were further subdivided into either hemorrhagic or microinvasive type, the latter showing at least one locally invasive area. Type 2 tumors, usually bigger than 1mm, have dense and irregular nuclei with little cytoplasm, are intercalated with the exocrine pancreas, show acute hemorrhage accompanied by distorted vessel morphology and

immune cells infiltration is evident. In type 2 tumors, detached tumor cell clusters within the tumor were often detected (Figure 31B), and we also detected tumor cell clusters in blood vessels located in the exocrine pancreas, indicative of tumor cell disaggregation (Figure 31C). Per pancreatic tissue section from mice analyzed at age 18 – 20 weeks, we found in average 5.5 +/- 1.8 normal/ hyperplasic islets, 5.5 +/- 1.6 type 1 lesions and 1.6 +/- 0.3 type 2 lesions (mean per mouse +/- SEM, 6 mice, 76 counted lesions). BrdU injection 2h before sacrifice and staining for incorporated BrdU revealed a proliferation rate of 10.1 +/- 0.7% of all tumor-constituting cells (mean of microscopic fields +/- SEM; 3 mice, 12 tumors, 27 microscopic fields). TUNEL stain, indicative for apoptosis, revealed 1.05 +/- 0.08% apoptotic cells within tumors (mean of microscopic fields +/- SEM; 4 mice, 9 tumors, 25 microscopic fields).

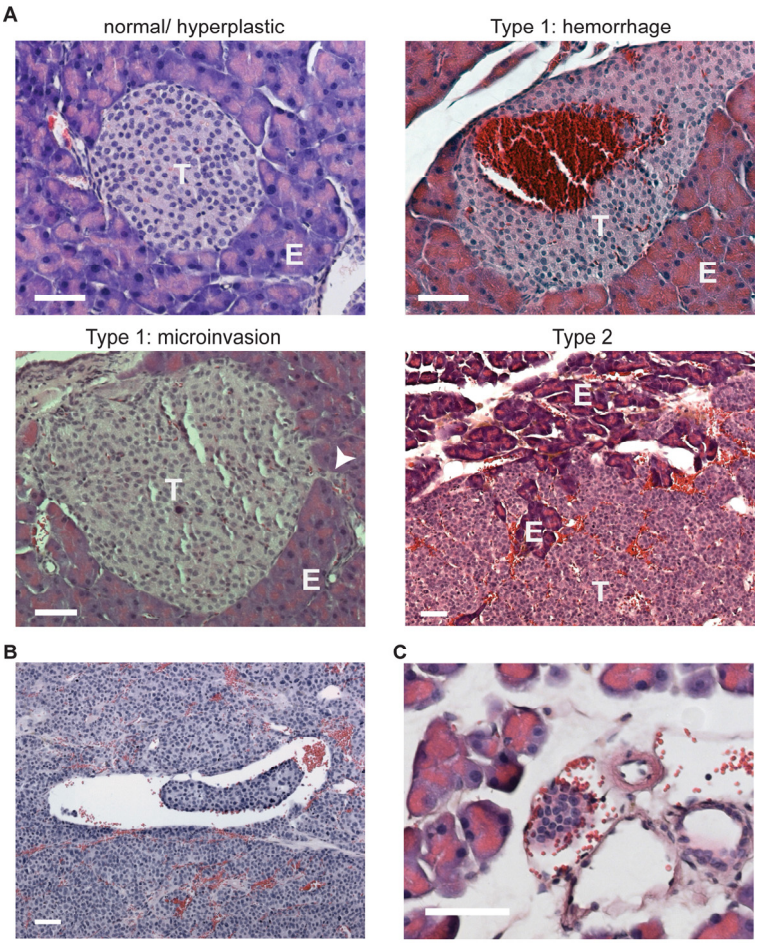

Figure 31. Representative Hematoxilin and Eosin stainings of RL-1 insulinomas found in pancreas. (**A**) Three types of endocrine lesions in RL-1 mice are found. Normal appearing hyperplasic islets (top left) with a maximal diameter of 200μm and have similar nucleus to cytoplasm ratio like normal islets. Type 1 lesions are markedly bigger and additionally show either hemorrhage (top right) and/ or microinvasion (bottom left, microinvasion indicated by arrowhead) into exocrine pancreas. Type 2 tumors have high nucleus density, prominent hemorrhage, intercalate with the exocrine pancreas and might show marked immune cell infiltration. (**B**) Type 2 tumors display internal loose tumor cell clusters in hemorrhagic areas. (**C**) Tumor cell clusters can be found in blood vessels within the exocrine pancreas as identified by the presence of erythrocytes and a clearly defined vascular lining. T: tumor, E: exocrine pancreas, scale bars: 50μm

By staining with the endothelial cell marker CD31, we found that larger tumors were poorly vascularized towards the tumor centre, whereas an outer rim was highly vascularized (Figure 32A). NG2, a marker for pericytes, was strictly colocalized to blood vessels in the tumor periphery (Figure 32A). In contrast, central tumor regions have few immuno-reactive CD31 positive vessels and the proteoglycan NG2 seems to stay behind as remnants of ancient intact vasculature.

E-Cadherin, an epithelial marker robustly expressed in β-cells of Langerhans islets, but eventually down-regulated in Rip1Tag2 tumors (Perl et al., 1998), was found to be retained in

hyperplastic and type 1 lesions (not shown), but was occasionally lost in type 2 lesions, with E-Cadherin positive and negative regions within the same tumor (Figure 32B).

Similar observations were made for insulin, one of the most characteristic β-cell markers. Lesions up to type 1 retained insulin expression (data not shown), albeit at reduced levels compared to islets, but type 2 tumors eventually down-regulated insulin expression in certain areas, as illustrated in Figure 32C. In order to determine major transcriptional changes that could be involved in the differential regulation of tumor onset and progression between RL-1 and Rip1Tag2 mice, we analyzed gene expression of total tumors by quantitiative PCR. A group of genes was analyzed that was shown to be important either for angiogenesis, namely VEGF-A, as well as a group of major transcriptional repressors of E-Cadherin expression, including SNAIL, SLUG, E47 and SIP1 (Figure 32D). However, none of these factors was differentially expressed.

It has previously been shown, that insulin like growth factor II (IGF-II) is an important mitogenic and anti-apoptotic factor for the growth of Rip1Tag2 insulinomas, as its expression correlates with hyperproliferation (Christofori et al., 1994) and growth of Rip1Tag2 tumors is severly impaired in IGF-II knockout mice (Christofori et al., 1995a). mRNA expression analysis revealed that RL-1 tumors dramatically up-regulate expression of IGF-II by more than 100-fold as compared to islets of Langerhans. In contrast, Insulin receptor (InsR) and IGF-1 receptor, known receptors for IGF-II, have unchanged expression levels between islets, Rip1Tag2 and RL-1 tumors (Figure 32E).

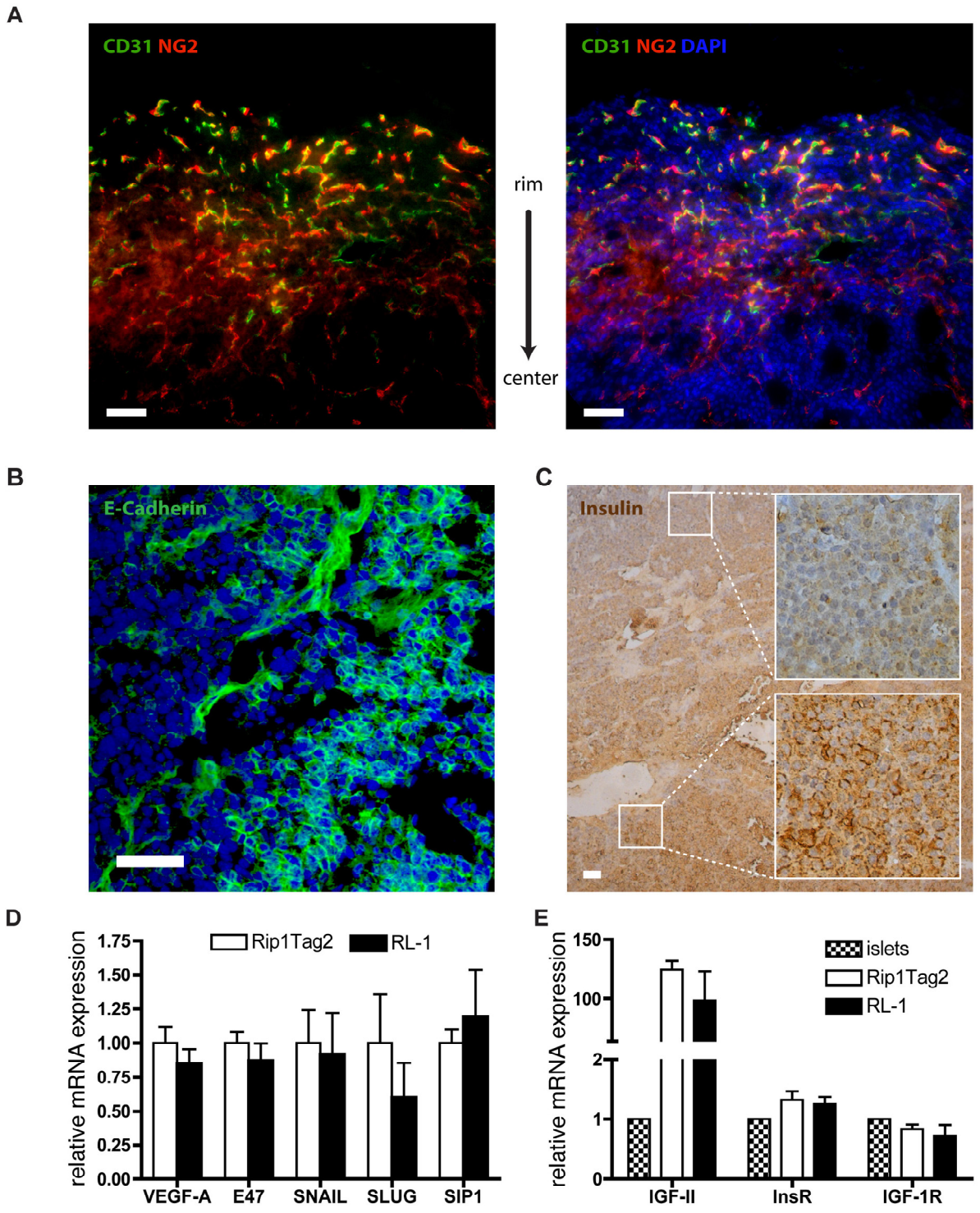

Figure 32. RL-1 tumors are poorly vascularized towards the centre and show heterogenous E-Cadherin and insulin expression**.** (**A**) Immunofluorescent staining of type 2 RL-1 tumor for endothelial marker CD31 and pericyte marker NG2 shows thorough coverage of blood vessels by pericytes in the tumor rim whereas central regions are almost devoid of CD31 reactive vessels but still are immunoreactive for the proteoglycan NG2 which might be leftovers from previous blood vessels. Background in red channel is from hemorrhage. (**B**) Whereas type 1 tumors keep E-Cadherin expression throughout the tumors, type 2 tumors might down-regulate E-Cadherin in some tumor areas. (**C**) Insulin stain illustrates partial down-regulation of insulin expression in regions of type 2 tumors. (**D**) & (**E**) Quantitative real-time PCR from macroscopic tumors of Rip1TAg2 and RL-1 mice. (**D**) No significantly different mRNA levels of the angiogenic factor VEGF-A or the E-Cadherin transcriptional repressors E47, SNAIL, SLUG or SIP1 were detected (N = 8 individual tumors from each genotype for VEGF-A and E47 and N = 3 individual tumors for SNAIL, SLUG and SIP1). (**E**): Insulinomas upregulate IGF-II compared to islets but the receptor levels are unchanged (two individual islet isolations, N = 8 individual tumors for Rip1TAg2, N = 4 for RL-1). Shown are means +/- SEM. Scale bars: 50μm.

Reduced infiltration by myeloid-derived suppressor cells (MDSC)

In addition to tumor cell intrinsic factors, it has been demonstrated in a number of experimental systems, that myeloid cells can be critical components in promotion of tumor angiogenesis and metastasis as well as in protection from anti-tumoral adaptive immune responses (reviewed in (Zumsteg and Christofori, 2009)). In particular, MDSC have been demonstrated to suppress activation of dendritic and cytotoxic T cells, and their abundance increases in peripheral blood and spleen with increasing tumor size. MDSC are characterized by a concomitant expression of CD11b, a myeloid marker, and Gr1, a granulocyte marker. By flow cytometry, we detected an increase of $CD11b^+$/ $Gr1^+$ MDSC in peripheral blood and spleen of insulinoma bearing mice as compared to their non-tumor bearing inbred strain. FVB/N mice have significantly less MDSC in peripheral blood and spleen as compared to C57BL/6 mice. We found a significantly reduced infiltration of MDSC into tumors of RL-1 mice as compared to tumors from Rip1Tag2 mice (Figure 33, left panel), a difference that was also detected in spleen and peripheral blood (Figure 33, middle and right panel).

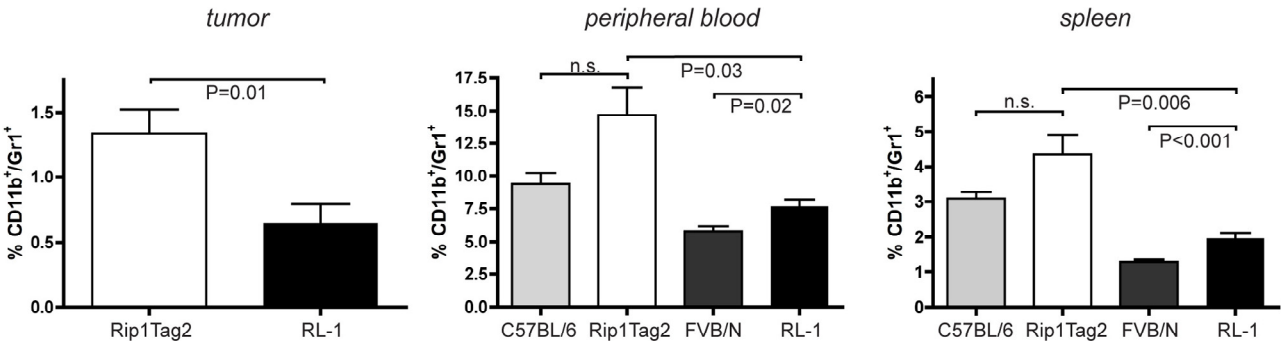

Figure 33. Reduced immune cell infiltration. RL-1 mice have significantly less $CD11b^+$/ $Gr1^+$ myeloid-derived suppressor cells in spleen, peripheral blood and tumors than Rip1Tag2 mice. This is also seen in the respective non tumor-bearing FVB/N vs. C57BL/6 strains. P values from unpaired two-tailed Student's t-test. Shown are means +/- SEM.

RL-1 mice develop lymph node and liver but rarely lung metastases

When we analyzed pancreatic lymph nodes for the presence of metastasis, we found 3 lymph node metastases in 3 out of 13 mice with totally 23 lymph nodes analyzed (Figure 34).

As normal mammalian cells do not express luciferase, the luciferase system offers a highly sensitive method to detect luciferase labeled cells in a luciferase negative environment, for example liver and lung in RL-1 mice (Figure 28). Insulinomas have been shown to metastasize to these organs in either man (Weber et al., 1995) or mice (Kopfstein et al., 2007). Out of 66 analyzed RL-1 single transgenic mice analyzed between 18 and 20 weeks of age, we detected luciferase activity at least threefold above background in liver from 19 mice (29%). When we correlated primary tumor size with normalized luciferase activity from the liver, a highly significant correlation

of tumor size and extent of hepatic metastasis was found (Figure 34B), with mice carrying primary tumors above 150 mm^3 having a 67% likelihood for liver metastases (Table 4). We confirmed the occurrence of metastases in liver by histology, and found structures strongly resembling pancreatic islets of Langerhans from cell shape and heamatoxylin/ eosin stain (Figure 34D, left panel). The β-cell origin of those cells was confirmed by immunohistochemical detection of insulin (Figure 34D, right panel), an antibody not labeling any particular structure in livers of wild-type mice. These metastases never reached macroscopic size and $insulin^+$ structures up to 150 μm diameter were identified. Using insulin staining, we identified in one particular mouse up to 20 insulin positive structures in one section, most often in the rim region and only rarely in central regions. When we divided $insulin^+$ area by the total section area, a ratio of 1/ 5800 was obtained. The normalized liver RLU (RLU/ μg lysate) in this mouse was 64, which is more than 30 fold above the detection level, suggesting that a 1/ 100'000 to 1/ 150'000 area fraction, corresponding to mass fraction could be detected by assessing *ex vivo* luciferase activity.

From the ratio of liver metastasis we obtained in single transgenic RL-1 mice, it seems obvious that a large cohort of mice carrying small to large lesions must be analyzed in order to faithfully determine the effect of modifier genes on metastasis probability. Nevertheless, liver metastasis were detected using *ex vivo* luciferase assays in RL-1;RipIGF1R, RL-1;$NCAM^{+/-}$ and RL-1;RipVEGF-C composite mice, as indicated in Figure 34C and Table 4, and also confirmed by insulin stain of liver sections (not shown). RL-1;RipIGF1R mice develop metastasis to a higher extent than single transgenic mice, but the number of mice is too small to yield statistically significant differences using Fisher's Exact test.

Detailed analysis of hepatic metastatic clusters revealed that most of them were partially or completely surrounded by CD31 and LYVE-1 positive vessels (Figure 34E). In contrast to many other organs, in which LYVE-1 is a marker for lymphatic vessels (Jackson et al., 2001) or a certain subset of macrophages (Schledzewski et al., 2006), hepatic sinusoidal endothelial cells express LYVE-1 (Mouta Carreira et al., 2001). The blood endothelial character of the vessels surrounding the metastatic nodules is highlighted by the erythrocytes present in the vessels (H & E stain, Figure 34D). Most metastatic nodules we detected were negative for the epithelial marker E-Cadherin, which is occasionally lost in type 2 primary tumors (Figure 32B). This indicates that these metastatic clusters had undergone an epithelial to mesenchymal transition. Surprisingly, within larger metastatic clusters, we found small patches of cells expressing E-Cadherin (Figure 34E). The proliferative nature of the metastatic nodules was confirmed by staining for Phospho-Histone-H3, a marker for mitosis (Figure 34E).

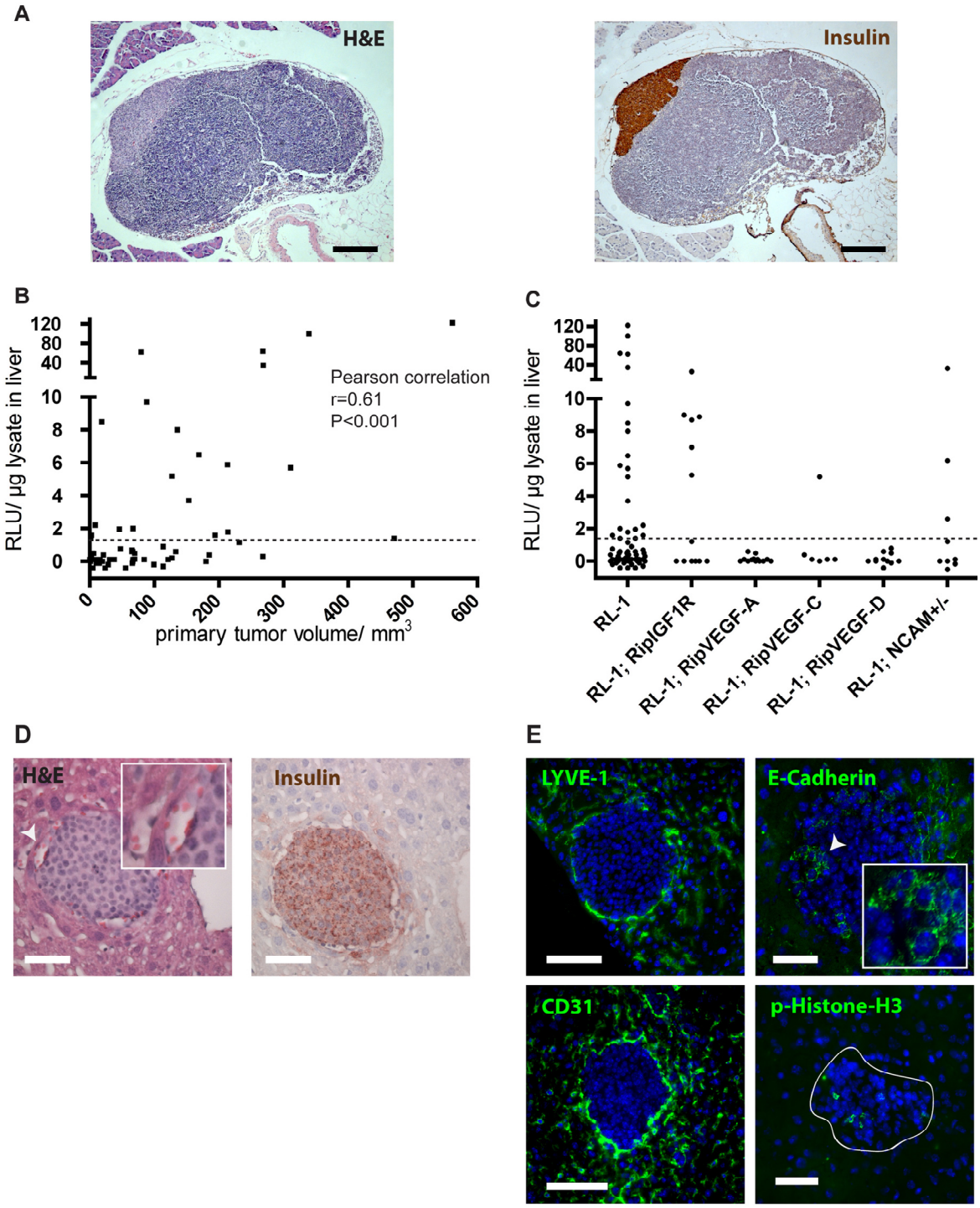

Figure 34. RL-1 tumors metastasize to the lymph node and liver. (**A**) RL-1 mice show lymph node metastasis in 3/13 mice (23%), as indicated by H & E and insulin staining of pancreatic lymph node showing metastasis. (**B**) Livers from 18 – 20 week old RL-1 mice were homogenized and assayed for *in vitro/ ex vivo* luciferase activity. Normalized luciferase activity in liver significantly correlates with primary tumor volume and is indicative of liver metastasis. Dashed line indicates the threshold defined as luciferase value 3 fold above background level (obtained with young RL-1 mice livers without primary tumors). (**C**) Composite mice also develop liver metastasis. No increase can be seen in lymphangiogenic tumor carrying RL1;RipVEGF-C or RL1;RipVEGF-D mice. Rather, as only a small number of composite mice had been analyzed, the lack of mice carrying large tumors makes it impossible to accurately compare the genotypes. RL1;RipIGF1R mice develop liver metastasis at a higher frequency but when categorized into different primary tumor size groups, fail to give significance (Fisher's exact test). (**D**) H & E stain (left panel) of liver histology shows insulin positive (right panel) metastasis (serial section), arrowhead in H & E indicates erythrocyte filled blood vessel (inset). (**E**): Metastatic nodules in the liver are surrounded by sinusoidal endothelial venules as indicated by LYVE-1 and CD31 stain (left panel); most metastatic cells lose E-Cadherin expression but some re-express this epithelial marker (arrowhead, right panel, inset). P-Histone-H3 staining shows proliferation of metastasis. Scale bars: (A): 200μm, (D) & (E): 50μm.

		Primary tumor size/ mm^3		
Genotype	***N***	***< 50***	***> 50 < 150***	***> 150***
RL-1	66	4/30 (16.7%)	5/21 (23.8%)	10/15 (66.7%)
RL-1;RipIGF1R	12	1/4 (25%)	3/6 (50%)	2/2 (100%)
RL-1;RipVEGF-A	14	0/11 (0%)	0/3 (0%)	none
RL-1;RipVEGF-C	6	1/4 (25%)	0/2 (0%)	none
RL-1;RipVEGF-D	13	0/10 (0%)	0/1 (0%)	0/2 (0%)
RL-1;NCAM$^{+/-}$	9	0/4 (0%)	2/4 (50%)	1/1 (100%)

Table 4. Metastasis frequency in liver. Mice are categorized according to primary tumor size and genotype. Numbers represent mice of category positive for liver metastasis (either by histology and/ or *in vitro* luciferase) per total mice analyzed in the respective category. N is total number of mice analyzed.

Using the same approach as for livers, we analyzed organ lysates from lungs and brains for *ex vivo* luciferase activity. In lung, we detected positive luciferase signals in RL-1 mice in 3/ 45, in RL-1;RipVEGF-D in 1/ 14 and in RL-1;RipIGF1R in 2/ 4 lungs analyzed, whereas in RL-1;RipVEGF-C, RL-1;RipVEGF-A and RL-1;NCAM$^{+/-}$ mice we did not detect positive signals. In contrast to liver, we were not able to detect metastases by histology in the controlateral lobe to the one that was used for the organ lysate. In brain, we detected luciferase values above background levels in a series of mice. Histological analysis of whole brains has never indicated any brain metastasis. We conclude that the insulin promoter can be activated in the brain (as previously shown in rats (Devaskar et al., 1993)) and as suggest the luciferase leakiness in brain lysates of young RL-1 mice) by yet unknown stimulus.

4.4.4. Discussion

In an attempt to modify the much-appreciated Rip1Tag2 tumor model, we successfully implemented luciferase *in vivo* imaging technology into a transgenic insulinoma model, driven by rat insulin promoter mediated expression of SV40 large T antigen. SV40 large T antigen is known to bind and inactivate the tumor suppressors p53 and pRB and is therefore a very potent oncoprotein often used to generate murine models of carcinogenesis (Ahuja et al., 2005). The Rip1Tag2 tumor model has proven to be extremely instructive in identifying molecules and cell types participating in the so-called angiogenic switch, i.e. the capacity of a tumor to ensure its own oxygen and nutrient supply by acquiring an extended blood vascular network. Yet, due to the location of insulinoma within the pancreas, it was not possible to use the Rip1Tag2 tumor model to monitor tumor growth over time. Highly specific expression in β-cells of Langerhans islets of a bicistronic mRNA coding for large T antigen and firefly luciferase enabled us to generate a transgenic mouse, that offers the possibility to observe tumor growth by bioluminescence over time and detect organ metastases with very high sensitivity by *in vitro/ ex vivo* analysis of organ lysates.

The low background of luminescence from normal tissue, the rapid turnover of luciferase enzyme, and the nonimmunogenic characteristics of luciferin make this method ideally suited for temporal *in vivo* imaging of gene expression. As primary tumors cause fatal hypoglycemica before metastases reach a macroscopic size, it was not possible to identify metastases by *in vivo* bioluminescence.

The rat insulin promoter 1 (from the rat insulin II gene) has been used in numerous transgenic mouse models to specifically target trangene expression to β-cells of Langerhans islets. In several reports, a small number of founder mice was sufficient to drive specific expression of transgenic gene products to the insulin secreting β-cells, indicating a high flexibility of this promoter concerning the genomic integration site. Indeed, all three founder mice we obtained expressed the transgene in the pancreas and developed insulinoma over time. However, aberrant expression in other tissues might be a problem, so using luciferase technology we were able to easily select the founder with the lowest levels of aberrant expression in other organs apart from the pancreas, a stringency level hard and cumbersome to reach using quantitiative PCR or antibody based protein detection methods. The genomic integration site in the H4 region of murine chomosome 3 is 100kb away from the next protein coding gene, neuronal growth regulator (Negr1), a gene mainly involved in the neural system. This integration site might confer the expression detected in brain lysates of RL-1 mice. When we crossed the RL-1 transgene into homozygosity, we did not encounter any abnormalities, yet as we did not find obvious differences in tumor development due to possible gene dosage effects between homozygous RL-1/RL-1 vs. RL-1/wt heterozygous mice, we analyzed mainly heterozygous mice.

Another important issue is the onset of transgene expression, which can vary widely between different founder lines, ranging from embryonic expression to onset after puberty. As we found T antigen mRNA and luciferase protein in total pancreas of newborn RL-1 mice, we assume that transgene expression begins before birth. The occurrence of hyperplastic islets at 7 weeks of age also suggests early β-cell transformation. However, the first macroscopic tumors are detected only after 10 weeks of age, indicating a slow progression from hyperplastic islets to macroscopic tumors. Alternatively, hyperplastic islets could be recognized by the murine immune system as foreign and lost by auto-immune responses. When we analyzed the proportion of cells that was labeled after a 5 day pulse of 5-bromodeoxyuridine, labeling cells during S-phase of the cell cycle, we indeed found only about 20% of $BrdU^+$ cells within RL-1 tumors (at 14 weeks) compared to a 50% labeling efficiency in Rip1Tag2 mice at 8 weeks of age (data not shown). This indicates that tumors from RL-1 mice have a slower proliferative rate than Rip1Tag2 mice but hyperplasia occurs already at early age. The massive upregulation of IGF-II in macroscopic tumors as compared to normal islets and the concomitant unchanged levels of the IGF-II receptors IGF-1R and Insulin

receptor strongly suggest an important role of IGF-II in tumorigenesis in RL-1 mice, as described for Rip1Tag2 mice.

Several lines of evidence point towards an impaired angiogenesis onset of RL-1 mice versus Rip1Tag2 mice. First, already small RL-1 tumors of type 1 can show substantial amount of hemorrhage, not observed like this in Rip1Tag2 tumors, suggesting growth of very delicate and torturous vessels. Even though total mRNA levels of VEGF-A do not differ between RL-1 and Rip1Tag2 mice, there might be differences in the bio-availability of angiogenic factors. VEGF-A, in particular the splice variant VEGF-A_{165} can be sequestered to heparan sulfate proteoglycans, in this form incapable of signaling to VEGF receptors (Gengrinovitch et al., 1999). Activity of matrix metalloproteinases or heparinases have been implicated in the control of VEGF-A release, and in a series of tumor models, it has been shown that MMP9 activity is crucial for tumor angiogenesis in different murine tumor models (Bergers et al., 2000; Coussens et al., 2000; Giraudo et al., 2004). Usually, different sources of MMP-9 exist in a tumor environment: the tumor cells, stromal fibroblast or inflammatory cells can be prominent sources of MMP-9. Particularly, myeloid derived-suppressor cells (MDSC) and tumor-associated macrophage have been shown to contribute substantially to support the angiogenic switch (reviewed (Zumsteg and Christofori, 2009)). We found that RL-1 tumor mice (in FVB/N background) have significantly less $Gr1^+/CD11b^+$ MDSC in blood, spleen and tumors as compared to Rip1Tag2 mice (in C57BL/6 background). It is tempting to speculate that differential infiltration of myeloid cells is crucial for the difference in tumor onset. Double transgenic RL-1;RipVEGF-A mice die at a much younger age than their single transgenic RL-1 counterparts, indicating that VEGF-A availability indeed limits tumor growth drastically. The smaller tumor volumes in RL-1;RipVEGF-A mice (as compared to RL-1 mice) detected prior to median survival age might be due to decreased body weight (just by the younger age) and the better vascularization, facilitating the release of insulin into the circulation. Both factors would increase the relative insulin burden and promote the finally fatal hypoglycemic state of the mice. However, as RL-1;RipIGF1R mice die at even younger age but have many more and bigger tumors than RL-1;RipVEGF-A mice, it is unlikely that body weight is a critical factor to explain the earlier decease of VEGF-A over-expressing mice.

Principally, all composite mice analyzed showed phenotypes similar to the ones already described. RL-1;RipVEGF-C and RL-1;RipVEGF-D showed peritumoral lymphangiogenesis, rarely detected in RL-1 single transgenic mice (data not shown). However, in contrast to Rip1Tag2 mice, we found lymph node metastases in single transgenic RL-1 mice. An exception to the described phenotypes is the occurrence of lung metastases that was found in 80% of Rip1Tag2;RipVEGF-D mice (Kopfstein et al., 2007). By analyzing lung lysates for luciferase activity, we only detected one potential metastasis carrier out of 14 RL-1;RipVEGF-D mice, which we could not confirm by histology. In contrast to the Rip1Tag2 insulinoma model, in RL-1 mice the transgenic expression of

VEGF-D does not trigger massive lymphocyte infiltration, an inflammatory stimulus that could potentially support metastatic events. RL-1;RipIGF1R mice showed massively accelerated tumor progression as can be seen by the survival time and the larger tumor burden. We conclude that IGF1R signaling co-operates with SV40 large T antigen for efficient oncogenic transformation.

Using luciferase *in vivo* imaging technology, growth of insulinomas could be observed and quantified over time, a technique already employed for transgenic mice developing pituitary or prostate tumors (Liao et al., 2007; Vooijs et al., 2002). We propose this mouse tumor model to test the efficacy of anti-tumor regimens in pre-clinical experiments. Some limitations of RL-1 mice include the thickness of subcutaneous fat layer that might increase especially when mice get older and gain weight and the inherent fluctuation of luciferase expression levels due to reduced insulin promoter activity in bigger tumors. However, by analyzing a large cohort of mice, we could observe 3 fold increase in average photon flow over a 25 day period, stressing the possibility to utilize this tumor model in quantitative manner.

Like insulinomas in humans, RL-1 mice develop liver metastasis (Hirshberg et al., 2005), and total metastasis burden correlates with primary tumor size. The partial surrounding of metastatic nodules by LYVE-1^+ sinusoidal endothelial vessels but the absence of intra-metastatic blood vessels, as judged by the lack of internal LYVE-1^+ or $CD31^+$ structures, indicates that the metastases do not yet execute an angiogenic program of their own, at least not sufficiently potent to induce intra-metastatic vasculature. That the LYVE-1^+ sinusoids do not completely surround the metastatic nodules suggests that the detected structures are not just stuck in blood vessels but rather start to establish their niche in the target organ. We find about 5% of cells positive for the mitosis marker Phospho-Histone H3, indicating the proliferating nature of the metastatic nodules. The almost complete loss of E-Cadherin in most metastatic nodules indicates that metastatic cell must have undergone at least a partial epithelial to mysenchymal transistion (EMT), a phenomenon often observed in tumors of epithelial tissues (carcinomas) (Hugo et al., 2007). However, if the occurrence of E-Cadherin positive cell patches means re-expression of E-Cadherin or if some metastatic cells have never shut down E-Cadherin expression, cannot be decided at this point.

The route of metastasis to the liver seems be rather haemogenic (primary intravasation into blood vessels) than lymphogenic (through lymphatics) by the following observation: lymphangiogenic RL-1;RipVEGF-C and RL-1;RipVEGF-D mice show tumor cell clusters within LYVE-1 positive lymphatic vessels (not shown), not observed in RL-1 mice, but do not have a higher liver metastasis rate or develop liver metastasis at smaller primary tumor sizes as compared to RL-1 mice.

In conclusion, we generated a transgenic mouse which holds promise to become a valuable tool to study the efficacy of pre-clinical therapeutic approaches in longitudinal analyses. The highly specific luciferase expression will be very valuable to utilize this mouse in studies aiming at detecting metastases promoting events. Finally, liver metastasis, the most common metastatic event in neuroendocrine tumors, can be studied at an early stage.

4.4.5. Materials and Methods

Generation of RipTag-IRES-Luciferase construct

The total cassette containing rat insulin promoter 1 regulatory region, SV40 early region and polyA signal was excised from pRIP1-Tag vector (Hanahan, 1985) using BamHI and cloned into BamHI of pBluescript II KS (Promega) vector in forward orientation, yielding pBS-RipTag-pA.

The SV40 polyA signal as well as 90bp of SV40-TAG cDNA was removed from this vector using BclI, cutting 90bp upstream of the SV40-TAG stop codon, and SalI, cutting in the pBS II multiple cloning site downstream of the insertion site. The removed SV40-TAG cDNA was restored by insertion of a BclI/ SalI digested PCR product (primers: “TAg Bcl fw” and “TAg 3’ end SalI rv”) into the BclI/ SalI opened pBS-RipTag-pA, the PCR fragment starting at the BclI site within the SV40-TAG cDNA and ending with the SV40-TAG stop codon with an additional SalI site for cloning, yielding pBS-RipTag-MCS. The PCR was performed on the original pRIP1-Tag.

A 163bp SV40 poly-adenylation signal was then reintroduced into pBS-RipTag-MCS, by ligating a XhoI/ KpnI digested PCR product (primers: “XhoI_TAg_pAsig_fwd” and “KpnI_TAg_pAsig_rv”) covering the poly-adenylation site of the SV40-Tag of pRIP1-Tag into the XhoI/ KpnI opened pBS-RipTag-MCS, yielding pBS-RipTag-MCS-pA.

IRES-Luciferase cassette was constructed by amplifying Luciferase out of pUHC13.3 (Gossen and Bujard, 1992) using “BamHI_Luc_fw“ and „ XhoI_Luc_rv“ into pcDNA3.1 (Invitrogen) using BamHI and XhoI, yielding pcDNA3.1-Luc. IRES was amplified out of pCCALL2-IRES-EGFP (kindly provided by Jody Haigh, Toronto, Canada) using “BamHI-XhoI-IRES_fw” and “BamHI-IRES-rv“ and cloned in forward orientation in pcDNA3.1-Luc using BamHI, yielding pcDNA3.1-IRES-Luc. IRES-Luc was cloned into pBS-RipTag-MCS-pA in forward orientation using XhoI, yielding pRTIL. pRTIL was sequenced and the predicted sequence confirmed.

Generation of transgenic mice

pRTIL was cut using NotI and linearized plasmid was purified over ultra-pure agarose gel elecrophoresis and extracted using GeneClean (Q-Bio gene). The linearized construct was micro-injected into pronuclei of fertilized FVB/N eggs according to standard techniques (Taketo et al., 1991). Embryos that survived microinjection were reimplanted the same day into pseudopregnant NMRI females that had been random-mated to vasectomized $B6D2F_1$ males. Genomic PCR identified 3 founder lines designated RL-1, RL-2 and RL-3. All animal experiments were approved by the “Basler Tierschutzkommission” and are covered by the licenses 1878, 1907 and 1908.

Determination of transgene integration site in RL-1 line by linker mediated PCR

The transgene integration site was principally determined by a method described for detecting transposon integration sites (Dupuy et al., 2005). 5 µg of genomic DNA from RL-1 mice isolated from liver was digested using 15U NlaIII and fragments subsequently isolated using QIAEX II gel extraction kit (Qiagen). To avoid amplification of concatamers of the trangene, the extracted DNA was then digested using SacII, eliminating amplification of transgene junctions and then again purified using QIAEX II. NlaIII linker was generated by annealing equimolar amount of "NlaIII linker+" and "NlaIII linker-" in NEB buffer 3 (New England Biolabs) at a concentration of 5mM. "NlaIII linker-" was 5' phosphate modified to aid linker ligation and 3' C3 spacer modified to avoid priming of Taq polymerase. Annealed NlaIII linker at a final concentration of 0.2mM was then ligated to 1/40 of the genomic NlaIII/ SacII double digested DNA using T4 DNA ligase. 1/20 of the ligation reaction was then used as template for the 1st PCR, using Taq polymerase and "NlaIII Lnkr pri" and RipRv2 primers. RipRv2 primer binds in the transgene and will lead to the preferential amplification of fragments containing transgenic DNA. No specific DNA fragments were detected after this PCR. Then 1/20 of the PCR product was used as template for a nested PCR using "NlaIII Nest lnkr pri" and RipRv3 primers. A specific band was detected and cloned into pGEM-T easy (Promega) vector. Sequencing of the construct confirmed integration of the transgene with a junction between host DNA and transgene consisting of a destroyed NotI site. Integration was in mouse Chromosome 3 as indicated in Figure 27.

Genotyping of transgenic mice

With the knowledge of the transgene integration site, a multiplex PCR could be designed yielding a 281bp amplicon for a transgene allele and a 501bp fragment of a wild-type allele using the primers RipMsChr3, MsCh3_24971617fw and MsCh3_24972117rv. Primer RipMsChr3 is spanning the transgene integration site.

Mice

All mice described carrying modifier genes have been characterized in the Rip1Tag2 tumor model previously (Gannon et al., 2002; Kopfstein et al., 2007; Lopez and Hanahan, 2002; Mandriota et al., 2001; Perl et al., 1999) and were coming from a C57BL/6 background and then continuously bred into FVB/N background.

In vivo luciferase bioluminescence

Prior to measurement, mice were shaved in the peritoneal region to maximize signal intensity from insulinomas. Mice were injected *intraperitoneally* with D-luciferin potassium salt (Gold BioTechnology, St. Louis, MO, U.S.A.) dissolved in sterile PBS at 15 mg/ml with a luciferin

dose of 150mg/kg body weight. 5 minutes after luciferin injection, mice were anaesthetized by inhalation of 3% isoflurane (Provet AG, Lyssach, Switzerland) with medical grade oxygen as carrier gas and placed in the dark chamber of the "NightOWL II LB 983" imaging system (Berthold Technologies, Bad Wildbad, Germany). For quantification experiments with multiple rounds of monitoring, timing of injection, anesthesia, and camera setting were standardized and kept constant throughout the experiment. Typical acquisition times were between 1 and 5 minutes with maximal binning. For quantification of light intensities in time course experiments, a constant analysis gate was defined and individual tumor photon counts were determined by centering the gate on the highest signal intensity for each time point.

FACS analysis of MDSC in peripheral blood, spleen and tumors

Peripheral blood was drawn directly by heart puncture of CO_2 sacrificed mice and transferred to EDTA anti-coagulated collection tube (Sarstedt). Staining was done using anti-CD11b-PE (Clone M1/70) and anti-Gr1-APC (Clone RB6-8C5) (eBioscience) and erythrocytes lysed prior to analysis using BD FACS lysing solution (BD Biosciences). Spleens were minced to single cells in PBS/ 5% FCS using 100μm nylon mesh followed by filtration over 40μm nylon mesh. Single cell suspensions of tumors from 12-13 week old Rip1Tag2 or 16-19 week old RL-1 mice were obtained by digestion for 60 minutes at 37°C in Dulbecco's Modified Eagle's Medium (DMEM) supplemented with 5% NU serum (Becton Dickinson), 0.2 mg/ml DNaseI, 1.2 U/ml Dispase II (Roche Applied Science).

Quantitative real time RT–PCR

Total RNA from tumors or total pancreas was prepared by homogenizing tissue using TRI Reagent (SIGMA), and reverse transcribed with random hexamer primers using M-MLV reverse transcriptase (SIGMA). cDNA was quantified on a ABI Prism 7000 light cycler (Applied Biosystems) using SYBR green PCR MasterMix (Fermentas) using the primers described in Table 5. Ct values were normalized against ribosomal protein L19 (RPL19) and fold induction calculated as $2^{\Delta\Delta ct}$.

Ex vivo quantification of organ lysate luciferase activity

Organs and tumors were homogenized into ice-cooled Reporter Lysis Buffer (Promega) using a Polytron PT1200 homogenizer (Kinematica AG, Switzerland). Samples were then centrifuged at 12'000 rcf for 10 minutes and supernatants stored at -20° C until further analysis. For quantification, 10μl of lysate were mixed with 50μl of Luciferase Assay Reagent (Promega) (either manually or by the sample injector) in white 96 well plates (Berthold Technologies) and luminescence measured on a Centro LB 960 luminometer (Berthold Technologies). Liver and lung lysates were found to have a high quenching activity and were used in a 1:5 dilution.

Tissue processing/ histology/ antibodies

For organ biopsies, mice were euthanized by CO_2 and organs quickly removed. Organs were either fixed at 4° C in 4% phosphate buffered paraformaldehyde (PFA) for 12 hours and then embedded in paraffin after ethanol/ xylene dehydration; alternatively organs were fixed at 4°C in 4% PFA for 2h, and cryo-preserved for 10 hours in 20% sucrose in PBS prior to embedding in OCT freezing matrix. Paraffin slides were cut 5 μm thick and rehydrated according to standard protocols. For immunohistochemical (IHC) stainings of PFA fixed, paraffin embedded specimens, antigen epitopes were retrieved by boiling slides in 10mM Na-Citrate buffer (pH6.0) for 10' in a microwave oven, endogenous peroxidase was quenched by treatment with 3% H_2O_2 for 10 minutes. Cryosections were cut 7 μm thick, postfixed for 5' in either 4% PFA or 70% ethanol and dried for 30' prior to rehydration in PBS. Slides were blocked for 30' in PBS/ 5% normal goat serum and then incubated with the primary antibody in blocking buffer at 4° C overnight. Antibodies used: rat a-CD31 1:50 (clone MEC13.3, B&D), guinea pig a-Insulin (DAKO) 1:100, rabbit anti-NG2 1:200 (Transduction Lab), rabbit anti-Phospho-Histone H3 (Upstate Biotechnology) 1:500, rabbit anti-mLYVE-1 (Reliatech) 1:100, rat anti-E-Cadherin (clone ECCD-2, Zymed) 1:100. IHC stainings were revealed by incubation with biotinylated secondary antibodies and ABC Elite detection kit using AEC substrate (all from Vector Laboratories) according to manufacturers instructions and counterstained using haematoxilin. Immunofluorescent stainings were revealed by incubation with $Alexa_{488}$ or $Alexa_{568}$ labeled secondary antibodies (Molecular Probes) and nuclei stained with DAPI (SIGMA). Western blot for large T antigen was done by lysing tumors in RIPA lysis buffer (25mM Tris-HCl pH 7.6, 150mM NaCl, 1% NP-40, 1% Sodium deoxycholate, 0.1% SDS), resolving 50 μg of cleared lysate by 10% SDS-PAGE and revealed using mouse Anti-SV40 T Antigen (Clone Ab-1; Calbiochem).

Statistical evaluations

All statistical tests were performed using GraphPad Prism 4.0c for Mac. Data was first tested for normality and when normality was fulfilled, unpaired, two-tailed student's t-test was applied. For non-gaussian data, Mann-Whitney non-parametric U test was performed. Survival data was analyzed by log-rank test. P values below 0.05 were considered to be statistically significant.

Primer name	**Sequence 5' -> 3'**	Comments
TAg Bcl fw	CTGTTCA**TGATCA**TAATCAGCCA	BclI site: bold
TAg 3' end SalI rv	GAGA**GTCGAC***TTA*TGTTTCAGGTTCAGGGG	SalI site: bold, STOP codon: italic
XhoI_TAg_pAsig_fwd	C**CTCGAG**AATGAATGCAATTGTTGTTGTTAAC	Xho site: bold
KpnI_TAg_pAsig_rv	GC**GGTACC**AGACATGATAAGATACATTGATG	KpnI site: bold
NlaIII linker+	GTAATACGACTCACTATAGGGCTCCGCTTAAGG GACCATG	
NlaIII linker-	Phos-GTCCCTTAAGCGGAG-C3 spacer	5' and 3' modified
NlaIII Lnkr pri	GTAATACGACTCACTATAGGGC	
NlaIII Nest lnkr pri	AGGGCTCCGCTTAAGGGAC	
RipRv2	GGTGTATTCTCCTGTAGTATCTTAGATTTGC	optimized not to bind to murine insulin promoter
RipRv3	GGTCAGCAACTCTCCATAAGAGGTG	optimized not to bind to murine insulin promoter
RipMsChr3	GTTCTAGA**GCGGCC**AAGTATT	NotI site from linearized transgene: bold
BamHI_Luc_fw	GATCG**GGATCC**AATATGCAAGCTTGGCATTCCG	BamHI site: bold
XhoI_Luc_rv	GATTAG**CTCGAG**ATCGTTACAATTTGGACTTTCCG	XhoI site: bold
BamHI-XhoI-IRES_fw	GAGTC**GGATCC***CTCGAG*AGCGCTTCAGGCC CCTCTCCCTCCCCCCCC	BamHI site: bold XhoI site: italic
BamHI-IRES-rv	ATCGAC**GGATCC**TTATCATCGTGTTTTTCAAA	BamHI site: bold
MsCh3_24971617fw	CATATGGCAGTGTAAACCAGT	Genotyping
MsCh3_24972117rv	AGTTCCCAGCATTCTTCATG	Genotyping
mVEGFA_420fw	ACTGGACCCTGGCTTTACTG	qPCR mVEGF-A
mVEGFA_497rv	TCTGCTCTCCTTCTGTCGTG	qPCR mVEGF-A
mE47_1671fw	GGACATTAACGAGGCCTTCCG	qPCR mE47
mE47_1822rv	TGGGGTTCAGGTTGCGTTCT	qPCR mE47
mSNAIL_566fw	CTCTGAAGATGCACATCCGAA	qPCR mSNAIL
mSNAIL_683rv	GGCTTCTCACCAGTGTGGGT	qPCR mSNAIL
mSLUG_671fw	TGTGTCTGCAAGATCTGTGGC	qPCR mSLUG
mSLUG_747rv	TCCCCAGTGTGAGTTCTAATGTG	qPCR mSLUG
mSIP1_325fw	GGAGGAAAAACGTGGTGAACTAT	qPCR mSIP1
mSIP1_403rv	GCAATGTGAAGCTTGTCCTCTT	qPCR mSIP1
mRPL19_fw	ATCCGCAAGCCTGTGACTGT	qPCR mRPL19
mRPL19_rv	TCGGGCCAGGGTGTTTTT	qPCR mRPL19
mIGF2_1244fw	CGCTTCAGTTTGTCTGTTCG	qPCR mIGF-2
mIGF2_1338rv	GCAGCACTCTTCCACGATG	qPCR mIGF-2
mIR_2623fw	TGCTCATGCCCTAAGACTGAC	qPCR mInsR
mIR_2747rv	GATCTTCGCTTTCGGGATG	qPCR mInsR

Table 5. Primers used for cloning of pRTIL, integration site extraction using LM-PCR, multplex genotyping PCR and real-time quantitative PCR (SYBR green).

5. References

Achen, M. G., and Stacker, S. A. (2008). Molecular control of lymphatic metastasis. Ann N Y Acad Sci *1131*, 225-234.

Ahn, G. O., and Brown, J. M. (2008). Matrix metalloproteinase-9 is required for tumor vasculogenesis but not for angiogenesis: role of bone marrow-derived myelomonocytic cells. Cancer Cell *13*, 193-205.

Ahuja, D., Saenz-Robles, M. T., and Pipas, J. M. (2005). SV40 large T antigen targets multiple cellular pathways to elicit cellular transformation. Oncogene *24*, 7729-7745.

Akashi, K., Traver, D., Miyamoto, T., and Weissman, I. L. (2000). A clonogenic common myeloid progenitor that gives rise to all myeloid lineages. Nature *404*, 193-197.

Allavena, P., Sica, A., Solinas, G., Porta, C., and Mantovani, A. (2008). The inflammatory micro-environment in tumor progression: the role of tumor-associated macrophages. Crit Rev Oncol Hematol *66*, 1-9.

Allavena, P., Signorelli, M., Chieppa, M., Erba, E., Bianchi, G., Marchesi, F., Olimpio, C. O., Bonardi, C., Garbi, A., Lissoni, A.*, et al.* (2005). Anti-inflammatory properties of the novel antitumor agent yondelis (trabectedin): inhibition of macrophage differentiation and cytokine production. Cancer Res *65*, 2964-2971.

Amato, R. J., Hernandez-McClain, J., Saxena, S., and Khan, M. (2008). Lenalidomide therapy for metastatic renal cell carcinoma. Am J Clin Oncol *31*, 244-249.

Ando, T., Jordan, P., Joh, T., Wang, Y., Jennings, M. H., Houghton, J., and Alexander, J. S. (2005). Isolation and characterization of a novel mouse lymphatic endothelial cell line: SV-LEC. Lymphat Res Biol *3*, 105-115.

Arany, Z., Foo, S. Y., Ma, Y., Ruas, J. L., Bommi-Reddy, A., Girnun, G., Cooper, M., Laznik, D., Chinsomboon, J., Rangwala, S. M.*, et al.* (2008). HIF-independent regulation of VEGF and angiogenesis by the transcriptional coactivator PGC-1alpha. Nature *451*, 1008-1012.

Asahara, T., Murohara, T., Sullivan, A., Silver, M., van der Zee, R., Li, T., Witzenbichler, B., Schatteman, G., and Isner, J. M. (1997). Isolation of putative progenitor endothelial cells for angiogenesis. Science *275*, 964-967.

Bailey, A. S., Willenbring, H., Jiang, S., Anderson, D. A., Schroeder, D. A., Wong, M. H., Grompe, M., and Fleming, W. H. (2006). Myeloid lineage progenitors give rise to vascular endothelium. Proc Natl Acad Sci U S A *103*, 13156-13161.

Baluk, P., Fuxe, J., Hashizume, H., Romano, T., Lashnits, E., Butz, S., Vestweber, D., Corada, M., Molendini, C., Dejana, E., and McDonald, D. M. (2007). Functionally specialized junctions between endothelial cells of lymphatic vessels. J Exp Med *204*, 2349-2362.

Baron, J. A., Sandler, R. S., Bresalier, R. S., Quan, H., Riddell, R., Lanas, A., Bolognese, J. A., Oxenius, B., Horgan, K., Loftus, S., and Morton, D. G. (2006). A randomized trial of rofecoxib for the chemoprevention of colorectal adenomas. Gastroenterology *131*, 1674-1682.

Barrera, P., Blom, A., van Lent, P. L., van Bloois, L., Beijnen, J. H., van Rooijen, N., de Waal Malefijt, M. C., van de Putte, L. B., Storm, G., and van den Berg, W. B. (2000). Synovial macrophage depletion with clodronate-containing liposomes in rheumatoid arthritis. Arthritis Rheum *43*, 1951-1959.

Benard, A., Ceredig, R., and Rolink, A. G. (2006). Regulatory T cells control autoimmunity following syngeneic bone marrow transplantation. Eur J Immunol *36*, 2324-2335.

Bergers, G., Brekken, R., McMahon, G., Vu, T. H., Itoh, T., Tamaki, K., Tanzawa, K., Thorpe, P., Itohara, S., Werb, Z., and Hanahan, D. (2000). Matrix metalloproteinase-9 triggers the angiogenic switch during carcinogenesis. Nat Cell Biol *2*, 737-744.

Bergers, G., Javaherian, K., Lo, K. M., Folkman, J., and Hanahan, D. (1999). Effects of angiogenesis inhibitors on multistage carcinogenesis in mice. Science *284*, 808-812.

Bertagnolli, M. M., Eagle, C. J., Zauber, A. G., Redston, M., Solomon, S. D., Kim, K., Tang, J., Rosenstein, R. B., Wittes, J., Corle, D.*, et al.* (2006). Celecoxib for the prevention of sporadic colorectal adenomas. N Engl J Med *355*, 873-884.

Bertolini, F., Shaked, Y., Mancuso, P., and Kerbel, R. S. (2006). The multifaceted circulating endothelial cell in cancer: towards marker and target identification. Nat Rev Cancer *6*, 835-845.

Bingle, L., Brown, N. J., and Lewis, C. E. (2002). The role of tumour-associated macrophages in tumour progression: implications for new anticancer therapies. J Pathol *196*, 254-265.

Bjorndahl, M., Cao, R., Nissen, L. J., Clasper, S., Johnson, L. A., Xue, Y., Zhou, Z., Jackson, D., Hansen, A. J., and Cao, Y. (2005). Insulin-like growth factors 1 and 2 induce lymphangiogenesis in vivo. Proc Natl Acad Sci U S A *102*, 15593-15598.

Brideau, G., Makinen, M. J., Elamaa, H., Tu, H., Nilsson, G., Alitalo, K., Pihlajaniemi, T., and Heljasvaara, R. (2007). Endostatin overexpression inhibits lymphangiogenesis and lymph node metastasis in mice. Cancer Res *67*, 11528-11535.

Buttler, K., Ezaki, T., and Wilting, J. (2008). Proliferating mesodermal cells in murine embryos exhibiting macrophage and lymphendothelial characteristics. BMC Dev Biol *8*, 43.

Calandra, G., McCarty, J., McGuirk, J., Tricot, G., Crocker, S. A., Badel, K., Grove, B., Dye, A., and Bridger, G. (2008). AMD3100 plus G-CSF can successfully mobilize CD34+ cells from non-Hodgkin's lymphoma, Hodgkin's disease and multiple myeloma patients previously failing mobilization with chemotherapy and/or cytokine treatment: compassionate use data. Bone Marrow Transplant *41*, 331-338.

Cao, R., Bjorndahl, M. A., Religa, P., Clasper, S., Garvin, S., Galter, D., Meister, B., Ikomi, F., Tritsaris, K., Dissing, S.*, et al.* (2004). PDGF-BB induces intratumoral lymphangiogenesis and promotes lymphatic metastasis. Cancer Cell *6*, 333-345.

Casanovas, O., Hicklin, D. J., Bergers, G., and Hanahan, D. (2005). Drug resistance by evasion of antiangiogenic targeting of VEGF signaling in late-stage pancreatic islet tumors. Cancer Cell *8*, 299-309.

Chang, L. K., Garcia-Cardena, G., Farnebo, F., Fannon, M., Chen, E. J., Butterfield, C., Moses, M. A., Mulligan, R. C., Folkman, J., and Kaipainen, A. (2004). Dose-dependent response of FGF-2 for lymphangiogenesis. Proc Natl Acad Sci U S A *101*, 11658-11663.

Cho, C. H., Koh, Y. J., Han, J., Sung, H. K., Jong Lee, H., Morisada, T., Schwendener, R. A., Brekken, R. A., Kang, G., Oike, Y.*, et al.* (2007). Angiogenic role of LYVE-1-positive macrophages in adipose tissue. Circ Res *100*, e47-57.

Christofori, G., Naik, P., and Hanahan, D. (1994). A second signal supplied by insulin-like growth factor II in oncogene-induced tumorigenesis. Nature *369*, 414-418.

Christofori, G., Naik, P., and Hanahan, D. (1995a). Deregulation of both imprinted and expressed alleles of the insulin-like growth factor 2 gene during beta-cell tumorigenesis. Nat Genet *10*, 196-201.

Christofori, G., Naik, P., and Hanahan, D. (1995b). Vascular endothelial growth factor and its receptors, flt-1 and flk-1, are expressed in normal pancreatic islets and throughout islet cell tumorigenesis. Mol Endocrinol *9*, 1760-1770.

Conejo-Garcia, J. R., Buckanovich, R. J., Benencia, F., Courreges, M. C., Rubin, S. C., Carroll, R. G., and Coukos, G. (2005). Vascular leukocytes contribute to tumor vascularization. Blood *105*, 679-681.

Coukos, G., Benencia, F., Buckanovich, R. J., and Conejo-Garcia, J. R. (2005). The role of dendritic cell precursors in tumour vasculogenesis. Br J Cancer *92*, 1182-1187.

Coussens, L. M., Fingleton, B., and Matrisian, L. M. (2002). Matrix metalloproteinase inhibitors and cancer: trials and tribulations. Science *295*, 2387-2392.

Coussens, L. M., Raymond, W. W., Bergers, G., Laig-Webster, M., Behrendtsen, O., Werb, Z., Caughey, G. H., and Hanahan, D. (1999). Inflammatory mast cells up-regulate angiogenesis during squamous epithelial carcinogenesis. Genes Dev *13*, 1382-1397.

Coussens, L. M., Tinkle, C. L., Hanahan, D., and Werb, Z. (2000). MMP-9 supplied by bone marrow-derived cells contributes to skin carcinogenesis. Cell *103*, 481-490.

Crnic, I., Strittmatter, K., Cavallaro, U., Kopfstein, L., Jussila, L., Alitalo, K., and Christofori, G. (2004). Loss of neural cell adhesion molecule induces tumor metastasis by up-regulating lymphangiogenesis. Cancer Res *64*, 8630-8638.

Cumano, A., Ferraz, J. C., Klaine, M., Di Santo, J. P., and Godin, I. (2001). Intraembryonic, but not yolk sac hematopoietic precursors, isolated before circulation, provide long-term multilineage reconstitution. Immunity *15*, 477-485.

Cumano, A., and Godin, I. (2007). Ontogeny of the hematopoietic system. Annu Rev Immunol *25*, 745-785.

Cursiefen, C., Chen, L., Borges, L. P., Jackson, D., Cao, J., Radziejewski, C., D'Amore, P. A., Dana, M. R., Wiegand, S. J., and Streilein, J. W. (2004). VEGF-A stimulates lymphangiogenesis and hemangiogenesis in inflammatory neovascularization via macrophage recruitment. J Clin Invest *113*, 1040-1050.

Dadras, S. S., Lange-Asschenfeldt, B., Velasco, P., Nguyen, L., Vora, A., Muzikansky, A., Jahnke, K., Hauschild, A., Hirakawa, S., Mihm, M. C., and Detmar, M. (2005). Tumor lymphangiogenesis predicts melanoma metastasis to sentinel lymph nodes. Mod Pathol *18*, 1232-1242.

Dadras, S. S., Paul, T., Bertoncini, J., Brown, L. F., Muzikansky, A., Jackson, D. G., Ellwanger, U., Garbe, C., Mihm, M. C., and Detmar, M. (2003). Tumor lymphangiogenesis: a novel prognostic indicator for cutaneous melanoma metastasis and survival. Am J Pathol *162*, 1951-1960.

Das, S., and Skobe, M. (2008). Lymphatic vessel activation in cancer. Ann N Y Acad Sci *1131*, 235-241.

de Bruijn, M. F., Ma, X., Robin, C., Ottersbach, K., Sanchez, M. J., and Dzierzak, E. (2002). Hematopoietic stem cells localize to the endothelial cell layer in the midgestation mouse aorta. Immunity *16*, 673-683.

De Palma, M., Venneri, M. A., Galli, R., Sergi Sergi, L., Politi, L. S., Sampaolesi, M., and Naldini, L. (2005). Tie2 identifies a hematopoietic lineage of proangiogenic monocytes required for tumor vessel formation and a mesenchymal population of pericyte progenitors. Cancer Cell *8*, 211-226.

de Visser, K. E., Korets, L. V., and Coussens, L. M. (2005). De novo carcinogenesis promoted by chronic inflammation is B lymphocyte dependent. Cancer Cell *7*, 411-423.

Debnath, J., Muthuswamy, S. K., and Brugge, J. S. (2003). Morphogenesis and oncogenesis of MCF-10A mammary epithelial acini grown in three-dimensional basement membrane cultures. Methods *30*, 256-268.

Devaskar, S. U., Singh, B. S., Carnaghi, L. R., Rajakumar, P. A., and Giddings, S. J. (1993). Insulin II gene expression in rat central nervous system. Regul Pept *48*, 55-63.

Dietrich, W. F., Radany, E. H., Smith, J. S., Bishop, J. M., Hanahan, D., and Lander, E. S. (1994). Genome-wide search for loss of heterozygosity in transgenic mouse tumors reveals candidate tumor suppressor genes on chromosomes 9 and 16. Proc Natl Acad Sci U S A *91*, 9451-9455.

Dragovich, T., Burris, H., 3rd, Loehrer, P., Von Hoff, D. D., Chow, S., Stratton, S., Green, S., Obregon, Y., Alvarez, I., and Gordon, M. (2008). Gemcitabine plus celecoxib in patients with advanced or metastatic pancreatic adenocarcinoma: results of a phase II trial. Am J Clin Oncol *31*, 157-162.

Du, R., Lu, K. V., Petritsch, C., Liu, P., Ganss, R., Passegue, E., Song, H., Vandenberg, S., Johnson, R. S., Werb, Z., and Bergers, G. (2008). HIF1alpha induces the recruitment of bone marrow-derived vascular modulatory cells to regulate tumor angiogenesis and invasion. Cancer Cell *13*, 206-220.

Dupuy, A. J., Akagi, K., Largaespada, D. A., Copeland, N. G., and Jenkins, N. A. (2005). Mammalian mutagenesis using a highly mobile somatic Sleeping Beauty transposon system. Nature *436*, 221-226.

Dvorak, H. F. (2002). Vascular permeability factor/vascular endothelial growth factor: a critical cytokine in tumor angiogenesis and a potential target for diagnosis and therapy. J Clin Oncol *20*, 4368-4380.

Ferron, M., and Vacher, J. (2005). Targeted expression of Cre recombinase in macrophages and osteoclasts in transgenic mice. Genesis *41*, 138-145.

Fingleton, B. (2003). Matrix metalloproteinase inhibitors for cancer therapy:the current situation and future prospects. Expert Opin Ther Targets *7*, 385-397.

Fischer, C., Jonckx, B., Mazzone, M., Zacchigna, S., Loges, S., Pattarini, L., Chorianopoulos, E., Liesenborghs, L., Koch, M., De Mol, M.*, et al.* (2007). Anti-PlGF inhibits growth of VEGF(R)-inhibitor-resistant tumors without affecting healthy vessels. Cell *131*, 463-475.

Folkman, J., Merler, E., Abernathy, C., and Williams, G. (1971). Isolation of a tumor factor responsible for angiogenesis. J Exp Med *133*, 275-288.

Forssell, J., Oberg, A., Henriksson, M. L., Stenling, R., Jung, A., and Palmqvist, R. (2007). High macrophage infiltration along the tumor front correlates with improved survival in colon cancer. Clin Cancer Res *13*, 1472-1479.

Foster, B. A., Gingrich, J. R., Kwon, E. D., Madias, C., and Greenberg, N. M. (1997). Characterization of prostatic epithelial cell lines derived from transgenic adenocarcinoma of the mouse prostate (TRAMP) model. Cancer Res *57*, 3325-3330.

Fritz-Six, K. L., Dunworth, W. P., Li, M., and Caron, K. M. (2008). Adrenomedullin signaling is necessary for murine lymphatic vascular development. J Clin Invest *118*, 40-50.

Gaffney, D. K., Winter, K., Dicker, A. P., Miller, B., Eifel, P. J., Ryu, J., Avizonis, V., Fromm, M., and Greven, K. (2007). A Phase II study of acute toxicity for Celebrex (celecoxib) and chemoradiation in patients with locally advanced cervical cancer: primary endpoint analysis of RTOG 0128. Int J Radiat Oncol Biol Phys *67*, 104-109.

Gale, N. W., Prevo, R., Espinosa, J., Ferguson, D. J., Dominguez, M. G., Yancopoulos, G. D., Thurston, G., and Jackson, D. G. (2007). Normal lymphatic development and function in mice deficient for the lymphatic hyaluronan receptor LYVE-1. Mol Cell Biol *27*, 595-604.

Gale, N. W., Thurston, G., Hackett, S. F., Renard, R., Wang, Q., McClain, J., Martin, C., Witte, C., Witte, M. H., Jackson, D.*, et al.* (2002). Angiopoietin-2 is required for postnatal angiogenesis and lymphatic patterning, and only the latter role is rescued by Angiopoietin-1. Dev Cell *3*, 411-423.

Gannon, G., Mandriota, S. J., Cui, L., Baetens, D., Pepper, M. S., and Christofori, G. (2002). Overexpression of vascular endothelial growth factor-A165 enhances tumor angiogenesis but not metastasis during beta-cell carcinogenesis. Cancer Res *62*, 603-608.

Gao, D., Nolan, D. J., Mellick, A. S., Bambino, K., McDonnell, K., and Mittal, V. (2008). Endothelial progenitor cells control the angiogenic switch in mouse lung metastasis. Science *319*, 195-198.

Garcia-Barros, M., Paris, F., Cordon-Cardo, C., Lyden, D., Rafii, S., Haimovitz-Friedman, A., Fuks, Z., and Kolesnick, R. (2003). Tumor response to radiotherapy regulated by endothelial cell apoptosis. Science *300*, 1155-1159.

Gatfield, J., and Pieters, J. (2000). Essential role for cholesterol in entry of mycobacteria into macrophages. Science *288*, 1647-1650.

Gengrinovitch, S., Berman, B., David, G., Witte, L., Neufeld, G., and Ron, D. (1999). Glypican-1 is a VEGF165 binding proteoglycan that acts as an extracellular chaperone for VEGF165. J Biol Chem *274*, 10816-10822.

Gerhardt, H., and Semb, H. (2008). Pericytes: gatekeepers in tumour cell metastasis? J Mol Med *86*, 135-144.

Gingrich, J. R., Barrios, R. J., Morton, R. A., Boyce, B. F., DeMayo, F. J., Finegold, M. J., Angelopoulou, R., Rosen, J. M., and Greenberg, N. M. (1996). Metastatic prostate cancer in a transgenic mouse. Cancer Res *56*, 4096-4102.

Giraudo, E., Inoue, M., and Hanahan, D. (2004). An amino-bisphosphonate targets MMP-9-expressing macrophages and angiogenesis to impair cervical carcinogenesis. J Clin Invest *114*, 623-633.

Gonzalez-Perez, A., Garcia Rodriguez, L. A., and Lopez-Ridaura, R. (2003). Effects of non-steroidal anti-inflammatory drugs on cancer sites other than the colon and rectum: a meta-analysis. BMC Cancer *3*, 28.

Gossen, M., and Bujard, H. (1992). Tight control of gene expression in mammalian cells by tetracycline-responsive promoters. Proc Natl Acad Sci U S A *89*, 5547-5551.

Grant, S. G., Seidman, I., Hanahan, D., and Bautch, V. L. (1991). Early invasiveness characterizes metastatic carcinoid tumors in transgenic mice. Cancer Res *51*, 4917-4923.

Greenberg, N. M., DeMayo, F., Finegold, M. J., Medina, D., Tilley, W. D., Aspinall, J. O., Cunha, G. R., Donjacour, A. A., Matusik, R. J., and Rosen, J. M. (1995). Prostate cancer in a transgenic mouse. Proc Natl Acad Sci U S A *92*, 3439-3443.

Gregory, C. A., Ylostalo, J., and Prockop, D. J. (2005). Adult bone marrow stem/progenitor cells (MSCs) are preconditioned by microenvironmental "niches" in culture: a two-stage hypothesis for regulation of MSC fate. Sci STKE *2005*, pe37.

Grosso, F., Jones, R. L., Demetri, G. D., Judson, I. R., Blay, J. Y., Le Cesne, A., Sanfilippo, R., Casieri, P., Collini, P., Dileo, P.*, et al.* (2007). Efficacy of trabectedin (ecteinascidin-743) in advanced pretreated myxoid liposarcomas: a retrospective study. Lancet Oncol *8*, 595-602.

Grunewald, M., Avraham, I., Dor, Y., Bachar-Lustig, E., Itin, A., Jung, S., Chimenti, S., Landsman, L., Abramovitch, R., and Keshet, E. (2006). VEGF-induced adult neovascularization: recruitment, retention, and role of accessory cells. Cell *124*, 175-189.

Guiducci, C., Vicari, A. P., Sangaletti, S., Trinchieri, G., and Colombo, M. P. (2005). Redirecting in vivo elicited tumor infiltrating macrophages and dendritic cells towards tumor rejection. Cancer Res *65*, 3437-3446.

Hamrah, P., Chen, L., Zhang, Q., and Dana, M. R. (2003). Novel expression of vascular endothelial growth factor receptor (VEGFR)-3 and VEGF-C on corneal dendritic cells. Am J Pathol *163*, 57-68.

Hanahan, D. (1985). Heritable formation of pancreatic beta-cell tumours in transgenic mice expressing recombinant insulin/simian virus 40 oncogenes. Nature *315*, 115-122.

Hanahan, D., Wagner, E. F., and Palmiter, R. D. (2007). The origins of oncomice: a history of the first transgenic mice genetically engineered to develop cancer. Genes Dev *21*, 2258-2270.

Hanahan, D., and Weinberg, R. A. (2000). The hallmarks of cancer. Cell *100*, 57-70.

Harris, R. E., Chlebowski, R. T., Jackson, R. D., Frid, D. J., Ascenseo, J. L., Anderson, G., Loar, A., Rodabough, R. J., White, E., and McTiernan, A. (2003). Breast cancer and nonsteroidal anti-inflammatory drugs: prospective results from the Women's Health Initiative. Cancer Res *63*, 6096-6101.

Hattori, K., Dias, S., Heissig, B., Hackett, N. R., Lyden, D., Tateno, M., Hicklin, D. J., Zhu, Z., Witte, L., Crystal, R. G.*, et al.* (2001). Vascular endothelial growth factor and angiopoietin-1 stimulate postnatal hematopoiesis by recruitment of vasculogenic and hematopoietic stem cells. J Exp Med *193*, 1005-1014.

He, L., He, X., Lowe, S. W., and Hannon, G. J. (2007). microRNAs join the p53 network--another piece in the tumour-suppression puzzle. Nat Rev Cancer *7*, 819-822.

He, Y., Rajantie, I., Ilmonen, M., Makinen, T., Karkkainen, M. J., Haiko, P., Salven, P., and Alitalo, K. (2004). Preexisting lymphatic endothelium but not endothelial progenitor cells are essential for tumor lymphangiogenesis and lymphatic metastasis. Cancer Res *64*, 3737-3740.

Hirakawa, S., Brown, L. F., Kodama, S., Paavonen, K., Alitalo, K., and Detmar, M. (2006). VEGF-C-induced lymphangiogenesis in sentinel lymph nodes promotes tumor metastasis to distant sites. Blood.

Hirakawa, S., Kodama, S., Kunstfeld, R., Kajiya, K., Brown, L. F., and Detmar, M. (2005). VEGF-A induces tumor and sentinel lymph node lymphangiogenesis and promotes lymphatic metastasis. J Exp Med *201*, 1089-1099.

Hiratsuka, S., Watanabe, A., Aburatani, H., and Maru, Y. (2006). Tumour-mediated upregulation of chemoattractants and recruitment of myeloid cells predetermines lung metastasis. Nat Cell Biol *8*, 1369-1375.

Hirshberg, B., Cochran, C., Skarulis, M. C., Libutti, S. K., Alexander, H. R., Wood, B. J., Chang, R., Kleiner, D. E., and Gorden, P. (2005). Malignant insulinoma: spectrum of unusual clinical features. Cancer *104*, 264-272.

Holash, J., Maisonpierre, P. C., Compton, D., Boland, P., Alexander, C. R., Zagzag, D., Yancopoulos, G. D., and Wiegand, S. J. (1999). Vessel cooption, regression, and growth in tumors mediated by angiopoietins and VEGF. Science *284*, 1994-1998.

Huang, Y., Chen, X., Dikov, M. M., Novitskiy, S. V., Mosse, C. A., Yang, L., and Carbone, D. P. (2007). Distinct roles of VEGFR-1 and VEGFR-2 in the aberrant hematopoiesis associated with elevated levels of VEGF. Blood *110*, 624-631.

Hugo, H., Ackland, M. L., Blick, T., Lawrence, M. G., Clements, J. A., Williams, E. D., and Thompson, E. W. (2007). Epithelial--mesenchymal and mesenchymal--epithelial transitions in carcinoma progression. J Cell Physiol *213*, 374-383.

Ichikawa-Shindo, Y., Sakurai, T., Kamiyoshi, A., Kawate, H., Iinuma, N., Yoshizawa, T., Koyama, T., Fukuchi, J., Iimuro, S., Moriyama, N.*, et al.* (2008). The GPCR modulator protein RAMP2 is essential for angiogenesis and vascular integrity. J Clin Invest *118*, 29-39.

Iwata, C., Kano, M. R., Komuro, A., Oka, M., Kiyono, K., Johansson, E., Morishita, Y., Yashiro, M., Hirakawa, K., Kaminishi, M., and Miyazono, K. (2007). Inhibition of cyclooxygenase-2 suppresses lymph node metastasis via reduction of lymphangiogenesis. Cancer Res *67*, 10181-10189.

Jackson, D. G., Prevo, R., Clasper, S., and Banerji, S. (2001). LYVE-1, the lymphatic system and tumor lymphangiogenesis. Trends Immunol *22*, 317-321.

Jeltsch, M., Kaipainen, A., Joukov, V., Meng, X., Lakso, M., Rauvala, H., Swartz, M., Fukumura, D., Jain, R. K., and Alitalo, K. (1997). Hyperplasia of lymphatic vessels in VEGF-C transgenic mice. Science *276*, 1423-1425.

Jeon, B. H., Jang, C., Han, J., Kataru, R. P., Piao, L., Jung, K., Cha, H. J., Schwendener, R. A., Jang, K. Y., Kim, K. S.*, et al.* (2008). Profound but dysfunctional lymphangiogenesis via vascular endothelial growth factor ligands from CD11b+ macrophages in advanced ovarian cancer. Cancer Res *68*, 1100-1109.

Jiang, S., Bailey, A. S., Goldman, D. C., Swain, J. R., Wong, M. H., Streeter, P. R., and Fleming, W. H. (2008). Hematopoietic stem cells contribute to lymphatic endothelium. PLoS ONE *3*, e3812.

Jin, H., Su, J., Garmy-Susini, B., Kleeman, J., and Varner, J. (2006). Integrin alpha4beta1 promotes monocyte trafficking and angiogenesis in tumors. Cancer Res *66*, 2146-2152.

Jung, S., Aliberti, J., Graemmel, P., Sunshine, M. J., Kreutzberg, G. W., Sher, A., and Littman, D. R. (2000). Analysis of fractalkine receptor CX(3)CR1 function by targeted deletion and green fluorescent protein reporter gene insertion. Mol Cell Biol *20*, 4106-4114.

Kajiya, K., Hirakawa, S., Ma, B., Drinnenberg, I., and Detmar, M. (2005). Hepatocyte growth factor promotes lymphatic vessel formation and function. Embo J *24*, 2885-2895.

Kalluri, R., and Zeisberg, M. (2006). Fibroblasts in cancer. Nat Rev Cancer *6*, 392-401.

Kaplan, R. N., Riba, R. D., Zacharoulis, S., Bramley, A. H., Vincent, L., Costa, C., MacDonald, D. D., Jin, D. K., Shido, K., Kerns, S. A.*, et al.* (2005). VEGFR1-positive haematopoietic bone marrow progenitors initiate the pre-metastatic niche. Nature *438*, 820-827.

Karkkainen, M. J., Haiko, P., Sainio, K., Partanen, J., Taipale, J., Petrova, T. V., Jeltsch, M., Jackson, D. G., Talikka, M., Rauvala, H.*, et al.* (2004). Vascular endothelial growth factor C is required for sprouting of the first lymphatic vessels from embryonic veins. Nat Immunol *5*, 74-80.

Kerjaschki, D., Huttary, N., Raab, I., Regele, H., Bojarski-Nagy, K., Bartel, G., Krober, S. M., Greinix, H., Rosenmaier, A., Karlhofer, F.*, et al.* (2006). Lymphatic endothelial progenitor cells contribute to de novo lymphangiogenesis in human renal transplants. Nat Med *12*, 230-234.

Khuder, S. A., and Mutgi, A. B. (2001). Breast cancer and NSAID use: a meta-analysis. Br J Cancer *84*, 1188-1192.

Kim, K. J., Li, B., Winer, J., Armanini, M., Gillett, N., Phillips, H. S., and Ferrara, N. (1993). Inhibition of vascular endothelial growth factor-induced angiogenesis suppresses tumour growth in vivo. Nature *362*, 841-844.

Kinder, S. J., Tsang, T. E., Quinlan, G. A., Hadjantonakis, A. K., Nagy, A., and Tam, P. P. (1999). The orderly allocation of mesodermal cells to the extraembryonic structures and the anteroposterior axis during gastrulation of the mouse embryo. Development *126*, 4691-4701.

Klagsbrun, M., Sasse, J., Sullivan, R., and Smith, J. A. (1986). Human tumor cells synthesize an endothelial cell growth factor that is structurally related to basic fibroblast growth factor. Proc Natl Acad Sci U S A *83*, 2448-2452.

Kopfstein, L., Veikkola, T., Djonov, V. G., Baeriswyl, V., Schomber, T., Strittmatter, K., Stacker, S. A., Achen, M. G., Alitalo, K., and Christofori, G. (2007). Distinct roles of vascular endothelial growth factor-D in lymphangiogenesis and metastasis. Am J Pathol *170*, 1348-1361.

Kortylewski, M., Kujawski, M., Wang, T., Wei, S., Zhang, S., Pilon-Thomas, S., Niu, G., Kay, H., Mule, J., Kerr, W. G.*, et al.* (2005). Inhibiting Stat3 signaling in the hematopoietic system elicits multicomponent antitumor immunity. Nat Med *11*, 1314-1321.

Kortylewski, M., and Yu, H. (2008). Role of Stat3 in suppressing anti-tumor immunity. Curr Opin Immunol *20*, 228-233.

Krasner, C. N., McMeekin, D. S., Chan, S., Braly, P. S., Renshaw, F. G., Kaye, S., Provencher, D. M., Campos, S., and Gore, M. E. (2007). A Phase II study of trabectedin single agent in patients with recurrent ovarian cancer previously treated with platinum-based regimens. Br J Cancer *97*, 1618-1624.

Kren, A., Baeriswyl, V., Lehembre, F., Wunderlin, C., Strittmatter, K., Antoniadis, H., Fassler, R., Cavallaro, U., and Christofori, G. (2007). Increased tumor cell dissemination and cellular senescence in the absence of beta1-integrin function. Embo J *26*, 2832-2842.

Kujawski, M., Kortylewski, M., Lee, H., Herrmann, A., Kay, H., and Yu, H. (2008). Stat3 mediates myeloid cell-dependent tumor angiogenesis in mice. J Clin Invest.

Kusmartsev, S., Eruslanov, E., Kubler, H., Tseng, T., Sakai, Y., Su, Z., Kaliberov, S., Heiser, A., Rosser, C., Dahm, P.*, et al.* (2008). Oxidative stress regulates expression of VEGFR1 in myeloid cells: link to tumor-induced immune suppression in renal cell carcinoma. J Immunol *181*, 346-353.

Kuwana, M., Okazaki, Y., Kodama, H., Izumi, K., Yasuoka, H., Ogawa, Y., Kawakami, Y., and Ikeda, Y. (2003). Human circulating CD14+ monocytes as a source of progenitors that exhibit mesenchymal cell differentiation. J Leukoc Biol *74*, 833-845.

Le Hir, H., Nott, A., and Moore, M. J. (2003). How introns influence and enhance eukaryotic gene expression. Trends Biochem Sci *28*, 215-220.

Leung, D. W., Cachianes, G., Kuang, W. J., Goeddel, D. V., and Ferrara, N. (1989). Vascular endothelial growth factor is a secreted angiogenic mitogen. Science *246*, 1306-1309.

Li, Q., Michaud, M., Stewart, W., Schwartz, M., and Madri, J. A. (2008). Modeling the neurovascular niche: murine strain differences mimic the range of responses to chronic hypoxia in the premature newborn. J Neurosci Res *86*, 1227-1242.

Liao, C. P., Zhong, C., Saribekyan, G., Bading, J., Park, R., Conti, P. S., Moats, R., Berns, A., Shi, W., Zhou, Z.*, et al.* (2007). Mouse models of prostate adenocarcinoma with the capacity to monitor spontaneous carcinogenesis by bioluminescence or fluorescence. Cancer Res *67*, 7525-7533.

Lin, E. Y., Li, J. F., Bricard, G., Wang, W., Deng, Y., Sellers, R., Porcelli, S. A., and Pollard, J. W. (2007). VEGF Restores Delayed Tumor Progression in Tumors Depleted of Macrophages. Mol Oncol *1*, 288-302.

Lin, E. Y., Li, J. F., Gnatovskiy, L., Deng, Y., Zhu, L., Grzesik, D. A., Qian, H., Xue, X. N., and Pollard, J. W. (2006). Macrophages regulate the angiogenic switch in a mouse model of breast cancer. Cancer Res *66*, 11238-11246.

Lin, E. Y., Nguyen, A. V., Russell, R. G., and Pollard, J. W. (2001). Colony-stimulating factor 1 promotes progression of mammary tumors to malignancy. J Exp Med *193*, 727-740.

Lin, J., Lalani, A. S., Harding, T. C., Gonzalez, M., Wu, W. W., Luan, B., Tu, G. H., Koprivnikar, K., VanRoey, M. J., He, Y.*, et al.* (2005). Inhibition of lymphogenous metastasis using adeno-associated virus-mediated gene transfer of a soluble VEGFR-3 decoy receptor. Cancer Res *65*, 6901-6909.

Lonnroth, C., Andersson, M., Arvidsson, A., Nordgren, S., Brevinge, H., Lagerstedt, K., and Lundholm, K. (2008). Preoperative treatment with a non-steroidal anti-inflammatory drug (NSAID) increases tumor tissue infiltration of seemingly activated immune cells in colorectal cancer. Cancer Immun *8*, 5.

Loomans, C. J., Wan, H., de Crom, R., van Haperen, R., de Boer, H. C., Leenen, P. J., Drexhage, H. A., Rabelink, T. J., van Zonneveld, A. J., and Staal, F. J. (2006). Angiogenic murine endothelial progenitor cells are derived from a myeloid bone marrow fraction and can be identified by endothelial NO synthase expression. Arterioscler Thromb Vasc Biol *26*, 1760-1767.

Lopez, T., and Hanahan, D. (2002). Elevated levels of IGF-1 receptor convey invasive and metastatic capability in a mouse model of pancreatic islet tumorigenesis. Cancer Cell *1*, 339-353.

Lu, L., Payvandi, F., Wu, L., Zhang, L. H., Hariri, R. J., Man, H. W., Chen, R. S., Muller, G. W., Hughes, C. C., Stirling, D. I.*, et al.* (2008). The anti-cancer drug lenalidomide inhibits angiogenesis and metastasis via multiple inhibitory effects on endothelial cell function in normoxic and hypoxic conditions. Microvasc Res.

Lugus, J. J., Park, C., and Choi, K. (2005). Developmental relationship between hematopoietic and endothelial cells. Immunol Res *32*, 57-74.

Lugus, J. J., Park, C., Ma, Y. D., and Choi, K. (2008). Both primitive and definitive blood cells are derived from Flk-1+ mesoderm. Blood.

Lyden, D., Hattori, K., Dias, S., Costa, C., Blaikie, P., Butros, L., Chadburn, A., Heissig, B., Marks, W., Witte, L.*, et al.* (2001). Impaired recruitment of bone-marrow-derived endothelial and hematopoietic precursor cells blocks tumor angiogenesis and growth. Nat Med *7*, 1194-1201.

Mandriota, S. J., Jussila, L., Jeltsch, M., Compagni, A., Baetens, D., Prevo, R., Banerji, S., Huarte, J., Montesano, R., Jackson, D. G.*, et al.* (2001). Vascular endothelial growth factor-C-mediated lymphangiogenesis promotes tumour metastasis. Embo J *20*, 672-682.

Maroulakou, I. G., Anver, M., Garrett, L., and Green, J. E. (1994). Prostate and mammary adenocarcinoma in transgenic mice carrying a rat C3(1) simian virus 40 large tumor antigen fusion gene. Proc Natl Acad Sci U S A *91*, 11236-11240.

Maruyama, K., Asai, J., Ii, M., Thorne, T., Losordo, D. W., and D'Amore, P. A. (2007). Decreased macrophage number and activation lead to reduced lymphatic vessel formation and contribute to impaired diabetic wound healing. Am J Pathol *170*, 1178-1191.

Maruyama, K., Ii, M., Cursiefen, C., Jackson, D. G., Keino, H., Tomita, M., Van Rooijen, N., Takenaka, H., D'Amore, P. A., Stein-Streilein, J.*, et al.* (2005). Inflammation-induced lymphangiogenesis in the cornea arises from CD11b-positive macrophages. J Clin Invest *115*, 2363-2372.

McDonnell, C. O., Bouchier-Hayes, D. J., Toomey, D., Foley, D., Kay, E. W., Leen, E., and Walsh, T. N. (2003). Effect of neoadjuvant chemoradiotherapy on angiogenesis in oesophageal cancer. The British journal of surgery *90*, 1373-1378.

Millauer, B., Shawver, L. K., Plate, K. H., Risau, W., and Ullrich, A. (1994). Glioblastoma growth inhibited in vivo by a dominant-negative Flk-1 mutant. Nature *367*, 576-579.

Motoike, T., Markham, D. W., Rossant, J., and Sato, T. N. (2003). Evidence for novel fate of Flk1+ progenitor: contribution to muscle lineage. Genesis *35*, 153-159.

Mouta Carreira, C., Nasser, S. M., di Tomaso, E., Padera, T. P., Boucher, Y., Tomarev, S. I., and Jain, R. K. (2001). LYVE-1 is not restricted to the lymph vessels: expression in normal liver blood sinusoids and down-regulation in human liver cancer and cirrhosis. Cancer Res *61*, 8079-8084.

Murakami, M., Zheng, Y., Hirashima, M., Suda, T., Morita, Y., Ooehara, J., Ema, H., Fong, G. H., and Shibuya, M. (2008). VEGFR1 tyrosine kinase signaling promotes lymphangiogenesis as well as angiogenesis indirectly via macrophage recruitment. Arterioscler Thromb Vasc Biol *28*, 658-664.

Murdoch, C., Tazzyman, S., Webster, S., and Lewis, C. E. (2007). Expression of Tie-2 by human monocytes and their responses to angiopoietin-2. J Immunol *178*, 7405-7411.

Nibbs, R. J., Gilchrist, D. S., King, V., Ferra, A., Forrow, S., Hunter, K. D., and Graham, G. J. (2007). The atypical chemokine receptor D6 suppresses the development of chemically induced skin tumors. J Clin Invest *117*, 1884-1892.

Noel, A., Jost, M., and Maquoi, E. (2008). Matrix metalloproteinases at cancer tumor-host interface. Semin Cell Dev Biol *19*, 52-60.

Nolan, D. J., Ciarrocchi, A., Mellick, A. S., Jaggi, J. S., Bambino, K., Gupta, S., Heikamp, E., McDevitt, M. R., Scheinberg, D. A., Benezra, R., and Mittal, V. (2007). Bone marrow-derived endothelial progenitor cells are a major determinant of nascent tumor neovascularization. Genes Dev *21*, 1546-1558.

Novak, A., Guo, C., Yang, W., Nagy, A., and Lobe, C. G. (2000). Z/EG, a double reporter mouse line that expresses enhanced green fluorescent protein upon Cre-mediated excision. Genesis *28*, 147-155.

Nozawa, H., Chiu, C., and Hanahan, D. (2006). Infiltrating neutrophils mediate the initial angiogenic switch in a mouse model of multistage carcinogenesis. Proc Natl Acad Sci U S A *103*, 12493-12498.

Ny, A., Koch, M., Schneider, M., Neven, E., Tong, R. T., Maity, S., Fischer, C., Plaisance, S., Lambrechts, D., Heligon, C.*, et al.* (2005). A genetic Xenopus laevis tadpole model to study lymphangiogenesis. Nat Med *11*, 998-1004.

Okabe, M., Ikawa, M., Kominami, K., Nakanishi, T., and Nishimune, Y. (1997). 'Green mice' as a source of ubiquitous green cells. FEBS Lett *407*, 313-319.

Oliver, G. (2004). Lymphatic vasculature development. Nat Rev Immunol *4*, 35-45.

Osada, T., Chong, G., Tansik, R., Hong, T., Spector, N., Kumar, R., Hurwitz, H. I., Dev, I., Nixon, A. B., Lyerly, H. K.*, et al.* (2008). The effect of anti-VEGF therapy on immature myeloid cell and dendritic cells in cancer patients. Cancer Immunol Immunother *57*, 1115-1124.

Overall, C. M., and Kleifeld, O. (2006a). Towards third generation matrix metalloproteinase inhibitors for cancer therapy. Br J Cancer *94*, 941-946.

Overall, C. M., and Kleifeld, O. (2006b). Tumour microenvironment - opinion: validating matrix metalloproteinases as drug targets and anti-targets for cancer therapy. Nat Rev Cancer *6*, 227-239.

Ozerdem, U. (2006). Targeting of pericytes diminishes neovascularization and lymphangiogenesis in prostate cancer. The Prostate *66*, 294-304.

Pacheco, A. V., Rasila, K., Lee, S. J., Rabinowitz, I., Elias, L., Lee, F. C., and Verschraegen, C. F. (2007). Phase II studies of antiangiogenic four drug regimens for the treatment of advanced renal cell carcinoma: FUNIL-retinoid and the FUNIL-thalidomide protocols. Urol Oncol.

Padera, T. P., Kadambi, A., di Tomaso, E., Carreira, C. M., Brown, E. B., Boucher, Y., Choi, N. C., Mathisen, D., Wain, J., Mark, E. J.*, et al.* (2002). Lymphatic metastasis in the absence of functional intratumor lymphatics. Science *296*, 1883-1886.

Pahler, J. C., Tazzyman, S., Erez, N., Chen, Y. Y., Murdoch, C., Nozawa, H., Lewis, C. E., and Hanahan, D. (2008). Plasticity in tumor-promoting inflammation: impairment of macrophage recruitment evokes a compensatory neutrophil response. Neoplasia *10*, 329-340.

Palumbo, A., Dimopoulos, M., Miguel, J. S., Harousseau, J. L., Attal, M., Hussein, M., Knop, S., Ludwig, H., von Lilienfeld-Toal, M., and Sonneveld, P. (2008). Lenalidomide in combination with dexamethasone for the treatment of relapsed or refractory multiple myeloma. Blood Rev.

Pan, P. Y., Wang, G. X., Yin, B., Ozao, J., Ku, T., Divino, C. M., and Chen, S. H. (2008). Reversion of immune tolerance in advanced malignancy: modulation of myeloid-derived suppressor cell development by blockade of stem-cell factor function. Blood *111*, 219-228.

Paz-Ares, L., Rivera-Herreros, F., Diaz-Rubio, E., Garcia, M., Casado, E., Cubedo, R., Gravalos, C., Alfaro, V., Gomez, J., Izquierdo, M. A., and Tabernero, J. (2007). Phase II study of trabectedin in pretreated patients with advanced colorectal cancer. Clin Colorectal Cancer *6*, 522-528.

Pelosi, E., Valtieri, M., Coppola, S., Botta, R., Gabbianelli, M., Lulli, V., Marziali, G., Masella, B., Muller, R., Sgadari, C.*, et al.* (2002). Identification of the hemangioblast in postnatal life. Blood *100*, 3203-3208.

Perl, A. K., Dahl, U., Wilgenbus, P., Cremer, H., Semb, H., and Christofori, G. (1999). Reduced expression of neural cell adhesion molecule induces metastatic dissemination of pancreatic beta tumor cells. Nat Med *5*, 286-291.

Perl, A. K., Wilgenbus, P., Dahl, U., Semb, H., and Christofori, G. (1998). A causal role for E-cadherin in the transition from adenoma to carcinoma. Nature *392*, 190-193.

Purhonen, S., Palm, J., Rossi, D., Kaskenpaa, N., Rajantie, I., Yla-Herttuala, S., Alitalo, K., Weissman, I. L., and Salven, P. (2008). Bone marrow-derived circulating endothelial precursors do not contribute to vascular endothelium and are not needed for tumor growth. Proc Natl Acad Sci U S A *105*, 6620-6625.

Religa, P., Cao, R., Bjorndahl, M., Zhou, Z., Zhu, Z., and Cao, Y. (2005). Presence of bone marrow-derived circulating progenitor endothelial cells in the newly formed lymphatic vessels. Blood *106*, 4184-4190.

Rinderknecht, M., and Detmar, M. (2008). Tumor lymphangiogenesis and melanoma metastasis. J Cell Physiol *216*, 347-354.

Risau, W., and Flamme, I. (1995). Vasculogenesis. Annu Rev Cell Dev Biol *11*, 73-91.

Ristimaki, A., Narko, K., Enholm, B., Joukov, V., and Alitalo, K. (1998). Proinflammatory cytokines regulate expression of the lymphatic endothelial mitogen vascular endothelial growth factor-C. J Biol Chem *273*, 8413-8418.

Roberts, N., Kloos, B., Cassella, M., Podgrabinska, S., Persaud, K., Wu, Y., Pytowski, B., and Skobe, M. (2006). Inhibition of VEGFR-3 activation with the antagonistic antibody more potently suppresses lymph node and distant metastases than inactivation of VEGFR-2. Cancer Res *66*, 2650-2657.

Romagnani, P., Annunziato, F., Liotta, F., Lazzeri, E., Mazzinghi, B., Frosali, F., Cosmi, L., Maggi, L., Lasagni, L., Scheffold, A.*, et al.* (2005). CD14+CD34low cells with stem cell phenotypic and functional features are the major source of circulating endothelial progenitors. Circ Res *97*, 314-322.

Romero, S., Stanton, G., DeFelice, J., Schreiber, F., Rago, R., and Fishman, M. (2007). Phase II trial of thalidomide and daily oral dexamethasone for treatment of hormone refractory prostate cancer progressing after chemotherapy. Urol Oncol *25*, 284-290.

Rosen, L. S., Gordon, D., Tchekmedyian, S., Yanagihara, R., Hirsh, V., Krzakowski, M., Pawlicki, M., de Souza, P., Zheng, M., Urbanowitz, G.*, et al.* (2003). Zoledronic acid versus placebo in the treatment of skeletal metastases in patients with lung cancer and other solid tumors: a phase III, double-blind, randomized trial--the Zoledronic Acid Lung Cancer and Other Solid Tumors Study Group. J Clin Oncol *21*, 3150-3157.

Sabin, F. R. (1902). On the origin of the lymphatic system from the veins, and the development of the lymph hearts and thoracic duct in the pig. Am J Anat *1*, 367–389.

Sacco, M. G., Cato, E. M., Ceruti, R., Soldati, S., Indraccolo, S., Caniatti, M., Scanziani, E., and Vezzoni, P. (2001). Systemic gene therapy with anti-angiogenic factors inhibits spontaneous breast tumor growth and metastasis in MMTVneu transgenic mice. Gene Ther *8*, 67-70.

Sachsenmeier, K. F., and Pipas, J. M. (2001). Inhibition of Rb and p53 is insufficient for SV40 T-antigen transformation. Virology *283*, 40-48.

Santini, D., Vincenzi, B., Galluzzo, S., Battistoni, F., Rocci, L., Venditti, O., Schiavon, G., Angeletti, S., Uzzalli, F., Caraglia, M.*, et al.* (2007). Repeated intermittent low-dose therapy with zoledronic acid induces an early, sustained, and long-lasting decrease of peripheral vascular endothelial growth factor levels in cancer patients. Clin Cancer Res *13*, 4482-4486.

Schledzewski, K., Falkowski, M., Moldenhauer, G., Metharom, P., Kzhyshkowska, J., Ganss, R., Demory, A., Falkowska-Hansen, B., Kurzen, H., Ugurel, S.*, et al.* (2006). Lymphatic endothelium-specific hyaluronan receptor LYVE-1 is expressed by stabilin-1+, F4/80+, CD11b+ macrophages in malignant tumours and wound healing tissue in vivo and in bone marrow cultures in vitro: implications for the assessment of lymphangiogenesis. J Pathol *209*, 67-77.

Schneider, M., Othman-Hassan, K., Christ, B., and Wilting, J. (1999). Lymphangioblasts in the avian wing bud. Dev Dyn *216*, 311-319.

Schomber, T., Zumsteg, A., Strittmatter, K., Crnic, I., Antoniadis, H., Littlewood-Evans, A., Wood, J., and Christofori, G. (2009). Differential effects of the vascular endothelial growth factor receptor inhibitor PTK787/ZK222584 on tumor angiogenesis and tumor lymphangiogenesis. Mol Cancer Ther *8*, 55-63.

Schoppmann, S. F., Birner, P., Stockl, J., Kalt, R., Ullrich, R., Caucig, C., Kriehuber, E., Nagy, K., Alitalo, K., and Kerjaschki, D. (2002). Tumor-associated macrophages express lymphatic endothelial growth factors and are related to peritumoral lymphangiogenesis. Am J Pathol *161*, 947-956.

Senger, D. R., Galli, S. J., Dvorak, A. M., Perruzzi, C. A., Harvey, V. S., and Dvorak, H. F. (1983). Tumor cells secrete a vascular permeability factor that promotes accumulation of ascites fluid. Science *219*, 983-985.

Shaked, Y., Bertolini, F., Man, S., Rogers, M. S., Cervi, D., Foutz, T., Rawn, K., Voskas, D., Dumont, D. J., Ben-David, Y.*, et al.* (2005). Genetic heterogeneity of the vasculogenic phenotype parallels angiogenesis; Implications for cellular surrogate marker analysis of antiangiogenesis. Cancer Cell *7*, 101-111.

Shojaei, F., Singh, M., Thompson, J. D., and Ferrara, N. (2008). Role of Bv8 in neutrophil-dependent angiogenesis in a transgenic model of cancer progression. Proc Natl Acad Sci U S A *105*, 2640-2645.

Shojaei, F., Wu, X., Malik, A. K., Zhong, C., Baldwin, M. E., Schanz, S., Fuh, G., Gerber, H. P., and Ferrara, N. (2007a). Tumor refractoriness to anti-VEGF treatment is mediated by CD11b+Gr1+ myeloid cells. Nat Biotechnol *25*, 911-920.

Shojaei, F., Wu, X., Zhong, C., Yu, L., Liang, X. H., Yao, J., Blanchard, D., Bais, C., Peale, F. V., van Bruggen, N.*, et al.* (2007b). Bv8 regulates myeloid-cell-dependent tumour angiogenesis. Nature *450*, 825-831.

Sica, A., and Bronte, V. (2007). Altered macrophage differentiation and immune dysfunction in tumor development. J Clin Invest *117*, 1155-1166.

Sinha, P., Clements, V. K., Bunt, S. K., Albelda, S. M., and Ostrand-Rosenberg, S. (2007). Cross-talk between myeloid-derived suppressor cells and macrophages subverts tumor immunity toward a type 2 response. J Immunol *179*, 977-983.

Skobe, M., Hawighorst, T., Jackson, D. G., Prevo, R., Janes, L., Velasco, P., Riccardi, L., Alitalo, K., Claffey, K., and Detmar, M. (2001). Induction of tumor lymphangiogenesis by VEGF-C promotes breast cancer metastasis. Nat Med *7*, 192-198.

Soucek, L., Lawlor, E. R., Soto, D., Shchors, K., Swigart, L. B., and Evan, G. I. (2007). Mast cells are required for angiogenesis and macroscopic expansion of Myc-induced pancreatic islet tumors. Nat Med *13*, 1211-1218.

Stacker, S. A., Caesar, C., Baldwin, M. E., Thornton, G. E., Williams, R. A., Prevo, R., Jackson, D. G., Nishikawa, S., Kubo, H., and Achen, M. G. (2001). VEGF-D promotes the metastatic spread of tumor cells via the lymphatics. Nat Med *7*, 186-191.

Su, J. L., Shih, J. Y., Yen, M. L., Jeng, Y. M., Chang, C. C., Hsieh, C. Y., Wei, L. H., Yang, P. C., and Kuo, M. L. (2004). Cyclooxygenase-2 induces EP1- and HER-2/Neu-dependent vascular endothelial growth factor-C up-regulation: a novel mechanism of lymphangiogenesis in lung adenocarcinoma. Cancer Res *64*, 554-564.

Suzuki, E., Kapoor, V., Jassar, A. S., Kaiser, L. R., and Albelda, S. M. (2005). Gemcitabine selectively eliminates splenic Gr-1+/CD11b+ myeloid suppressor cells in tumor-bearing animals and enhances antitumor immune activity. Clin Cancer Res *11*, 6713-6721.

Taketo, M., Schroeder, A. C., Mobraaten, L. E., Gunning, K. B., Hanten, G., Fox, R. R., Roderick, T. H., Stewart, C. L., Lilly, F., Hansen, C. T., and et al. (1991). FVB/N: an inbred mouse strain preferable for transgenic analyses. Proc Natl Acad Sci U S A *88*, 2065-2069.

Tammela, T., Zarkada, G., Wallgard, E., Murtomaki, A., Suchting, S., Wirzenius, M., Waltari, M., Hellstrom, M., Schomber, T., Peltonen, R.*, et al.* (2008). Blocking VEGFR-3 suppresses angiogenic sprouting and vascular network formation. Nature *454*, 656-660.

Tang, Y., Zhang, D., Fallavollita, L., and Brodt, P. (2003). Vascular endothelial growth factor C expression and lymph node metastasis are regulated by the type I insulin-like growth factor receptor. Cancer Res *63*, 1166-1171.

Thurston, G., Noguera-Troise, I., and Yancopoulos, G. D. (2007). The Delta paradox: DLL4 blockade leads to more tumour vessels but less tumour growth. Nat Rev Cancer *7*, 327-331.

Thurston, G., Suri, C., Smith, K., McClain, J., Sato, T. N., Yancopoulos, G. D., and McDonald, D. M. (1999). Leakage-resistant blood vessels in mice transgenically overexpressing angiopoietin-1. Science *286*, 2511-2514.

Van Rooijen, N. (1989). The liposome-mediated macrophage 'suicide' technique. J Immunol Methods *124*, 1-6.

Van Rooijen, N., and Sanders, A. (1994). Liposome mediated depletion of macrophages: mechanism of action, preparation of liposomes and applications. J Immunol Methods *174*, 83-93.

Venneri, M. A., De Palma, M., Ponzoni, M., Pucci, F., Scielzo, C., Zonari, E., Mazzieri, R., Doglioni, C., and Naldini, L. (2007). Identification of proangiogenic TIE2-expressing monocytes (TEMs) in human peripheral blood and cancer. Blood *109*, 5276-5285.

Vooijs, M., Jonkers, J., Lyons, S., and Berns, A. (2002). Noninvasive imaging of spontaneous retinoblastoma pathway-dependent tumors in mice. Cancer Res *62*, 1862-1867.

Wang, S., Gao, J., Lei, Q., Rozengurt, N., Pritchard, C., Jiao, J., Thomas, G. V., Li, G., Roy-Burman, P., Nelson, P. S.*, et al.* (2003). Prostate-specific deletion of the murine Pten tumor suppressor gene leads to metastatic prostate cancer. Cancer Cell *4*, 209-221.

Weber, H. C., Venzon, D. J., Lin, J. T., Fishbein, V. A., Orbuch, M., Strader, D. B., Gibril, F., Metz, D. C., Fraker, D. L., Norton, J. A., and et al. (1995). Determinants of metastatic rate and survival in patients with Zollinger-Ellison syndrome: a prospective long-term study. Gastroenterology *108*, 1637-1649.

Wicki, A., Wild, D., Storch, D., Seemayer, C., Gotthardt, M., Behe, M., Kneifel, S., Mihatsch, M. J., Reubi, J. C., Macke, H. R., and Christofori, G. (2007). [Lys40(Ahx-DTPA-111In)NH2]-Exendin-4 is a highly efficient radiotherapeutic for glucagon-like peptide-1 receptor-targeted therapy for insulinoma. Clin Cancer Res *13*, 3696-3705.

Wigle, J. T., and Oliver, G. (1999). Prox1 function is required for the development of the murine lymphatic system. Cell *98*, 769-778.

Yamashita, J., Itoh, H., Hirashima, M., Ogawa, M., Nishikawa, S., Yurugi, T., Naito, M., Nakao, K., and Nishikawa, S. (2000). Flk1-positive cells derived from embryonic stem cells serve as vascular progenitors. Nature *408*, 92-96.

Yancopoulos, G. D., Davis, S., Gale, N. W., Rudge, J. S., Wiegand, S. J., and Holash, J. (2000). Vascular-specific growth factors and blood vessel formation. Nature *407*, 242-248.

Yang, L., DeBusk, L. M., Fukuda, K., Fingleton, B., Green-Jarvis, B., Shyr, Y., Matrisian, L. M., Carbone, D. P., and Lin, P. C. (2004). Expansion of myeloid immune suppressor Gr+CD11b+ cells in tumor-bearing host directly promotes tumor angiogenesis. Cancer Cell *6*, 409-421.

Yuan, L., Moyon, D., Pardanaud, L., Breant, C., Karkkainen, M. J., Alitalo, K., and Eichmann, A. (2002). Abnormal lymphatic vessel development in neuropilin 2 mutant mice. Development *129*, 4797-4806.

Zeisberger, S. M., Odermatt, B., Marty, C., Zehnder-Fjallman, A. H., Ballmer-Hofer, K., and Schwendener, R. A. (2006). Clodronate-liposome-mediated depletion of tumour-associated macrophages: a new and highly effective antiangiogenic therapy approach. Br J Cancer *95*, 272-281.

Zelek, L., Yovine, A., Brain, E., Turpin, F., Taamma, A., Riofrio, M., Spielmann, M., Jimeno, J., and Misset, J. L. (2006). A phase II study of Yondelis (trabectedin, ET-743) as a 24-h continuous intravenous infusion in pretreated advanced breast cancer. Br J Cancer *94*, 1610-1614.

Zetter, B. R. (2008). The scientific contributions of M. Judah Folkman to cancer research. Nat Rev Cancer *8*, 647-654.

Zumsteg, A., and Christofori, G. (2009). Corrupt policemen: inflammatory cells promote tumor angiogenesis. Curr Opin Oncol *21*, 60-70.

6. Curriculum Vitae

Personal

- Birth date and place: October 9, 1977, Biel/ Switzerland
- Citizenship: Swiss
- Status: Single, no children

Education

- 1989 – 1992: Gymnasium, Kantonsschule Solothurn
- 1992 – 1997: Oberreal-Gymnasium, Kantonsschule Solothurn.
- January 1997: Matura Typus C (mathematics and natural sciences)
- 1997 – 2002: Studies in Biology II (molecular biology & biochemistry), Biozentrum, Universität Basel
- March 2002: Graduation as dipl. phil. nat. biologist from the University of Basel

Professional experience/ research

- 9/2000 – 8/2001: Diploma student
  In the Division of Pharmacology/ Neurobiology of the Biozentrum, University of Basel, I worked in the laboratory of Prof. Dr. UA Meyer on a diploma project concerning the mechanisms of drug-mediated induction of murine housekeeping 5-aminolevulinate synthase.
- 11/2002 – 5/2003: PhD student in the group of Prof. Jürg Tschopp, subgroup of Prof. Pascal Schneider, Institut de Biochimie, Université de Lausanne. In this position, I worked on a project to identify a novel receptor for the TNF family member APRIL.
- 9/2003 – 8/2004: Trainee at the Novartis Institutes for Biomedical Research, Oncology/ Angiogenesis program. In this position, I worked on a project to define the contribution of bone marrow-derived (stem-)cells to angiogenesis in different tumor & angiogenesis models in mice.
- 11/2004 – 2/2009: PhD thesis research in the laboratory of Prof. Gerhard Christofori, Departement Biomedizin, University of Basel.

7. Conferences

- 2005: MVA Ascona, Tumor-Host Interaction and Angiogenesis: Basic Mechansims and Therapeutic Perspectives, Monte Verità, Ascona, Switzerland. Poster presentation: "Different macrophage subsets in the lymphangiogenic phenotype of tumors from Rip1Tag2/NCAM-deficient mice

- 2007: 7th ESH Euroconference on Angiogenesis, Albufeira, Portugal. Poster presentation: "Myeloid cells contribute to tumor lymphangiogenesis"

- 2007: Cellular and Molecular Mechanisms of Tumor Progression and Metastasis. Seeon, Germany. 1st International Kloster Seeon Meeting of the DFG SPP1190 "The tumor – vessel interface". Poster presentation: "Myeloid cells contribute to tumor lymphangiogenesis"

- 2008: Metabolism and Cancer. Symposion CIG (Center for Integrative Genomics), Lausanne, Switzerland.

8. Workshops/ courses

- EMBO practical course: "Genome, transcriptome and miRNome analysis of single cells". August 27 – September 1, 2006, Cologne, Germany

- EMBnet Course: "Introduction to Statistics for Biologists", Biozentrum, University of Basel. 5 - 9 March 2007

- Experimental Course on "Antibody Phage Technology", Department of Chemistry and Applied Biosciences, ETH Zürich, Institute of Pharmaceutical Sciences, February 4 - 8, 2008, Zürich, Switzerland

9. Publications

Fraser DJ, Zumsteg A, Meyer UA: Nuclear receptors constitutive androstane receptor andpregnane X receptor activate a drug-responsive enhancer of the murine 5-aminolevulinic acid synthase gene. *J Biol Chem.* 2003 Oct 10;278(41):39392-401

Ingold K, Zumsteg A et al: Identification of proteoglycans as the APRIL-specific binding partners. *J Exp Med.* 2005 May 2;201(9):1375-83

Adrian Zumsteg, Gerhard Christofori: Corrupt policemen: inflammatory cells promote tumor angiogenesis. *Current Opinion in Oncology*, 21 (1), 2009, p.60-70

Schomber T, Zumsteg A, Strittmatter K, Crnic I, Antoniadis H, Littlewood-Evans A, Wood J, Christofori G: Differential effects of the vascular endothelial growth factor receptor inhibitor PTK787/ZK222584 on tumor angiogenesis and tumor lymphangiogenesis. *Mol Cancer Ther.* 2009 Jan;8(1):55-63.

Adrian Zumsteg*, Vanessa Baeriswyl*, Natsuko Imaizumi, Reto Schwendener, Curzio Rüegg, and Gerhard Christofori: Myeloid cells contribute to tumor lymphangiogenesis (submitted). *equally contributing authors

Adrian Zumsteg, Karin Strittmatter, Daniela Klewe-Nebenius, Helena Antoniadis and Gerhard Christofori: Improved mouse model of β-cell carcinogenesis (in preparation).

Adrian Zumsteg, Karin Strittmatter, Christoph Caviezel, Carlos García-Echeverría, Francesco Hoffmann, and Gerhard Christofori: Compensatory role of insulin receptor upon IGF-1R blockade in an insulinoma mouse model (in preparation).

10. Patents

US Patent US2005118601: MEYER URS (CH); FRASER DAVID J (CH); KAUFMANN MICHEL R (CH); PODVINEC MICHAEL (CH); ZUMSTEG ADRIAN (CH): Enhancer sequence of the 5-aminolevulinic acid synthase gene: Nucleic acid sequences mediating chemical compound induced 5-aminolevulinate synthase gene (ALAS1) expression are disclosed. Said sequences comprise at least a DR-4 binding site. Furthermore, in vitro methods for testing chemical compounds for modulation of heme and/or P 450 cytochromes synthesis are described.

11. Prices/ Awards

2007: BioValley Science Day: “Roche Poster-Awards”, 2nd place, 1500 Swiss Francs. First authors: Adrian Zumsteg and Vanessa Baeriswyl. Title: „Myeloid cells contribute to tumor lymphangiogenesis“

12. Lectures

2008: “Genetic tracing strategies to study cellular plasticity in mice”, Lecture series “Genetic approaches in biomedical research”, University of Basel.

13. Acknowledgements

I would like to thank especially my supervisor Gerhard Christofori to give me the opportunity to conduct my PhD studies in his laboratory. Many, many discussion with him resulted in even more ideas, much more than I could finally approach in experimental studies. In particular, he helped me to improve my scientific thinking by sharpening my senses of what might be a useful and what might be a “time-filler” experiment. Nevertheless, he also encouraged me, the group in general, to follow my own ideas, initiate side-projects, to pick up little findings within my results and formulate hypotheses eventually unrelated to the original project. In a laboratory providing an extremely supportive and friendly atmosphere, I survived more than one scientific drought, without taking too much psychological damage… (I hope).

I would like to thank Roland Jost for taking care of an almost uncountable number of mice. He was always very helpful in conducting my mouse experiments, in setting up complicated breedings and in providing the right mouse at the right spot at the right time. I pay respect to his extraordinary work ethics and appreciate his taking responsibility beyond his duties.

I thank Vanessa Baeriswyl, with whom I co-conducted part of the experiments shown here. She developed many productive ideas that resulted in key experiments for our joint project. Working with her was big fun and also encouraged me to think and work a little harder.

I thank Karin Strittmatter for helping me coping with all the mice and their organs mentioned above. She introduced me in the art of histology, and was an invaluable support in conducting my experiments in general. And: the parties at her house will have cult status in our lab for many years!

I thank Mahmut Yilmaz for bearing up with me the long time of a PhD thesis. Side by side we dived more deeply into the dangerous ocean called science, without losing our breath. I enjoyed discussions with him about science, politics and “dokus”.

I especially thank Helena Antoniadis, Petra Schmidt and Ursula Schmieder for doing a lot of work I was not too keen to do.

I thank Ernesta, Anna, Lorenz, Lukas, Chantal, Miguel, Fabienne, Tibor, Angie, Lucie, Dorothea, Ulrike, Akiko, Imke, Andreas, Neha and Francois for support, a good atmosphere, their stamina in taking my jokes, and for sharing with me their enthusiasm for science and parties.

Finally, I thank my parents for their love and encouragement for the last 31 years.